SECONDARY ATOMIZATION OF COAL-WATER FUELS FOR GAS TURBINE APPLICATION

Final Report

By

T. U. Yu, S.W. Kang and
J.M. Beer

Energy Laboratory Report No. MIT-EL 88-008

December 1988

DOE/MC/23253-F

SECONDARY ATOMIZATION OF COAL-WATER FUELS FOR GAS TURBINE APPLICATIONS

Final Report

T.U. Yu, S.W. Kang and J.M. Beér

Principal Investigators:

J.M. Beér
T.U. Yu

The Energy Laboratory and
Department of Chemical Engineering
Massachusetts Institute of Technology
Cambridge, Massachusetts 02139

December 1988

Prepared for

U.S. Department of Energy
Morgantown Energy Technology Center
Morgantown, WV

Work Performed Under Contract Number: DE-AC21-86MC23253

DISCLAIMERS

FOREWORD

Contract number DE-AC21-86MC23253 covered research carried out at the Massachusetts Institute of Technology during the period September 30, 1986-September 30, 1988. The Technical Monitor of this work at the DOE Morgantown Energy Technology Center was Mr. H. Fred Bauer and, since April 28, 1988, is now Mr. Michael H. McMillian.

ACKNOWLEDGEMENTS

The contributions of members of the MIT-CRF group to the experimental program, and of Ms. Bonnie Caputo in the report preparation, are gratefully acknowledged.

ABSTRACT

The main research objective is to determine the effect of coal-water fuel (CWF) treatment on atomization quality when applied to an ultrafine coal water fuel (solids loading ~ 50%) and at elevated pressures. The fuel treatment techniques are expected to produce secondary atomization, i.e., disruptive shattering of CWF droplets subsequent to their leaving the atomizing nozzle. Upon combustion, the finer fuel droplets would then yield better burnout and finer fly ash size distribution, which in turn could reduce problems of turbine blade erosion. The parallel objective was to present quantitative information on the spray characteristics of CWF (average droplet size and spray shape and angle) with and without fuel treatment for purposes of application to the design of CWF-burning gas turbine combustors.

The experiments include laser diffraction droplet size measurements and high speed photographic studies of CWF sprays in the MIT Spray Test Facility to determine mean droplet size (mass median diameter), droplet size distribution, and spray shape and angle. For the spray tests at elevated pressures, pressure vessels were constructed and installed in the spray test rig. For support of data analyses, a capillary tube viscometer was used to measure the CWF viscosity at the high shear rate that occurs in an atomizer ($> 10^4$ sec^{-1}).

A semi-empirical relationship was developed giving the CWF spray droplet size as a function of the characteristic dimensionless parameters of twin-fluid atomization, including the Weber number, the Reynolds number, and the air-to-fuel mass flow ratio. The correlation was tested experimentally and good agreement was found between calculated and measured drop sizes when the high shear viscosity of the CWF was used in the semi-empirical equation.

Water and CWF spray tests at elevated pressure were made. Average droplet sizes measured as a function of atomizing air-to-fuel ratios (AFRs) at various chamber pressures show that the droplet mass median diameter (MMD) decreases with increasing AFR at a given chamber pressure and increases with increasing chamber pressure at a given AFR. In particular, the results show that droplet sizes of CWF sprays decrease with increasing chamber pressure if the atomizing air velocity is held constant.

Of the fuel treatment techniques investigated, the heating of CWF (flash-atomization) was found to be very effective in reducing droplet size, not only at atmospheric pressure but also at elevated pressure. Secondary atomization by CO_2 absorption (used in a previous study) had given favorable results on CWF combustion, but in this present case this fuel treatment did not seem to have any observable effect on the drop size distribution of the CWF spray at room temperature.

The spray angle was observed to reduce with increasing chamber pressure for given atomizing conditions (AFR, fuel flow rate, fuel temperature). The decreasing entrainment rate per unit length of spray with increasing chamber pressure was mainly responsible for the reduction of the spray angle. The heating of the CWF increased the spray angle, both at atmospheric and elevated pressures. A model was developed to predict spray angle change for the effects of the flash-atomization as a function of AFR, fuel flow rate, and the superheat of the water.

Table of Contents

Table of Contents (Continued)

LIST OF FIGURES

LIST OF FIGURES (Continued)

LIST OF FIGURES (Continued)

LIST OF FIGURES

LIST OF TABLES

EXECUTIVE SUMMARY

One of the principal problems of coal-burning gas turbine technology is the prevention of turbine blade erosion by fly ash particles. Early studies at MIT have shown that the particle size distribution (p.s.d.) within a coal-water fuel (CWF) flame correlates more closely with the size distribution of the atomized fuel spray than with the initial p.s.d. of the coal particles in the slurry. This is because there is a tendency for the coal particles to agglomerate within individual droplets while the water is evaporating, and agglomerates subsequently undergo thermal decomposition in the flame. Large particles formed through agglomeration take longer to burn out and produce large fly ash particles which accelerate turbine blade erosion. One route to finer p.s.d. of the spray droplets and of the fly ash is secondary atomization induced by fuel treatments: the atomizer would deliver as fine a spray as readily achievable, but fuel treatment would cause further disintegration of the atomized droplets, yielding finer droplet p.s.d. for combustion.

The main research objective was to determine the effectiveness of the coal-water fuel treatments on atomization quality when applied to an ultrafine coal-water fuel (solids loading reduced to 50%) and under gas turbine operating conditions (atomization at elevated pressures).

A parallel objective was to present quantitative information on the spray characteristics (mean droplet size, radial distribution of droplet size, and spray shape) of CWF with and without fuel treatment, at atmospheric and elevated chamber pressures.

Three systems of atomized sprays were studied:

1) Water sprays heated to a range of temperatures at atmospheric pressure. Since the fuel treatment affects only the water fraction of the CWF, this study at zero solids loading was expected to show the maximum effects of secondary atomization.

2) CWF sprays heated at atmospheric pressure to different temperatures. The effects of varying solids concentration of the CWF, both upon the fuel viscosity and on the effectiveness of the fuel treatments, were determined at atmospheric pressure.

3) Sprays at elevated pressure. Effects of chamber pressure on the effectiveness of secondary atomization were determined for water and CWF sprays within a pressurized spray test rig.

The experiments included laser diffraction droplet size measurements and photographic studies in the MIT Spray Test Facility to determine mean droplet size (mass median diameter), droplet size distribution, spray shape and spray angle. For the spray tests at elevated pressures, a high pressure spray rig has been constructed and installed. The spray rig is equipped with windows to give visual access for laser optical and photographic studies. For support of data analyses, physical properties of CWF such as viscosity and surface tension were determined. Since CWFs are non-Newtonian and their effective viscosity varies with the shear rate, the CWF viscosity was determined at the high shear rate that occurs in twin-fluid atomizers

($> 10^4$ sec^{-1}). A capillary tube viscometer was modified to permit measurement of CWF viscosity at high shear rate and at elevated temperature.

From the experimental and theoretical (modeling) studies several conclusions were drawn. A semi-empirical relationship was developed giving the CWF spray droplet size as a function of the characteristic dimensionless parameters of twin-fluid atomization including the Weber number, the ratio of the square root of the Weber number to the Reynolds number, and the air-to-fuel mass flow ratio. The correlation was tested experimentally and good agreement was found between calculated and measured drop sizes when the high shear viscosity of the CWF was used in the semi-empirical equation.

With increasing chamber pressure, the mass median droplet size in twin-fluid atomized sprays was found to increase if both the atomizing air and the fuel mass flow rates were maintained constant, but the droplet size decreased for the case when the atomizing air velocity was kept constant, with a concomitant increase of the atomizing air flow rate.

Among the three fuel treatment techniques tested (fuel heating, CO_2 absorption, and their combination) the CWF heating was found to be very effective in reducing the spray droplet size, not only at atmospheric but also at elevated pressures. Reduction in droplet size for the effect of CWF temperature up to levels of the saturation temperature of the CWF is explained by the corresponding reduction in the CWF effective viscosity; above this temperature the superheated liquid flash-vaporizes upon its passage through the atomizer, with the result of droplet disintegration and hence finer atomization. The effect of secondary (flash) atomization upon the spray size distribution depends also on the original (primary) atomized droplet sizes: large droplets are more likely to be disrupted because of their smaller surface tension. This is an especially favorable feature of secondary atomization because large droplets are likely to cause difficulties with burn-out and impingement on structural parts of the combustor or gas turbine.

Secondary atomization by CO_2 absorption (used in a previous study) had given favorable results on CWF combustion, but in this present case this fuel treatment did not seem to have any observable effect on the drop size distribution of the CWF spray at room temperature. It is considered that the improvements found in flame stability and carbon burn-out in sprays with CO_2 absorption in the CWF were due to the rapid bubble formation in the atomized droplets upon their injection into the flame, an effect that does not occur at room temperature.

Photographic studies of the spray angle revealed that the angle decreases with increasing chamber pressure, but the spray angle will increase even at elevated pressure as a result of heating of the CWF to cause flash-atomization. The effect of flash-atomization on the spray angle change is important because a wider angle makes for improved flame stability and promotes carbon burn-out efficiency. A model was developed to predict spray angle change for the effects of flash (secondary) atomization. A relationship is given between the change in the spray angle on the one hand, and the superheat of the water in the CWF and the mass flow rates of the CWF and the atomizing air, on the other.

In light of the established benefits of secondary (thermal) atomization at elevated pressure, the following recommendations are made to promote the successful application of secondary atomization to coal-burning gas turbine combustors:

1) The correlations for droplet size and spray angle should be tested for a wide range of atomizer types, fuel types, and chamber pressures, to broaden the areas of their applicability.

2) The effect of the high temperature combustion environment on the droplet size and shape of flash-atomized CWF sprays needs to be determined as a function of the ambient pressure.

3) Existing atomizers should be characterized for their amenability to operation under conditions of flash-atomization. The relationship between spray angle, linear momentum of the spray, and droplet size on the one hand, and flame stability, carbon burnout, and fly ash formation on the other, should be studied with the objective of establishing a better mechanistic understanding of the effect of atomization quality upon gas turbine combustion characteristics.

1. INTRODUCTION

One of the principal problems of coal-burning gas turbine technology is the prevention of turbine blade erosion by fly ash particles. Coal-water fuels (CWFs) are carefully prepared with minimal ash contents and ultrafine coal particle size distribution to reduce the number of large particles that would not follow streamlines around blades but impact on them. When fly ash particles are very small they may still form deposits on the blades by particle and turbulent gas diffusion processes, necessitating down-time for maintenance, with concomitant reduction in availability of the gas turbine plant. The deposition problem, however, is of secondary importance to that of blade erosions, which results in the direct destruction of the blades. Early studies at MIT have shown that the particle size distribution (p.s.d.) within a CWF flame correlates more closely with the size distribution of the atomized fuel spray than with the initial p.s.d. of the coal particles in the slurry. This is because there is a tendency for the coal particles to agglomerate within individual droplets while the water is evaporating during coal-water slurry combustion, and the agglomerates then undergo thermal decomposition in the flame. Large particles formed through agglomeration take longer to burn out, and produce large fly ash particles that accelerate turbine blade erosion. Burnout and ash deposition mechanisms for a CWF droplet are represented in Figure 1-1.

In pulverized coal combustion it is known that finer grinding of the coal will yield reduced fly ash p.s.d. The relationship between coal particle size and fly ash size, however, is less straightforward for CWF. A finer coal p.s.d. in the slurry could permit use of smaller atomizer nozzle orifices. This might lead to finer fly ash p.s.d. via improved atomization, with the fineness of atomization being related to the orifice dimensions of the atomizer. Unfortunately, finer p.s.d. of the solids loading leads also to increased slurry viscosity, and this, in turn, may lead to coarser atomization unless the viscosity is reduced by means of an additive or by diluting the slurry with water.

One possible route to finer p.s.d. of the spray droplets and of the fly ash is secondary atomization by fuel treatment; the atomizer would deliver as fine a spray as readily achievable, but fuel treatment or additives would cause further disintegration (microexplosion) of the atomized droplets, yielding finer droplet p.s.d. for combustion.

Several treatments to produce secondary atomization (microexplosions) in atomized droplets have been studied to date, three of which were used in this work:

1) CWF heating. This method was first studied in Germany (1) and later successfully tested at the Babcock & Wilcox Company (2). When a pressurized fuel is heated to a level approaching its saturation temperature, the water in the slurry "flash-vaporizes" as its pressure is rapidly reduced in the atomizing nozzle (flash-atomization). The resulting volumetric change causes the droplets to shatter after they leave the nozzle, thereby yielding a substantial reduction in p.s.d.

2) CO_2 Absorption. This method was initially proposed at MIT (3). Carbon dioxide is dissolved in the fuel by injection into the CWF transport

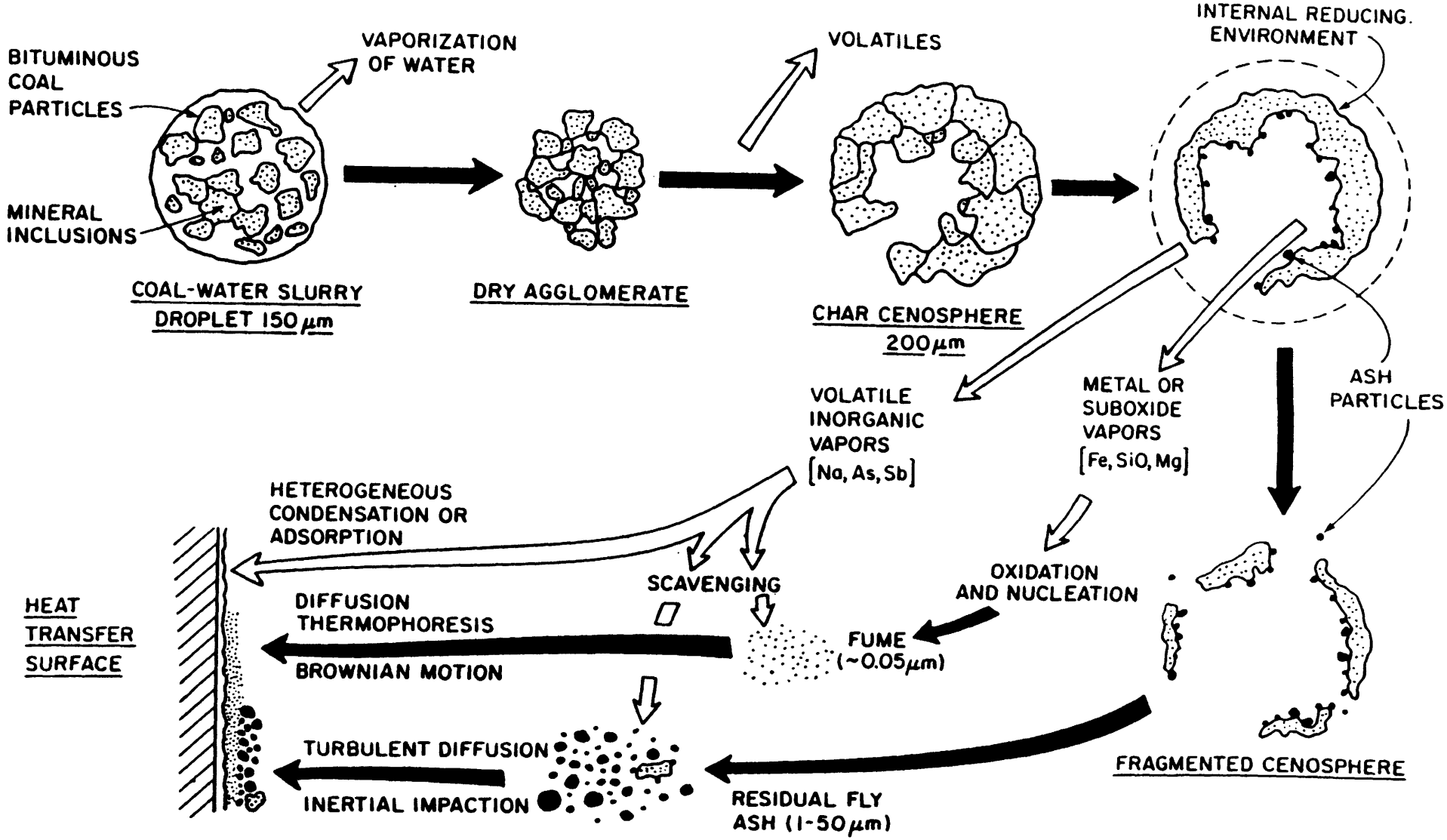

Figure 1-1. Burn-out and Ash Deposition Mechanisms of a Bituminous Coal-Water Fuel Droplet

line between the pump and fuel nozzle. During the pressure release in the atomizing nozzle, the dissolved CO_2 evolves in gaseous form and disrupts CWF droplets.

3) Combination of thermal and CO_2 absorption treatments. When CO_2 is dissolved in a CWF slurry heated in the course of thermally assisted atomization, the dissolved CO_2 generates additional disruptive droplet shattering. The combination of techniques may be useful when there is a low temperature limit to which the fuel can be exposed due to the rheological properties of the CWF (e.g., risk of pipeline blockage).

Some basic characteristics of these treatment techniques are presented in Appendix A. The effectiveness of such methods of secondary atomization of boiler fuels was demonstrated previously (4,5,6) in the MIT Combustion Research Facility (CRF) and the Spray Test Facility (STF). The experimental results have shown that these fuel treatments reduce p.s.d. of droplets and fly ash particles significantly. A summary of the results, which highlights the effects of secondary atomization on flame stability, carbon burnout, and size distribution of particles within a flame, is presented in Appendix B.

The secondary atomization techniques can be used to improve spray fineness for gas turbine applications where the operating combustor pressure is about 10 atm and an ultrafine CWF is used. Using ultrafine-grind CWF instead of regular or fine-grind CWF has several advantages in regard to improving effectiveness of secondary atomization. Ultrafine CWF has a water mass fraction in the order of 50%, compared to regular coal-water fuels that have about 30% water content. At a higher water fraction, more steam can be vaporized through the thermal (or flash) atomization. For the CO_2 absorption technique, this higher fraction of water can absorb more CO_2 gas and thereby generate stronger CO_2 bubbling effects.

While secondary atomization techniques were expected to work at elevated ambient pressure, it was uncertain how effective they would be in reducing droplet sizes in the coal-water fuel spray obtained at gas turbine operating conditions. The research described in this report was oriented to provide answers to this question.

2. RESEARCH OBJECTIVES AND APPROACH

The main research objective was to determine the effectiveness of the CWF treatments on atomization quality when applied to an ultrafine coal-water fuel (solids loading reduced to 50%) and to gas turbine operating conditions (atomization at elevated pressures). Three fuel treatment techniques were studied : (1) heating of CWF under pressure to produce steam as the pressure drops during passage of the CWF through the atomizer nozzle, (2) absorption of CO_2 gas in the CWF to produce a similar effect, and (3) a combination of the two treatments above. These techniques were expected to produce secondary atomization, that is, disruptive shattering of CWF droplets subsequent to their leaving the atomizing nozzle, and to lead to better burnout and finer fly ash size distribution.

A parallel objective was to present quantitative information on the spray characteristics (mean droplet size, radial distribution of droplet

size, and spray shape) of CWF with and without fuel treatment, applicable to the design of CWF-burning gas turbine combustors.

The experiments included laser diffraction droplet size measurements and high-speed photographic studies in the MIT Spray Test Facility to determine mean droplet size (mass median diameter), droplet size distribution, and spray shape and angle. For the spray tests at elevated pressures, a high-pressure spray rig was constructed and installed. The spray rig is equipped with windows to provide visual access for laser optical and photographic studies. For support of data analyses, physical properties of CWF such as viscosity and surface tension were measured. Since the CWF is non-Newtonian and its effective viscosity varies with the shear rate, the CWF viscosity was determined at the high shear rate that occurs in an atomizer (greater than 10^4 sec^{-1}) using a capillary tube viscometer. The capillary tube viscometer was modified to permit measurement of CWF viscosity at high shear rate and at elevated temperature.

In order to meet the above-mentioned objectives, three systems of atomized sprays were studied:

1) Water sprays heated to a range of temperatures at atmospheric pressure. Since the fuel treatment affects only the water fraction of the CWF, this study at zero solids loading was expected to show the maximum effects of secondary atomization.

2) CWF sprays heated at atmospheric pressure to different temperatures. The effects of varying solids concentration of the CWF, both upon the fuel viscosity and on the effectiveness of the fuel treatments, were determined at atmospheric pressure.

3) Sprays at elevated pressure. Effects of chamber pressure on the effectiveness of secondary atomization were determined for water and CWF sprays within a pressurized spray test rig.

3. EXPERIMENTAL APPARATUS

3.1 SPRAY TEST FACILITY

A schematic diagram of the spray test facility (STF) used to characterize CWF spray at atmospheric pressure is shown in Figure 3-1. CWF is delivered to the spray nozzle through a flow meter (Micro Motion Model C 25) by a Moyno pump that can provide injection pressure up to 4 MPa. Fuel pressure and temperature are measured at the atomizing gun entrance. Atomizing air is supplied at pressures up to 7 MPa. It passes through a pressure regulator, flow meter, and flexible stainless steel hose, to a spray nozzle. Atomizing air pressure and temperature are measured at the entrance of the fuel gun. A spray gun transporting the CWF and the atomizing air can be adjusted vertically and horizontally to permit the traversing of different segments of the conical spray by the laser beam of an optical spray analyzer.

Two sides of the 49 in. x 18 in. x 40 in. chamber are made of plexiglas for optical observation and measurement. About half of the other sides of the chamber have honeycomb sections through which air to be entrained by the

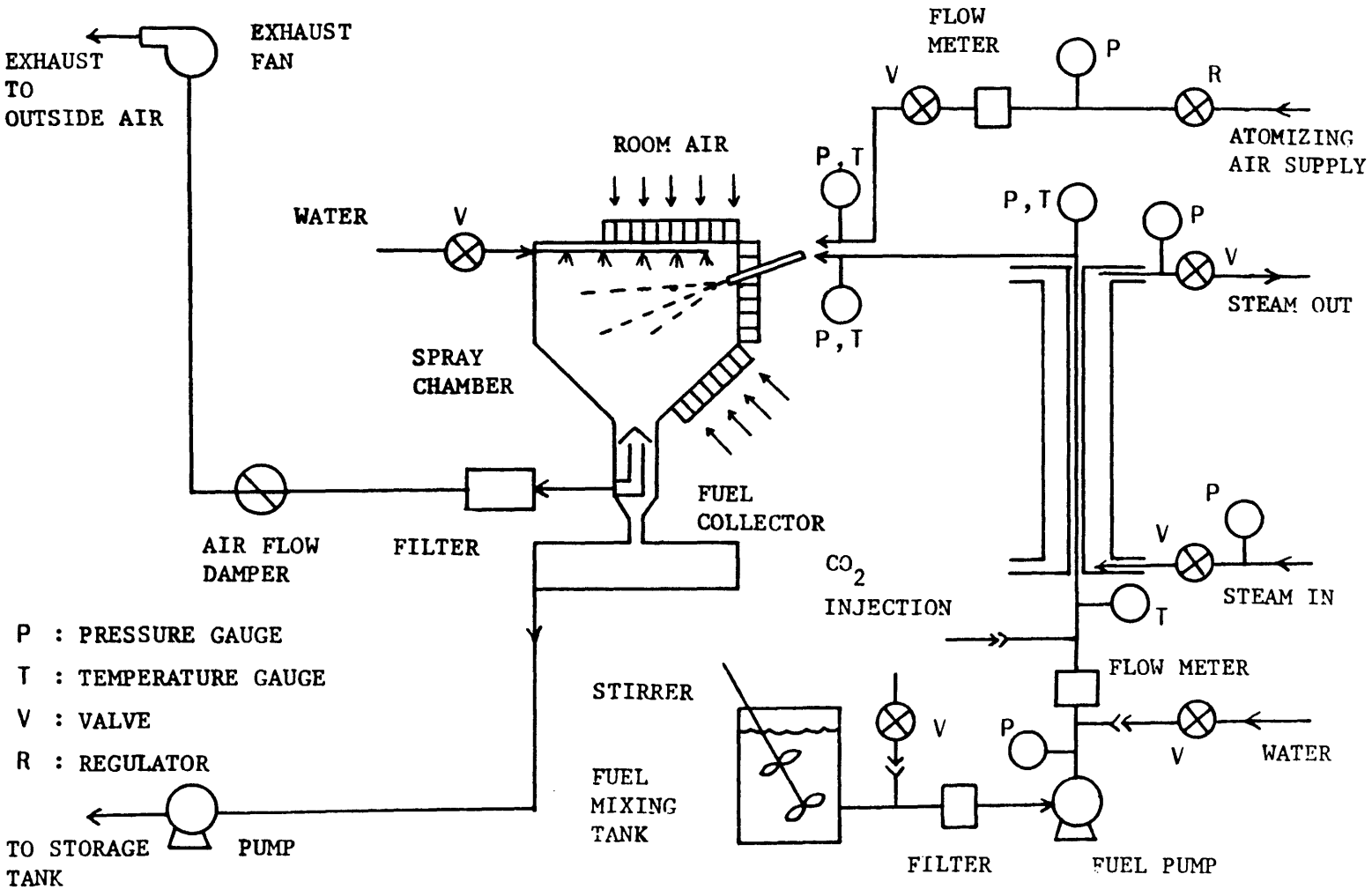

Figure 3-1. Schematic Diagram of Spray Test Facility

spray can pass. The supply of outside air is necessary to suppress the recirculation of small particles into the path of the laser beam.

Air at room temperature enters through the honeycomb sections when the exhaust fan is switched on. This entrained air flow and the atomizing air stream are separated from the fuel at the exit from the spray chamber and then flow through a filter and a flexible hose en route to the exhaust system. The used fuel is collected in a storage tank.

For the CWF heating, steam-heated lines connecting the fuel pump to the spray test facility are used to preheat the experimental CWF to the desired temperature. Each line is about 12 m long and equipped with gauges for monitoring pressures and temperatures of both steam and CWF.

For the study of fuel treatment by CO_2 absorption, a 15-cm section containing a CO_2 injection assembly is inserted into the main fuel line at the high-pressure side of the fuel pump. The maximum CO_2 flow rate that could be injected into the line without producing pulsating sprays or flames was approximately 4 g/kg CWF. This is about 50% of the theoretical saturation limit of CO_2 absorption by the water in the CWF.

3.2 HIGH-PRESSURE SPRAY TEST RIG

For the spray tests at elevated pressures, a high-pressure spray test rig was constructed and installed in the spray test facility (STF). A schematic diagram of this test rig is presented in Figure 3-2. Detail drawings of the pressure vessels are given in Appendix C. Existing equipment available in the STF, such as the fuel pump, steam-heated fuel lines, high-pressure air supply, flow meters, gauges, and other fuel and air-handling systems, are shared by the atmospheric pressure and pressurized spray test facilities. The pressurized spray test rig was designed to permit continuous operation for a period of 1 hour at a fuel flow rate of 6 lb/min; a second interconnected pressurized tank is used for storage of the expended CWF. The wedge-shaped honeycomb on the top of the pressure vessel serves to reduce the flow rate of air necessary to prevent recirculation of fine particles in the region of the path of the laser beam. The air supplied for atomization and prevention of particle recirculation is continuously exhausted through a pressure regulator which controls the exhaust flow rate so as to maintain the pressure at a set level. A particle separator is installed after the pressure regulator to remove airborne particles from the exhaust air. The main vertical vessel is furnished with four optical windows. One set of large optical windows is intended for visual and photographic observation. The other set is for measurement of spray droplet size distribution with the laser diffraction analyzer. A small flow of air or nitrogen is allowed to flow into a chamber behind each window to prevent deposition of CWF particles on the windows.

3.3 LASER DIFFRACTION DROPLET SIZE ANALYZER

The spray test facility is equipped with a laser diffraction size analyzer (Figure 3-3) for droplet size measurements. The operational principle of the laser diffraction analyzer (7) is based on the relationship between the droplet sizes along the laser beam shown on the spray and the radial energy distribution of light in a Fraunhofer diffraction pattern

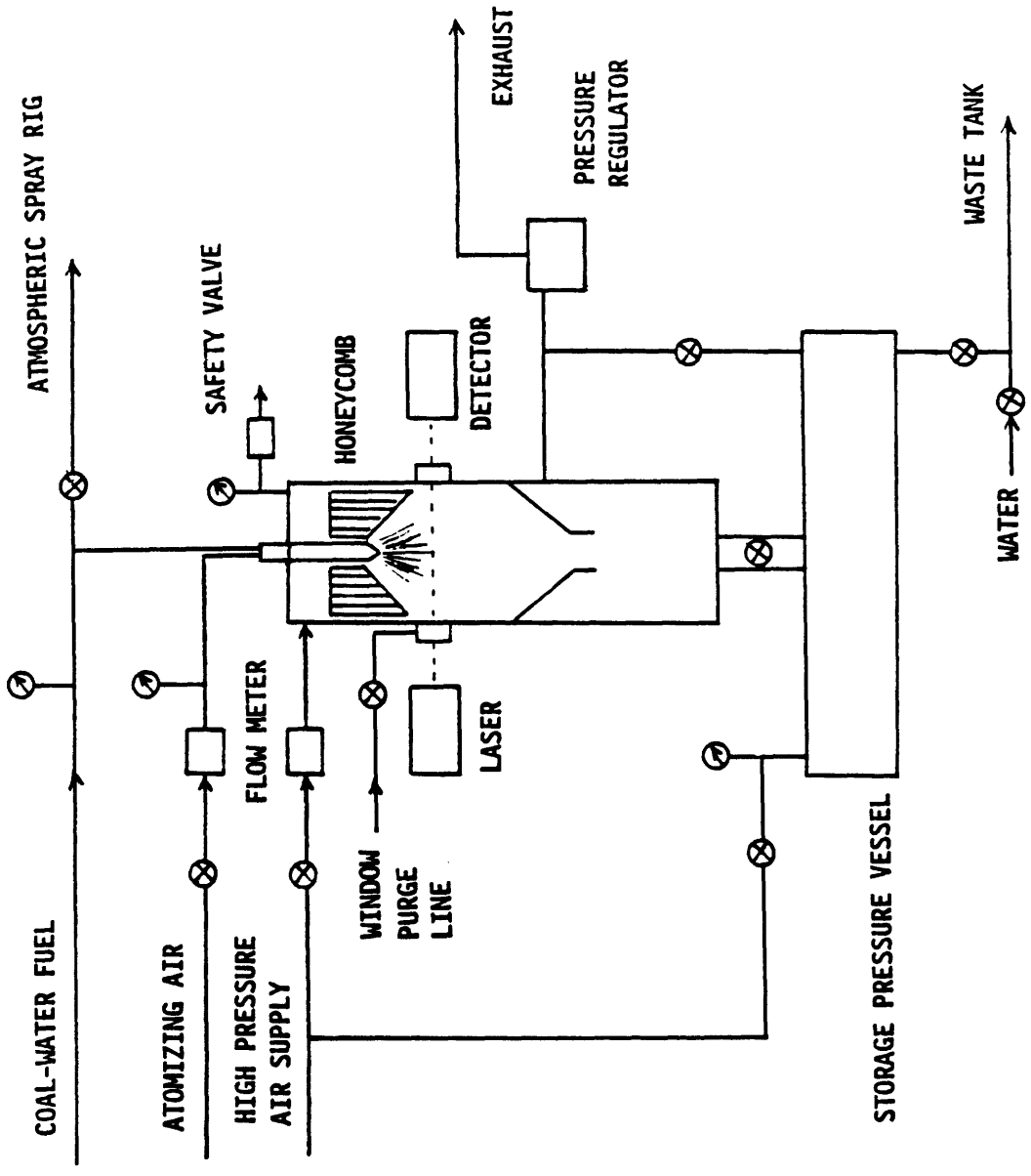

Figure 3-2. Schematic Diagram of High Pressure Spray Test Rig

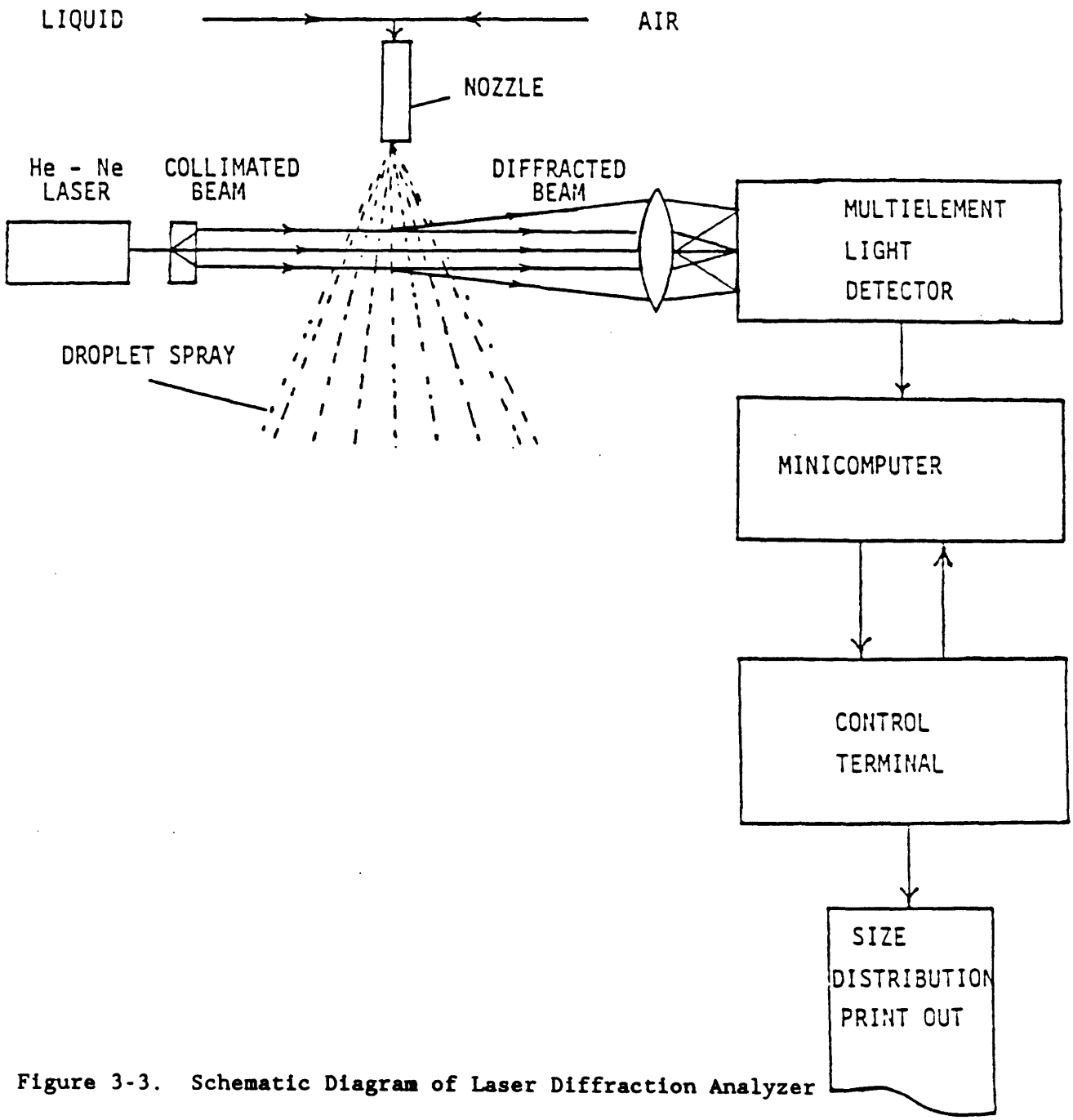

Figure 3-3. Schematic Diagram of Laser Diffraction Analyzer

(alternate bright and dark rings). This analyzer (Type 2600 HSD), manufactured by Malvern Instruments Inc., allows a laser light source to pass light through the two plexiglas plates perpendicular to the fuel spray flow. A 31-annular-element photodetector receives the laser light diffracted by the spray droplets from the other side of the chamber. A control terminal processes the signals from the photodetector and feeds them into a minicomputer. The computer is programmed to yield the particle size distribution, in various different functional forms, such as Normal, Log Normal, Rosin Rammler, or Model Independent.

In the experiments, a 300-mm focal length lens was used for the laser diffraction particle size measurements. This gave an observable size range between 5.8 and 564 μm. The laser light transmissivity of the spray was monitored, and measured average droplet sizes were corrected to account for multiple scattering effects in the measurement according to the empirical calibration technique developed by Dodge (8). The laser beam was aimed perpendicular to the spray centerline, at a distance of 10 in. from the nozzle tip. A laser beam guide tube (3/4 in. O.D.) was placed coaxially with the laser beam between the laser source and the center of the spray so as to reduce the path length of the laser beam crossing the spray, and hence the effects of multiple scattering. For chordal scans of the spray, the guide tube was moved along its radial direction perpendicular to the spray.

3.4 CAPILLARY TUBE VISCOMETER

A capillary tube viscometer developed at MIT (9) was used to measure viscosities of CWF at shear rates up to 10^5 sec^{-1}. The essential feature of the capillary tube viscometer is the measurement of a frictional pressure drop associated with the laminar flow of fluid at a given rate through a long, smooth, cylindrical tube of known dimensions. Under conditions of steady, fully developed flow through a capillary tube, the shear stress at the tube wall can be expressed as

$$\tau_w = \frac{D\Delta P}{4L} \tag{1}$$

where ΔP is the pressure drop associated with the laminar flow of fluid through a tube of diameter D and length L. The shear rate at the tube wall for a steady, laminar flow of time-independent fluid can be expressed as

$$\dot{\gamma}_w = \frac{3n+1}{4n}\,\frac{8V}{D} \tag{2}$$

where V is the average flow velocity in the tube, and

$$n = \frac{\Delta[\ell n\ (D\Delta P/4L)]}{\Delta[\ell n\ (8V/D)]} \tag{3}$$

By analogy with Newtonian fluids, an apparent viscosity is defined as

$$\mu_a = \tau_w/\dot{\gamma}_w \tag{4}$$

for the corresponding shear rate.

When the measurements made on the capillary tube viscometer are converted into a logarithmic plot of $D\Delta P/4L$ versus $8V/D$, n is evaluated as the slope of the curve at a particular value of τ_w. The corresponding wall shear rate and apparent viscosity are found from Eq. (2) and Eq. (4), respectively. Eq. (3) shows that it is also possible to write

$$\tau_w = \frac{D\Delta P}{4L} = K \left(\frac{8V}{D}\right)^n \tag{5}$$

where K is the intercept at an $8V/D$ of unity on the logarithmic plot of $D\Delta P/4L$ versus $8V/D$. Since Eq. (2) is based on the assumption of laminar flow in the tube, this condition can be confirmed by checking that the generalized Reynolds number is less than 2100:

$$Re_{gen} = \frac{D^n V^{2-n} \rho}{K\, 8^{n-1}} < 2100 \tag{6}$$

where ρ is the fluid density.

In practice, the pressure drop measured over the capillary tube can be expressed as

$$\Delta P_T = \Delta P + \Delta P_{excess} \tag{7}$$

where ΔP is the frictional pressure drop in fully developed flow and ΔP_{excess} is the excess frictional pressure drop because of entrance losses and additional friction effects. The excess frictional pressure drop should be constant when measurements of ΔP_T are made for two tubes of different lengths, L_1 and L_2, but with the same diameter and at the same flow rate (i.e., same average velocity). Therefore, the excess frictional pressure drop can be cancelled out from Eq. (7), if the pressure drops measured with tubes of different lengths but with the same diameter and at the same flow rate are subtracted, to yield

$$\Delta P_{21} = \Delta P_{T2} - \Delta P_{T1} = (\Delta P)_2 - (\Delta P)_1$$

The values of ΔP_{21} and $L_{21} = L_2 - L_1$ can then be used in place of ΔP and L, respectively, in Eqs. (1) through (5) to determine the apparent viscosity and shear rate.

A schematic diagram of the capillary tube viscometer is presented in Figure 3-4. A cylindrical pressure vessel, 2 ft long and 0.5 ft inside diameter, designed for a maximum working pressure of 2000 psia, is used to store CWF. When the cylindrical vessel is pressurized by compressed air, CWF in the vessel is forced to flow through a capillary tube to a Micro Motion flow meter. The applied pressure is measured by the pressure transducer and recorded together with the CWF mass flow rate on a minicomputer through an A/D converter. The capillary tubes used have an inside diameter of 1.5 mm and a length of 1.0 to 10.0 cm.

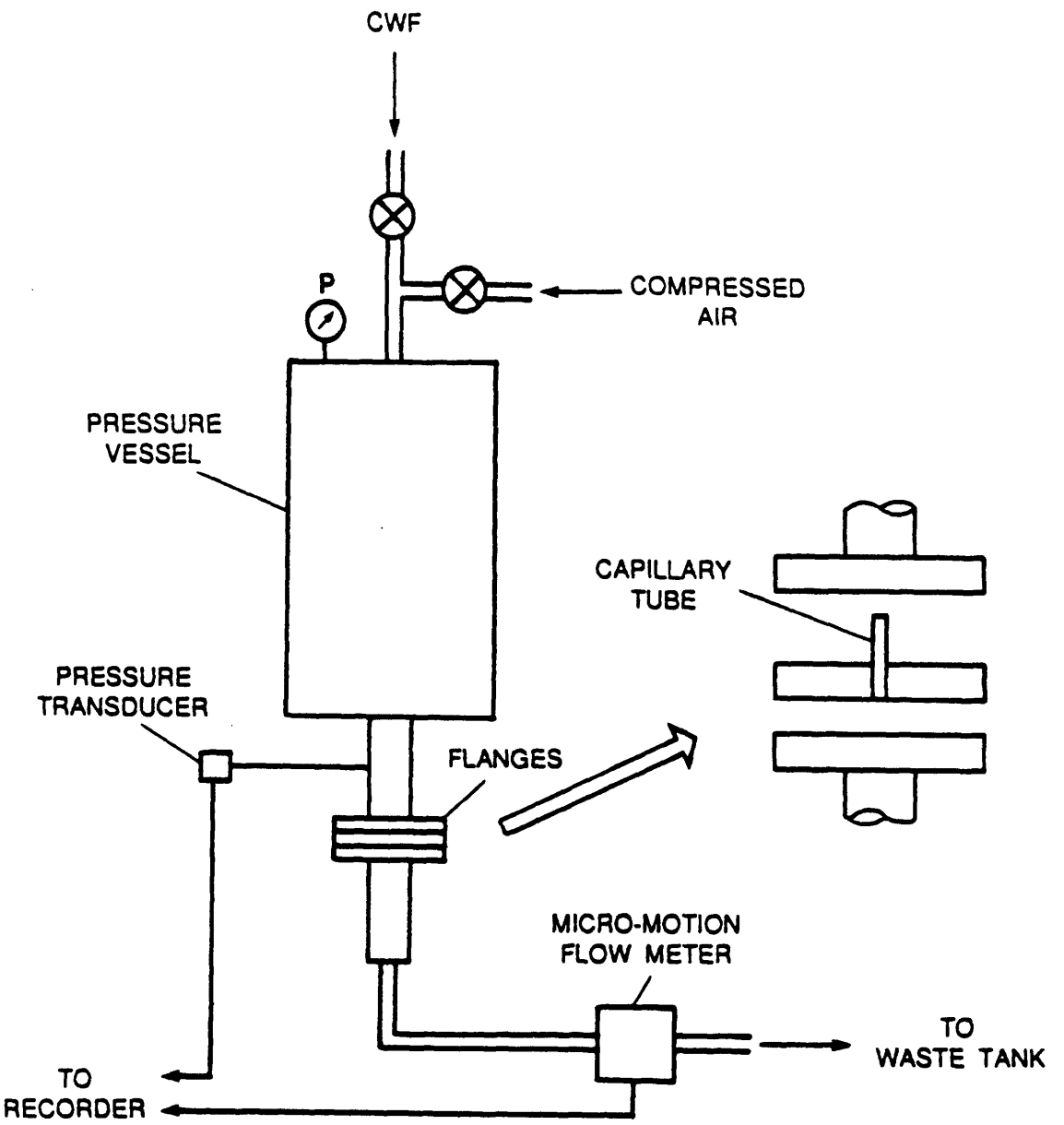

Figure 3-4. Schematic Diagram of Capillary Tube Viscometer

3.5 PHOTOGRAPHIC APPARATUS

The spray test facility and the high-pressure spray test rig were used to take photographs of water or CWF sprays at atmospheric and elevated pressures, respectively. For the atmospheric spray case the nozzle gun was placed on the top of the spray chamber perpendicular to the floor. The gun was adjusted vertically so as to locate the spray properly on the camera. Pictures were taken through a front window (15 in. x 17 in.) of the chamber. For the pressurized spray case the nozzle gun moved further inside the high-pressure chamber so that the nozzle tip could be viewed from outside through the large window (5 in. diameter) of the high-pressure spray test rig.

Two types of instant films were used. One was Polaroid 55 with a film speed of ISO 50; the other was Polaroid 57 with a film speed of ISO 3000. The Polaroid 55 was used for water sprays, while the Polaroid 57 was used for CWF sprays.

A 4 in. x 5 in. view camera with a 200-mm lens and extension bellows and a flashlight were used for photographing sprays.

3.6 ATOMIZER

A schematic diagram of the atomizer used for most of the spray tests is shown in Figure 3-5a. This twin-fluid atomizer (developed by Occidental Research Corp. and KVB, Inc.) is of the internal-mixing type and has a single-exit orifice. In combustion experiments carried out in the MIT Combustion Research Facility, this atomizer was found to be capable of producing fine CWF sprays and stable flames (5,6).

A nozzle (Figure 3-5b) developed and provided by the General Electric Co. was also used to study the effects of nozzle type on the effectiveness of fuel treatments. The GE nozzle is a twin-fluid air-blast-type atomizer.

4. PRIMARY ATOMIZATION AT ATMOSPHERIC PRESSURE

4.1 BACKGROUND

Upon atomization of coal-water fuel (CWF) into a combustor, CWF droplets undergo rapid evaporation and heating, followed by ignition. During these stages coal particles tend to agglomerate within CWF droplets. The resulting coal particle size distribution is then determined more by the size distribution of the atomized CWF spray than by the initial size distribution of the coal particles. Therefore, the atomization quality (i.e., fineness of CWF spray droplets) is considered to be a most important factor in determining the carbon conversion efficiency of CWF and the resultant fly-ash particle size distribution. The fineness of the atomized spray, in turn, is a sensitive function of the effective CWF viscosity.

In non-Newtonian fluids such as CWF, the effective viscosity is shear-rate dependent, and this dependence can take two distinct forms: shear thinning (pseudoplastic) and shear thickening (dilatant). The behavior of some CWFs is complicated by their changing from one type of behavior to the other as the shear rate is varied. Hence, it is important to determine

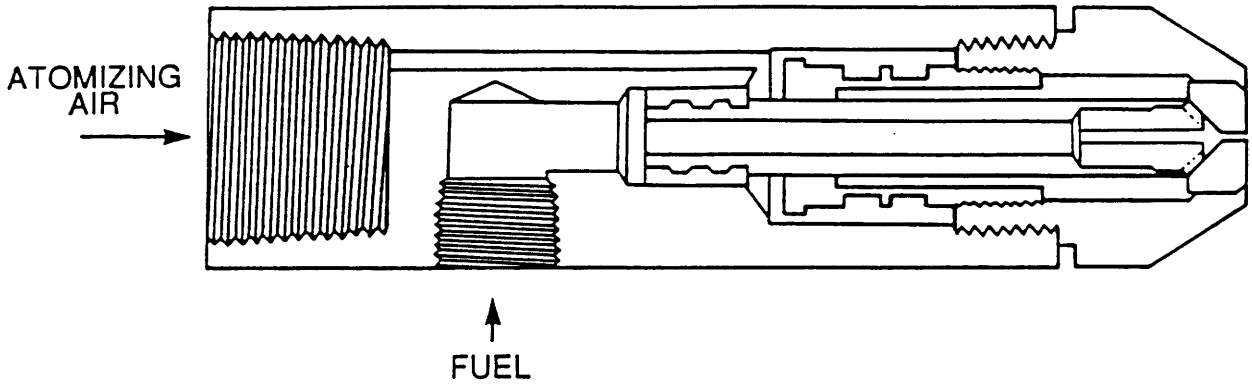

Figure 3-5. (a) Schematic Diagram of OR-KVB Nozzle, Nozzle exit diameter 3.175 or 2.79 mm

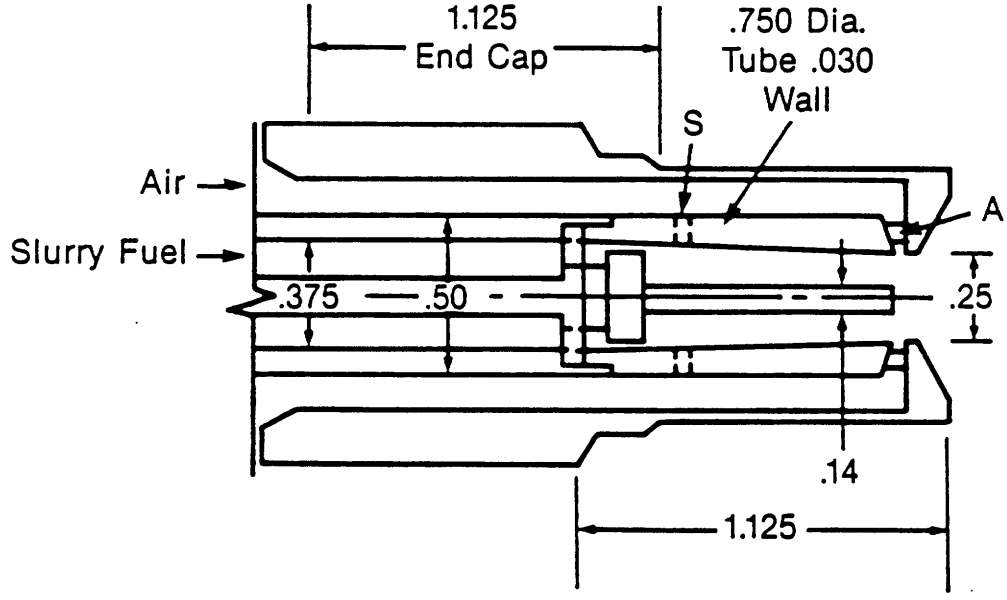

Figure 3-5. (b) Schematic of GE Nozzle Geometry, Dimensions in inches, Center passage (0.14 in. dia.) for auxiliary fuel, Holes at 'S' pre-mix air with slurry, Vanes at 'A' provide swirl

effective viscosities at high shear rates commensurate with those that arise in twin-fluid atomizers.

In the majority of experimental studies reported in the technical literature on CWF atomization, no attempt has been made to correlate measured droplet size distributions with rheological properties of CWF. Where such an effort was made, low shear rate values of the viscosity were used. Daley et al. (2) reported experimental data showing acceptable correlation between spray droplet size and viscosity at low shear rates (less than 500 sec^{-1}). Spray droplet size and viscosity at shear rates up to 10^4 sec^{-1} were measured by Tsai and Knell(10); they reported significant changes in effective viscosity as they varied the shear rate from low to high values, and found a better correlation between atomization quality and fuel viscosity when high shear viscosity data were used. The apparent contradiction between the conclusions drawn by investigators of these two studies (2,10) stems from the limited range of fuel types tested. The shear thinning (pseudoplastic) behavior at increased shear rates can be predicted with reasonable approximation from low shear rate viscosity data. However, it can be expected that as the shear rate is increased to high values, a limit is reached beyond which the fluid becomes dilatant (11). Hence, it is considered that predictions of rheological behavior of CWF during atomization can be made only if the representative shear rate during atomization is assessed, and the effective viscosity is experimentally determined at these representative shear rates.

4.2 EXPERIMENTAL DATA FROM PREVIOUS STUDIES

Under the aegis of the MIT Electric Utility Program, a large body of experimental data of spray drop size and high shear viscosity of CWFs has become available (12,13). Solids loadings, coal particle size distributions, and chemical additives of CWFs were found to have little influence on a fuel's surface tension but strong influence on its non-Newtonian viscosity. Some of the experimental data obtained in this separately funded study were used for the development of a relationship between the fineness of atomization and rheological properties of the fuel and parameters of the atomization process.

Six CWFs provided by several commercial vendors were tested for measurements of spray droplet size, high shear viscosity, and surface tension. In the designation of CWF type; the letters A, B, C, and D refer to coal type, Reg, Fine, and U-Fine refer to the fineness of the coal in the CWF (i.e., regular-grind, fine-grind, ultrafine-grind); and the numbers 70, 69, 66, etc. to the weight percentage of solids loading.

The surface tensions of these CWFs were measured by a Rosano Surface Tensiometer (Model LG-709827). The surface tension of a CWF was found to vary little with coal particle size distribution, coal type, and chemical additive (14).

CWF viscosity data (12,13), measured by the capillary tube viscometer, are plotted in Figures 4-1b through 4-4b as a function of shear rate in the range of 10^3 to 10^5 sec^{-1}. The results show that CWF viscosity is highly dependent on shear rate (non-Newtonian characteristics of CWF viscosity). Viscosity is also strongly dependent upon solids loading (dilution) and coal

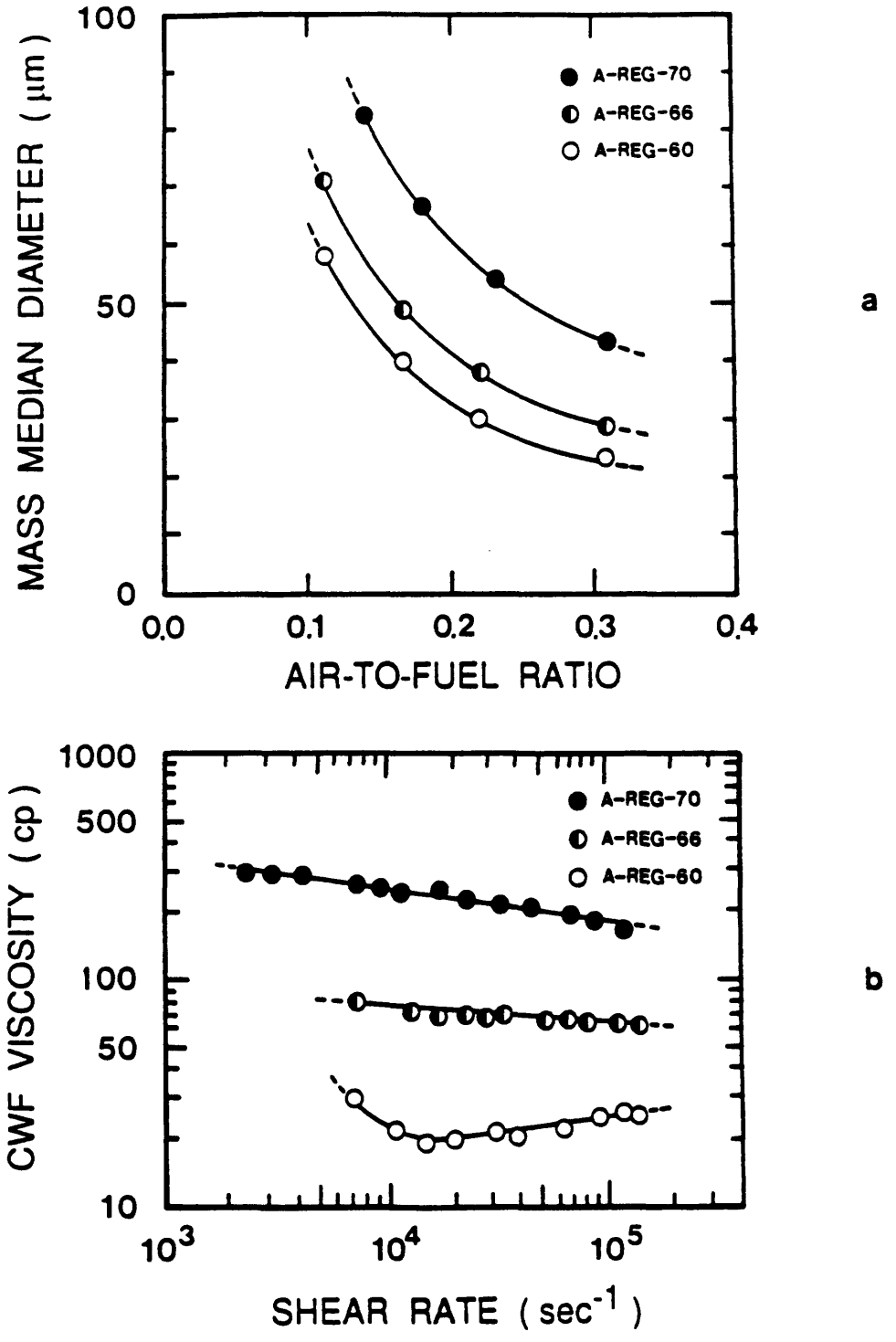

Figure 4-1. Effect of Dilution on MMD and Viscosity of CWF (A-Reg) (a) MMD versus AFR, (b) CWF Viscosity versus Shear Rate

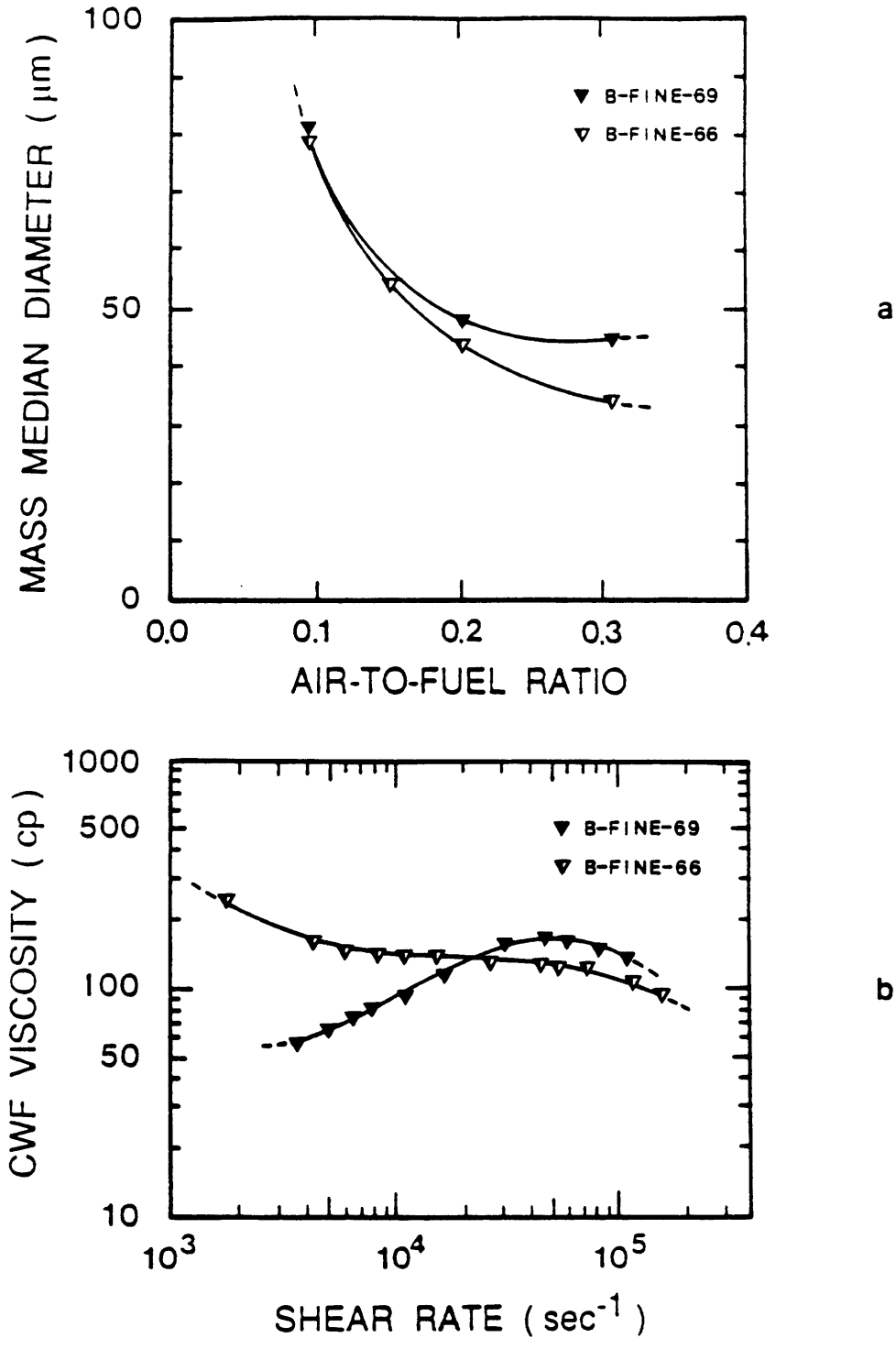

Figure 4-2. Effect of Dilution on MMD and Viscosity of CWF (B-Fine) (a) MMD versus AFR, (b) CWF Viscosity versus Shear Rate

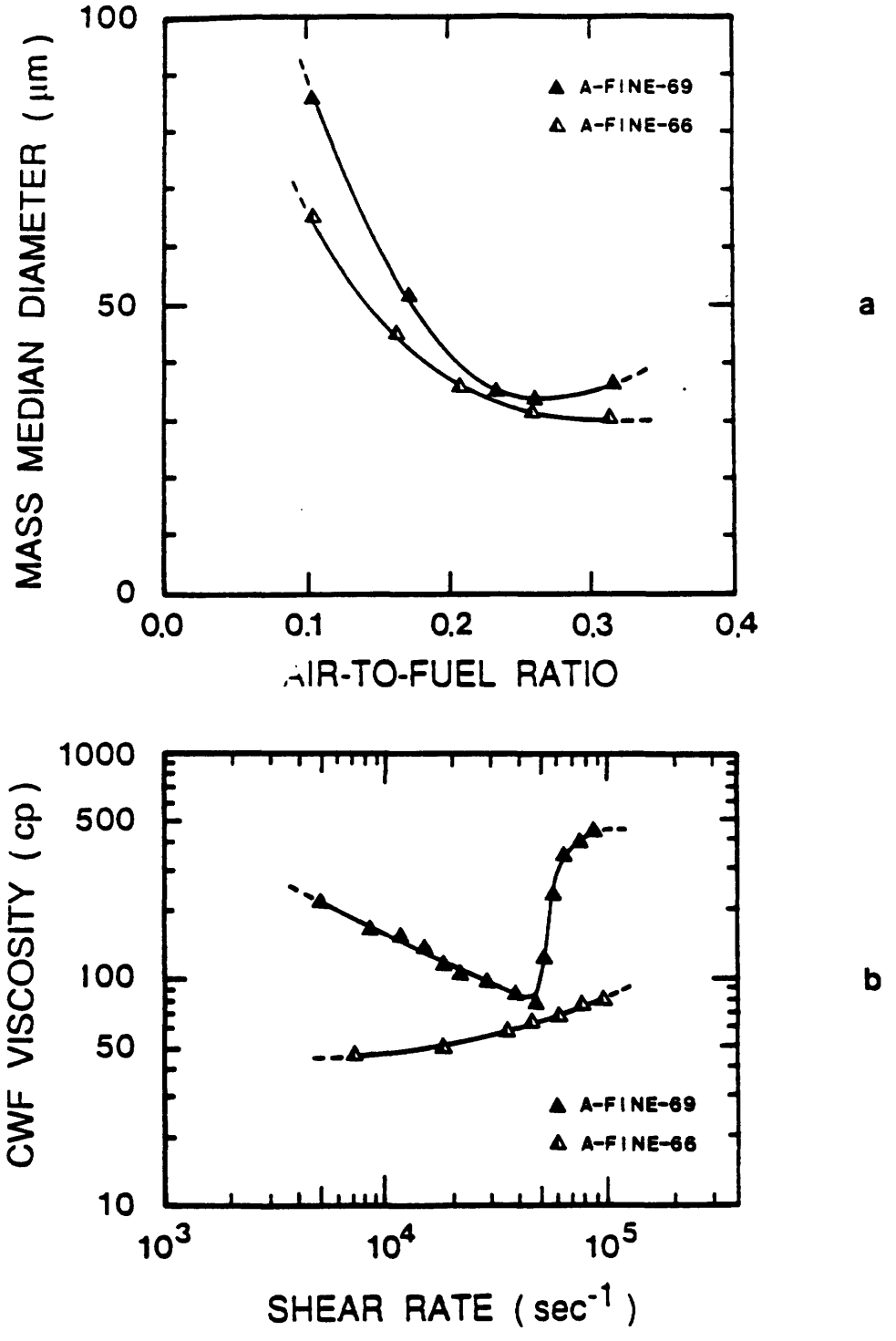

Figure 4-3. Effect of Dilution on MMD and Viscosity of CWF (A-Fine) (a) MMD versus AFR, (b) CWF Viscosity versus Shear Rate

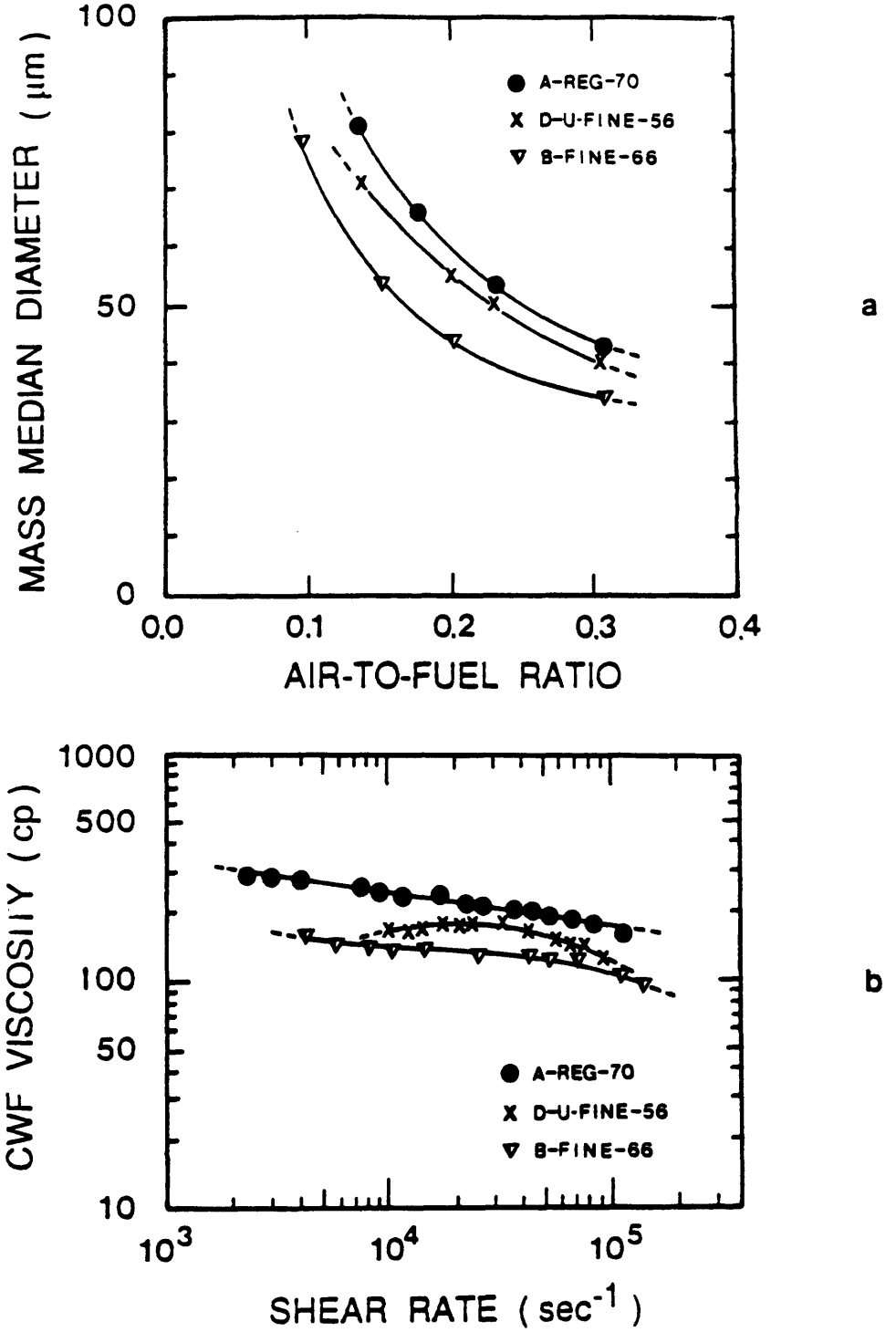

Figure 4-4. Effect of Coal Particle Size Distribution on MMD and Viscosity of CWFs (A-Reg, B-Fine, & D-U-Fine) (a) MMD versus AFR, (b) CWF Viscosity versus Shear Rate

particle size distribution. Dilution of CWF with water, in general, reduces the viscosity (Figure 4-1b), but some CWFs show reverse trends at certain shear rates (Figure 4-2b). One of the CWFs, A-Fine-69, is shear thinning at low shear rates, but as the shear rate increases above 5 x 10^4 sec^{-1}, it suddenly becomes shear thickening (Figure 4-3b).

The mass mean diameters (MMDs) of CWF sprays, measured by using the laser diffraction spray analyzer, are shown in Figures 4-1a through 4-4a plotted as a function of the air-to-fuel ratio (AFR). Since the fuel flow rate is kept constant at 2.7 kg/min during the experiments, the shear rate increases as the atomizing air flow rate increases. In general, as shown in Figures 4-1a through 4-4a, MMDs monotonically decrease with increasing AFR.

The spray droplet size, however, does not always decrease with increasing AFR (see B-Fine-69 in Figure 4-2a). The leveling off of the reduction in MMD in the AFR range of 0.2 to 0.3 is consistent with the increasing viscosity of the CWF in the corresponding shear rate range of 3 x 10^4 to 5 x 10^4 sec^{-1}. In Figure 4-3a, MMDs of the A-Fine-69 are found to decrease with increasing AFR up to AFR = 0.25, but beyond this value the droplet size increases because of the increasing viscosity of the fuel with increasing shear rate.

Figure 4-1a shows the effect of CWF dilution with water on the MMD of the CWF spray. The MMDs decrease with increasing dilution (decreasing solids loading) due to the corresponding reduction in CWF viscosity, as shown in Figure 4-1b.

The effect of coal particle size distribution on MMD and CWF viscosity is shown in Figure 4-4. In the shear rate range of 10^4 to 10^5 sec^{-1}, the viscosity of A-Reg-70 CWF is the highest and that of B-Fine-66 is the lowest. However, in the case of the ultrafine fuel sample, the solids loading (D-U-Fine-56) is such that the effective viscosity values lie between those plotted for the other two fuels. Relative rankings of droplet size data for the three fuels are in accord with the effective viscosity values shown in Figure 4-4.

The viscosity at low shear rate was measured by a commercial viscometer (HAAKE RV-12) to check the consistency of viscosities at the middle range of shear rate (10^3 to 10^4 sec^{-1}). The data are presented in Figures 4-5 and 4-6. These results show that the viscosities measured by the capillary tube viscometer and the commercial viscometer (HAAKE RV-12) agree reasonably well in the shear rate range of 10^3 to 10^4 sec^{-1}.

The significance of the use of high shear rate viscosities is highlighted by the data in Figures 4-3, 4-4 and 4-6. As the AFR is increased, the droplet size of A-Fine-69 CWF reaches a minimum (Figure 4-3a). At the corresponding value of the shear rate, a sudden increase in the viscosity can be observed, as discussed above (Figure 4-3b). In the case of the three fuels shown in Figures 4-4 and 4-6, it has already been pointed out that rankings of droplet sizes are in accord with rankings of high shear rate (in the range of 2 x 10^4 to 6 x 10^4 sec^{-1}) viscosity data. Reliance on low shear rate (less than 10^4 sec^{-1}) viscosities shown in Figure 4-6, however, would lead one to expect the wrong order in the fineness of atomized droplet sizes of the three CWFs tested.

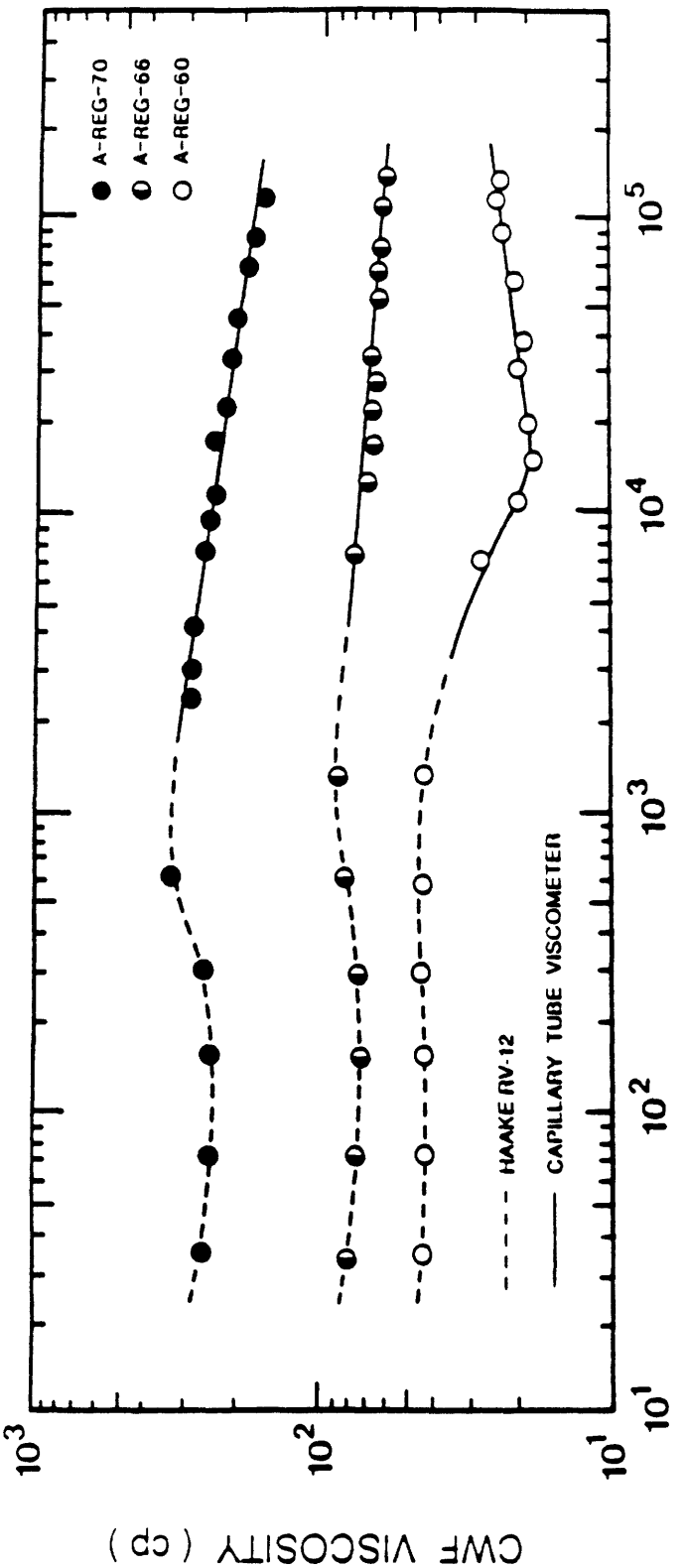

Figure 4-5. Effect of Dilution on CWF Viscosity at Low and High Shear Rates

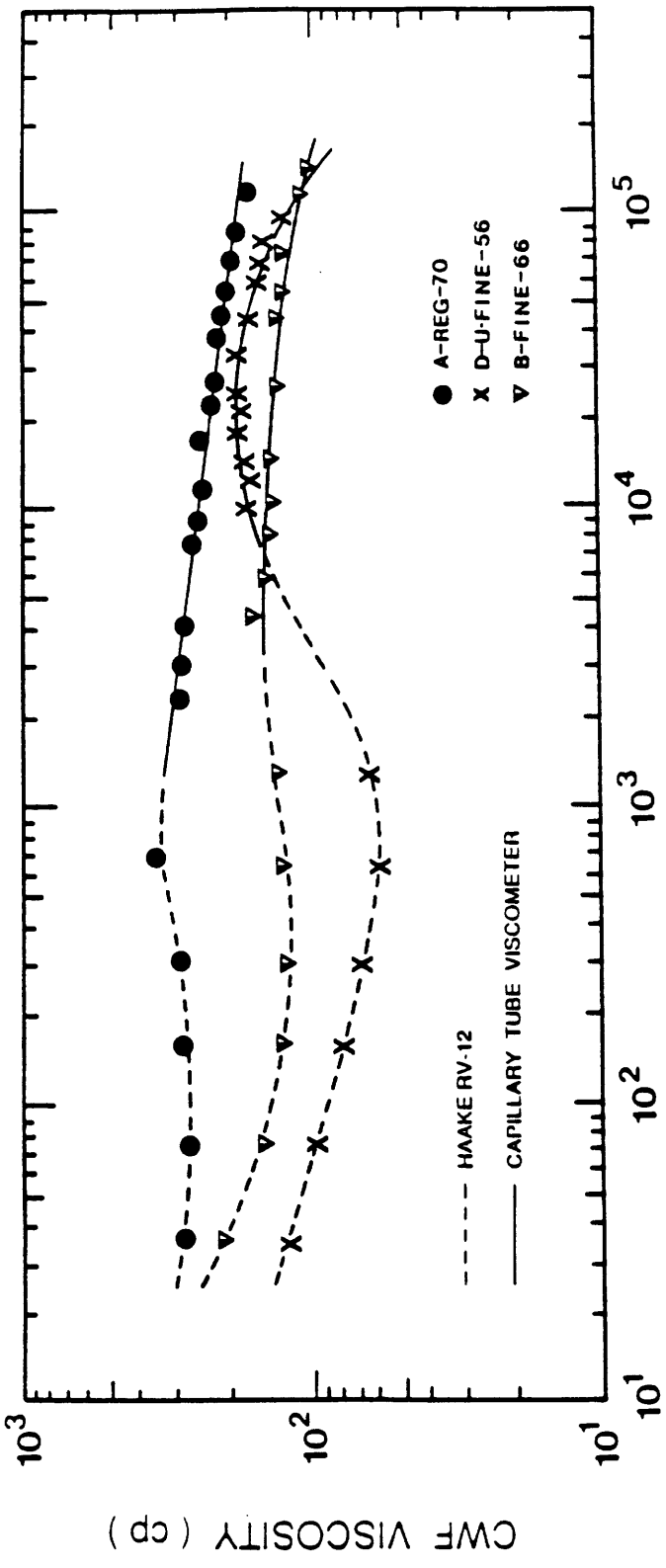

Figure 4-6. Effect of Size Distribution of Coal Particles on CWF Viscosity at Low and High Shear Rates

4.3 DEVELOPMENT OF A SEMI-EMPIRICAL CORRELATION OF TWIN-FLUID ATOMIZATION

4.3.1 Representative Shear Rate During CWF Atomization

Since CWF shows non-Newtonian fluid behavior, the shear rate needs to be known for determining the viscosity of CWF during atomization. The actual shear rate during atomization is varied with the position of the CWF jet within the atomizer due to the changes of liquid thickness and relative velocity between atomizing air and CWF (see Fig. 4-7). However, an accurate calculation of the continuously varying shear rate at the atomizing air/fuel interface is not possible because of the inadequate quantitative understanding of the physical process of twin-fluid atomization. An approximate shear rate, which is expressed as a function of air velocity, liquid velocity, and characteristic dimension of the liquid jet in the mixing chamber, is derived below.

The mass conservation and momentum equations for the liquid jet in the mixing chamber of the atomizer (Figure 4-7) can be given as

Mass Conservation Equation

$$\rho_L U_{L1} A_1 = \rho_L U_{L2} A_2 \tag{8}$$

Momentum Equation

$$\frac{d}{dt}\int_{cv} \rho \vec{v}\, dV + \int_{cs} \rho \vec{v}\,(\vec{v} - \vec{v}_{cs}).\,\vec{n}\, dA = \vec{F}_{cv}(t) \tag{9}$$

or, equivalently,

$$\rho_L U_{L2}^2 A_2 - \rho_L U_{L1}^2 A_1 = \Delta P A + \tau A_{side} \tag{10}$$

where ρ_L = density of liquid
U_{L1} = liquid velocity at position 1
U_{L2} = liquid velocity at position 2
A_1 = cross-sectional area of liquid jet at position 1
A_2 = cross-sectional area of liquid jet at position 2
A_{side} = side area of liquid jet between positions 1 and 2
τ = shear stress at the air/liquid interface
ΔP = pressure drop between positions 1 and 2, and assumed to be negligible

From eqs. (8) and (10), the area of the contracted liquid jet (A_2) can be calculated.

The characteristic dimension for the representative shear rate is expressed as the average value of the contracted liquid jet radius and fuel port radius. The representative shear rate, $\partial u/\partial y$, is expressed as

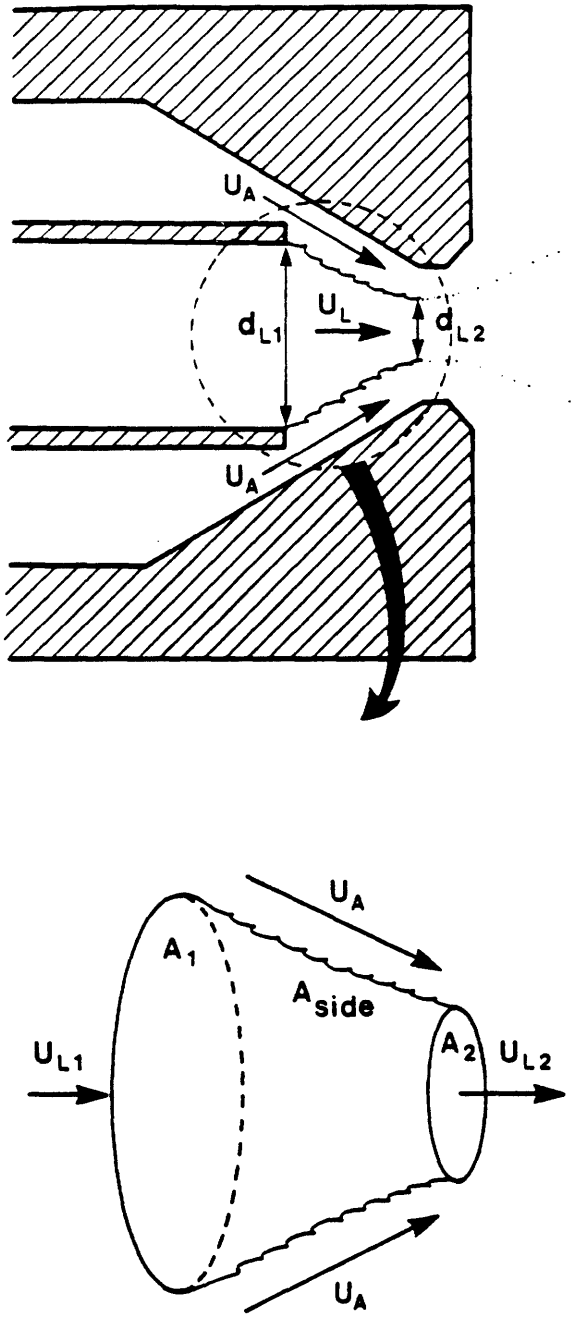

Figure 4-7. Control Volume of Contracted Liquid Jet in Mixing Chamber of Twin-Fluid Atomizer

$$\frac{\partial u}{\partial y} = \frac{U_A - U_L}{\frac{\left(\frac{d_{L1}}{2} + \frac{d_{L2}}{2}\right)}{2}} = \frac{4U_R}{d_{L1} + d_{L2}} \qquad (11)$$

where U_A = velocity of atomizing air in mixing chamber
U_L = velocity of liquid jet in mixing chamber ($\approx U_{L1} \approx U_{L2}$)
U_R = relative velocity between liquid jet and atomizing air
d_{L1} = diameter of fuel port
d_{L2} = diameter of contracted liquid jet at position 2

Representative shear rates for the OR-KVB atomizer (Figure 3-5), used in the present atomization study, for the air-to-fuel mass flow rate ratios of 0.1, 0.2, and 0.3 were calculated as 2.0×10^4 to 4.0×10^4 sec^{-1}, 3.0×10^4 to 4.7×10^4 sec^{-1}, and 4.0×10^4 to 6.0×10^4 sec^{-1}, respectively.

4.3.2 Basic Form of Correlation

Miesse (15) proposed that the atomization phenomena of liquid streams could be described by two independent dimensionless groups: the Reynolds number (Re) and the Weber number (We).

In the case of liquid-jet disintegration due to the influence of the surrounding air, the droplet sizes are governed by the ratio of the disruptive aerodynamic force $\rho_A U_R^2$ to the consolidating surface tension force σ_L/D_o. This dimensionless ratio is known as the Weber number, We, and is expressed as

$$We = \frac{\rho_A U_R^2 D_o}{\sigma_L}$$

where ρ_A = density of surrounding air
U_R = relative velocity between liquid jet and surrounding air
D_o = diameter of liquid jet
σ_L = surface tension of liquid

In the case of liquid jet breakup occurring without the influence of the surrounding air, dimensional analysis suggests that the atomization quality is dependent on the jet diameter D_o and the liquid properties: density ρ_L, surface tension σ_L, and viscosity μ_L. The breakup mechanism is found to depend on the Z number, which is obtained as the ratio of the square root of the Weber number to the Reynolds number; that is,

$$Z = \frac{We^{0.5}}{Re} = \frac{\mu_L}{\sqrt{\sigma_L \rho_L D_o}}$$

According to Lefebvre (16,17), the main factors governing the average droplet size of liquids of low viscosity are liquid surface tension, air density, and air velocity; for liquids of high viscosity, the effects of air properties are less significant, and the average droplet size becomes more dependent on the liquid properties, especially viscosity.

In the present study, the Weber number We and the Z number are used in a correlation expressed as follows:

$$\frac{MMD}{D_o} = a\,(We)^b \left(1 + \frac{1}{AFR}\right)^c + d \left(\frac{We}{Re^2}\right)^e \left(1 + \frac{1}{AFR}\right)^f \qquad (12)$$

where MMD = mass mean diameter of atomized CWF droplets
D_o = characteristic dimension of the atomizer, defined as the diameter of fuel port
AFR = air-to-fuel mass flow rate ratio
a,b,c,d,e,f = empirical constants, determined by experimental data

The two terms on the right-hand side of Eq. (12) correspond to two different mechanisms for liquid jet breakup: jet disintegration due to the influence of the surrounding air, and jet breakup occurring without the influence of the surrounding air. That is, the first term represents the competition between jet-consolidating surface tension force and aerodynamic shearing force, which leads to jet destruction; the second term accounts for the competition between viscous restoring force and surface tension force, which leads to jet breakup in the absence of surrounding air effects.

The basic form of the correlation [Eq. (12)] can also be expressed as

$$\frac{MMD}{D_o} = a \left(\frac{\sigma_L}{\rho_A U_R^2 D_o}\right)^{-b} \left(1 + \frac{1}{AFR}\right)^c + d \left(\frac{\mu_L^2}{\rho_L \sigma_L D_o}\right)^e \left(1 + \frac{1}{AFR}\right)^f \qquad (13)$$

During the atomization tests, the surface tension σ_L and density ρ_L of the liquid varied little among the CWFs tested, and the fuel port diameter D_o was maintained at 3.8 mm.

4.3.3 Correlation for the OR-KVB Atomizer

The MMDs of the atomized droplets for six CWFs are plotted as a function of high shear viscosity for AFRs of 0.1, 0.2, and 0.3 in Figure 4-8. Linear relationships are apparent between MMD and CWF viscosity for given values of AFR. These relationships imply that the empirical constant e in Eq. (13) has the value of 0.5, which makes the exponent of the viscosity, μ_L, unity.

The CWF atomization data were substituted into Eq. (13) to determine the empirical constants a through f. Finally, the dimensionally correct equation for MMD/D_o is expressed as

$$\frac{MMD}{D_o} = 0.0263 \left(\frac{\sigma_L}{\rho_A U_R^2 D_o}\right)^{0.25} \left(1 + \frac{1}{AFR}\right)^{0.5}$$

$$+ 0.0050 \left(\frac{\mu_L^2}{\rho_L \sigma_L D_o}\right)^{0.5} \left(1 + \frac{1}{AFR}\right)^{0.75} \qquad (14)$$

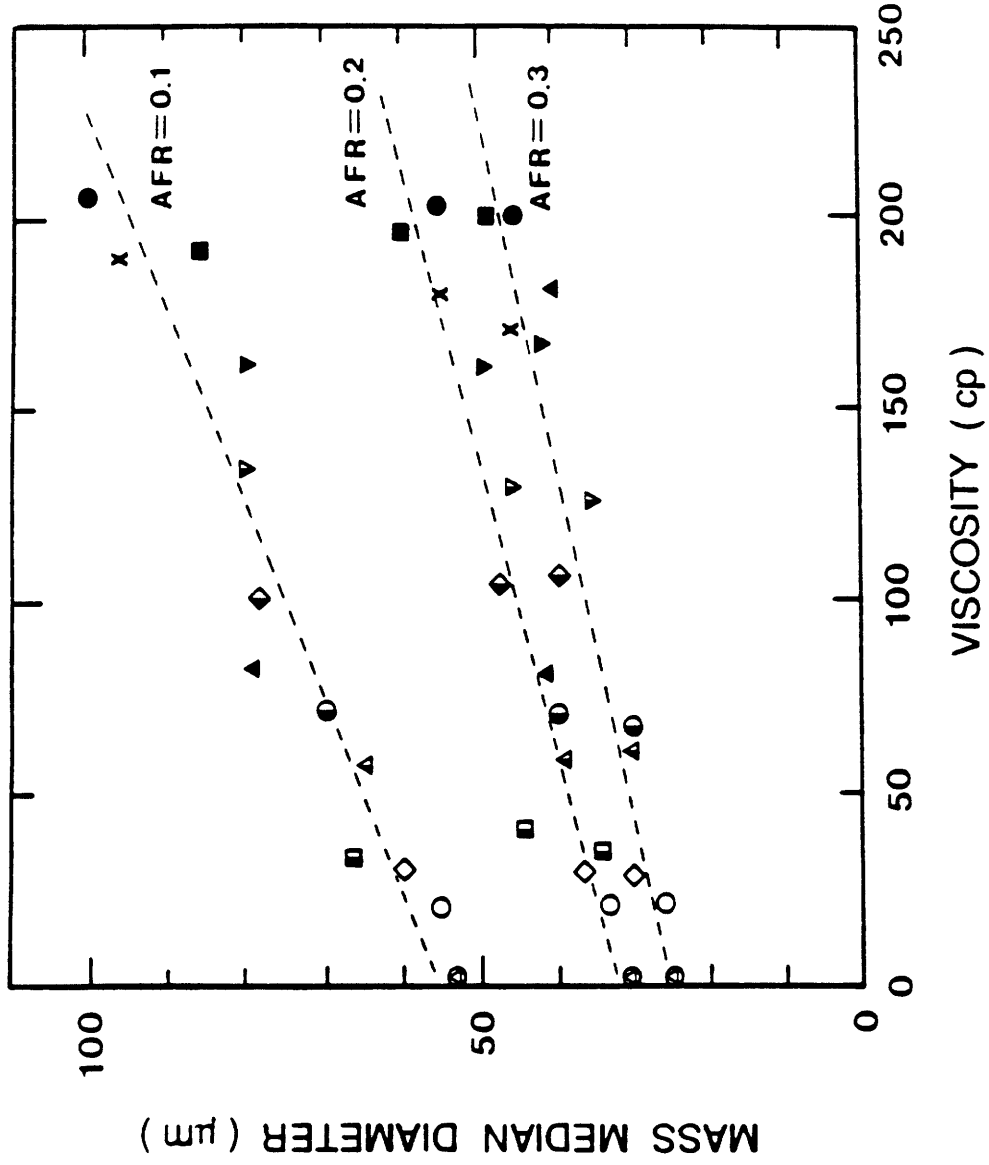

Figure 4-8. Variation of Mass Median Diameters of Spray Droplets as a Function of High Shear CWF Viscosity at AFRs = 0.1, 0.2 & 0

In Eq. (14) the units of the physical variables are as follows:

MMD: m
D_o: m
σ_L: kg/sec^2
ρ_A: kg/m^3
ρ_L: kg/m^3
U_R: m/sec
μ_L: kg/m.sec

The viscosity term in Eq. (14) is replaced by the power law expression to account for the non-Newtonian rheology of CWF as

$$\mu = K \dot{\gamma}^{n-1} \tag{15}$$

where K = consistency index
n = flow behavior index
$\dot{\gamma}$ = shear rate

From Eqs. (14) and (15), the CWF atomization correlation for the OR-KVB atomizer is established as

$$\frac{MMD}{D_o} = 0.0263 \left(\frac{\sigma_L}{\rho_A U_R^2 D_o}\right)^{0.25} \left(1 + \frac{1}{AFR}\right)^{0.5}$$

$$+ 0.0050 \left(\frac{(K\dot{\gamma}^{n-1})^2}{\rho_L \sigma_L D_o}\right)^{0.5} \left(1 + \frac{1}{AFR}\right)^{0.75} \tag{16}$$

The comparison of the measured MMDs with the calculated MMDs, using Eq. (16), is illustrated in Figure 4-9. The correlation [Eq. (16)] of CWF atomization for the OR-KVB atomizer is found to closely agree with experimental results if the high shear viscosity (i.e., viscosity obtained at the representative shear rate of the present study) of the CWF was substituted into Eq. (16). The comparisons of measured MMDs with those calculated by assuming viscosities at low shear rates (100 sec^{-1}) are also shown in Figure 4-9. The comparison illustrates the sensitivity of the atomization correlation to the use of the correct value of the CWF viscosity (i.e., CWF viscosity at a high shear rate).

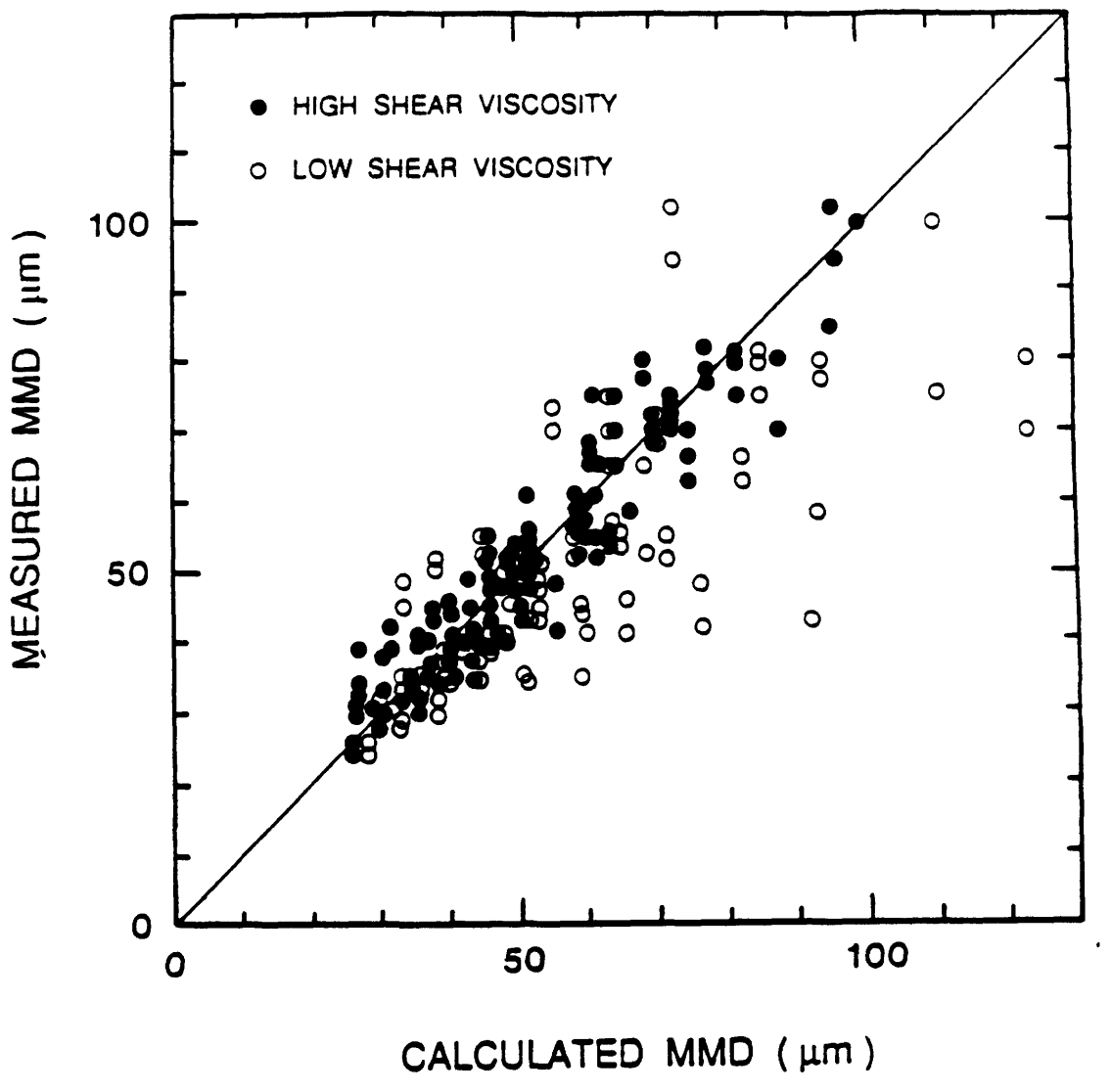

Figure 4-9. Comparisons of Measured MMDs with Calculated MMDs for Low Shear Viscosities and for High Shear Viscosities

5. SECONDARY ATOMIZATION AT ATMOSPHERIC PRESSURE

Since the fuel treatments affect only the water fraction of the CWF, water spray tests were made to determine the maximum effects of secondary atomization. CWF sprays with various solids loading were also tested.

5.1 WATER SPRAY TESTS

5.1.1 Droplet Size Measurement

5.1.1.1 Thermal Atomization

Water spray tests at atmospheric pressure have been performed in the spray test facility (Section 3.1) for the three fuel treatments proposed. The OR-KVB nozzle (air-assist nozzle) and the GE nozzle (air-blast nozzle) were used (see Section 3.6). Droplet size measurements were made by means of the laser diffraction size analyzer. The laser beam was aimed perpendicular to the spray axis and 10 in. away from the nozzle tip.

Figure 5-1b shows effects of water temperature on average spray droplet size (mass median diameter) for the OR-KVB and GE atomizing nozzles. With increasing water temperature, MMDs were observed to decrease. The reduction in MMDs up to a water temperature of 100°C is due to the corresponding reduction of the water viscosity, which is shown in of Figure 5-1a. As the water temperature is raised above 100°C, the viscosity continues to decrease but at a much lower rate. However, the rate of change of droplet size (slope of curve A in Figure 5.1b) is significantly increased at temperatures above 100°C. It is concluded, therefore, that the main cause of the droplet size reduction observed at temperatures above 100°C is disruptive flash-vaporization.

Temperature increase to produce flash-atomization was found to be less effective in reducing droplet sizes for the GE nozzle. The difference between the behavior of the two atomizers is due partly to the much higher atomizing air flow rate which is required by the GE nozzle for proper atomization and which, in turn, produces finer atomization by mechanical means. Also, the GE atomizer is operated at a smaller pressure drop (30 psig instead of 155 psig for the OR-KVB), which corresponds to a smaller enthalpy of the superheat available for flash-vaporization upon pressure drop across the atomizing nozzle.

Radial droplet size distributions were also measured by moving the laser guide-tube radially from the spray center to the spray edge. The radial variation of MMD was calculated from the light intensity variation across the width of the spray. Figure 5-2 shows radial droplet size distributions of water sprays obtained with the OR-KVB and GE nozzles for different temperatures; the droplet sizes are finer toward the spray center. This is because the entrained air takes fine droplets to the center, leaving the coarser ones on the edge of the spray (17). With increasing water temperature, MMDs were found to decrease in all radial locations.

5.1.1.2 CO_2 Absorption

Secondary atomization can be achieved not only by heating but also by the absorption of CO_2 in the liquid (see Appendix B). The CO_2 so absorbed nucleates and forms bubbles as the pressure is reduced during the passage of the liquid through the atomizing nozzle. Within the scope of the present project, experiments were carried out to test the effectiveness of CO_2-assisted secondary atomization of water and CWF. The MMD of water sprays plotted as a function of the mass concentration of CO_2 in water is

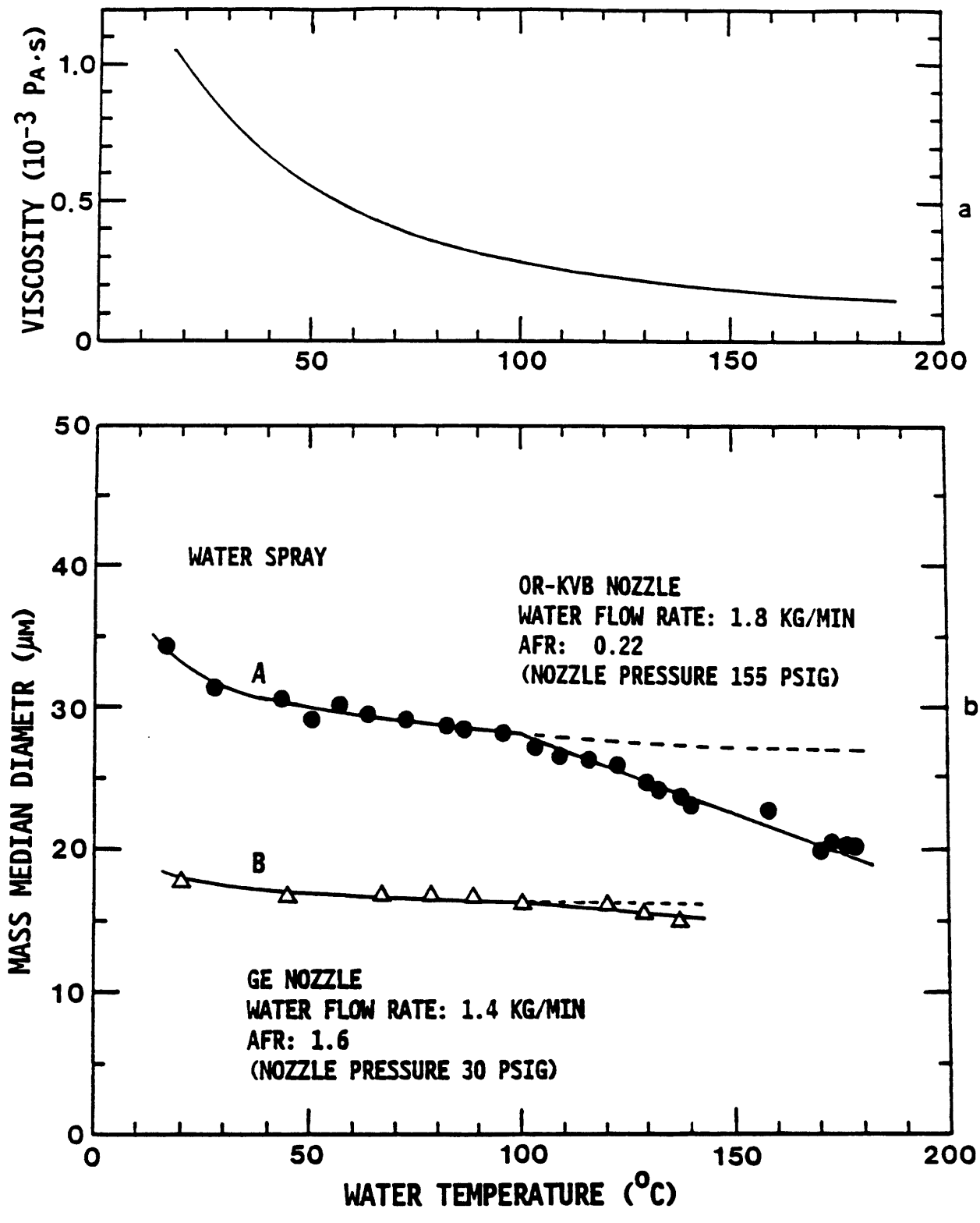

Figure 5-1. Top: Water Viscosity
Bottom: Effect of Water Temperature on Mass Median Diameter of Water Spray at Atmospheric Pressure

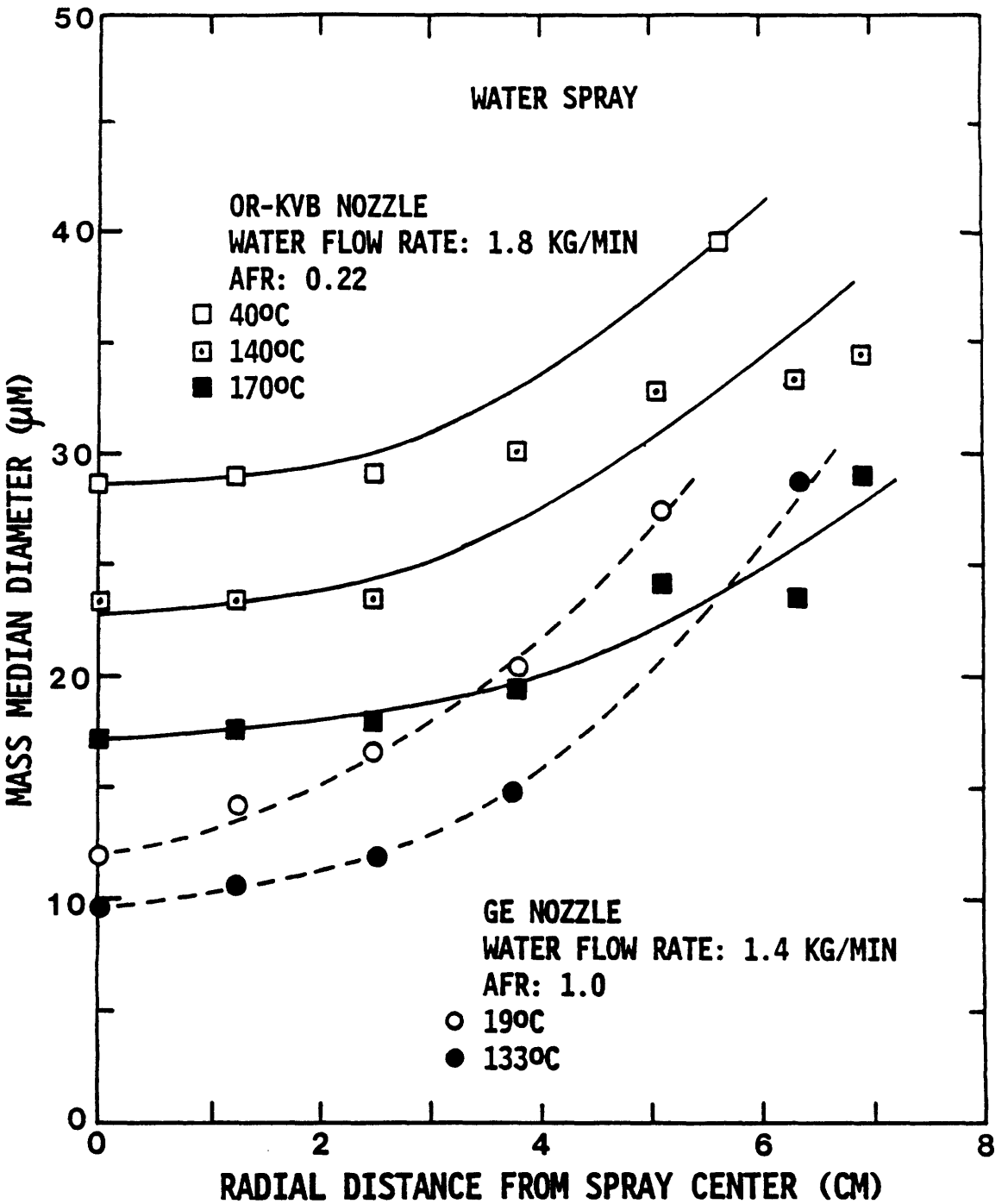

Figure 5-2. Radial Distributions of Mass Median Diameter of Water Sprays for OR-KVB and GE Nozzles at Atmospheric Pressure

shown in Figure 5-3. There was no observable effect of CO_2 absorption upon MMD of water sprays. When the CO_2 mass concentration reached about 0.8%, a low-frequency fluctuation of the spray was observed; this persisted when further increase in CO_2 concentration was made. No attempt was made to inhibit the fluctuations, since the onset occurs at a CO_2 mass-loading which is close to saturation level at the pump pressure (See Appendix B).

It was expected that at room temperature the evolution of CO_2 would have only a minor effect due to the relatively small volume change in the droplet upon the formation of CO_2 bubbles compared to that due to flash-atomization (see Appendix A). It should be noted, however, that despite this small change in the droplet volume, clearly observable improvements in combustion characteristics (burnout length and efficiency) were found with CO_2 absorption in CWF sprays (see Appendix B). It is possible that the sudden heating of the droplets upon their injection into the flame accentuates the effect of the absorbed CO_2 by causing droplet disruption due to an enhanced rate of bubble formation.

5.1.2 Photographic Study of Spray Angle and Shape

Figure 5-4 shows four pictures of water sprays taken at AFRs of 0.1 and 0.3 and water temperatures of 100°C and 160°C. Heating to 160°C produced a larger observable change in spray shape and angle at AFR 0.1. A smaller angle change at AFR 0.3 with heating to 160°C is attributable to the higher axial momentum of the spray relative to expansion of water vapor.

When water is heated near its saturation temperature at high pressure and discharged to the environment at a lower pressure through an atomizer, the water flash-vaporizes. This action of volumetric increase causes the spray angle to increase.

5.2 CWF SPRAY TESTS

5.2.1 High Shear Viscosity Measurement

The ultrafine-grind CWFs used were provided by the OXCE Company with two different shipments. Specifications of the two CWFs such as solids loading and viscosity are given in Table 1.

Viscosity of the two CWFs (CWF-A and CWF-B) used for the spray tests was measured using the capillary tube viscometer. CWF-A and CWF-B were diluted to solids loadings of 64% and 50%, respectively. Figures 5-5 and 5-6 show the measured CWF viscosity of CWF-A and CWF-B as a function of the shear rate, which ranged from 10^3 to 10^5 sec^{-1}. (CWF-A was also used in a separately funded DOE-PETC program in which MIT was a subcontractor to Combustion Engineering, Inc. The viscosity data of Figure 5-5 have been shared between the two projects.) Viscosity values of CWF-A at the top of Figure 5-5 are lower than those obtained by the CWF OXCE. This difference is expected since the CWF was diluted to 64% from 67.5%. The same is true for the case of CWF-B, shown in Figure 5-6.

High shear viscosities measured at two elevated CWF temperatures (60° or 75° and 100°C) are compared with those at room temperature, 25°C, in Figures 5-5 and 5-6 for CWF-A and CWF-B, respectively. For the

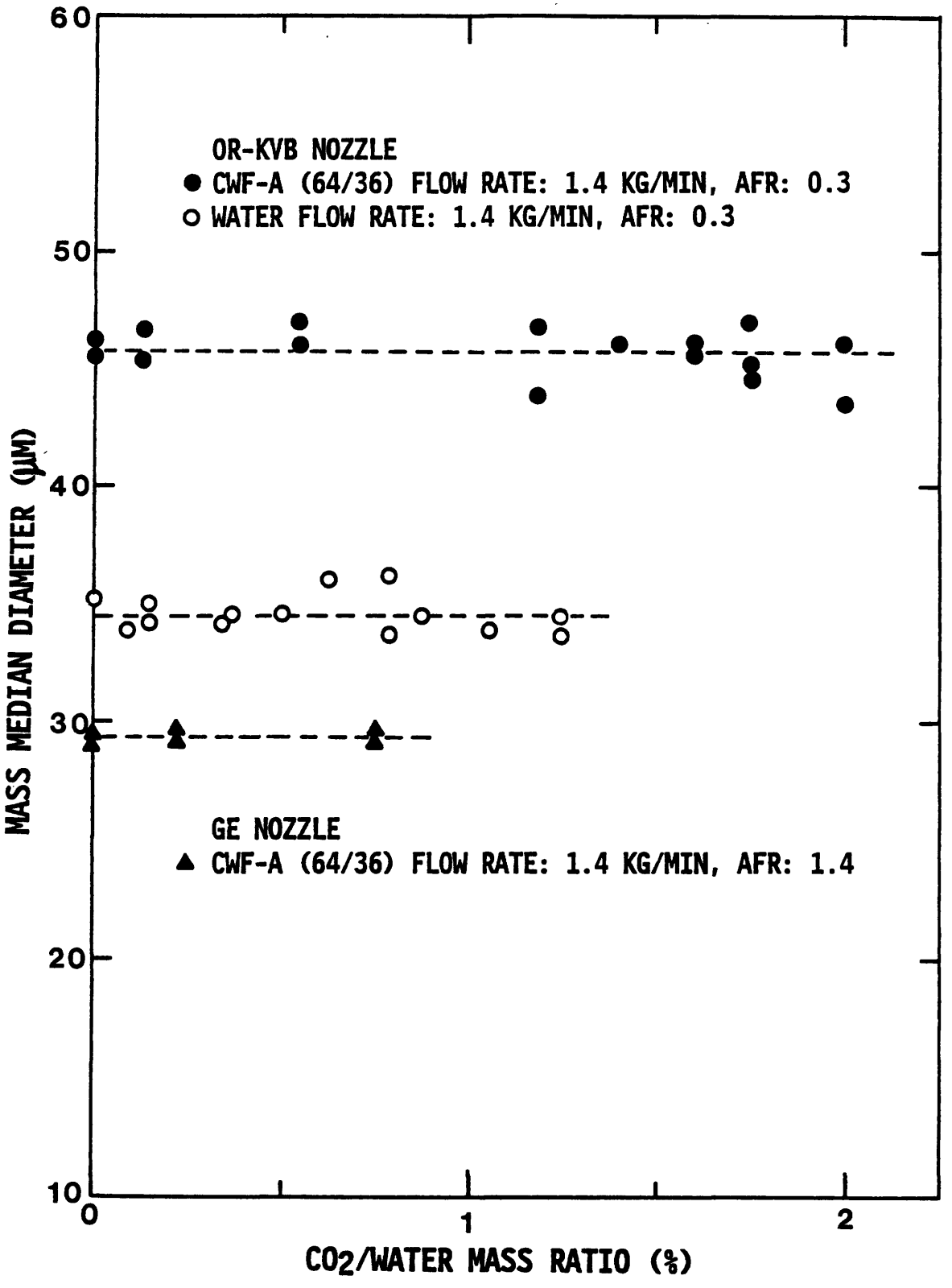

Figure 5-3. Effects of CO_2 Concentration on Mass Median Diameter of Water and CWF Sprays

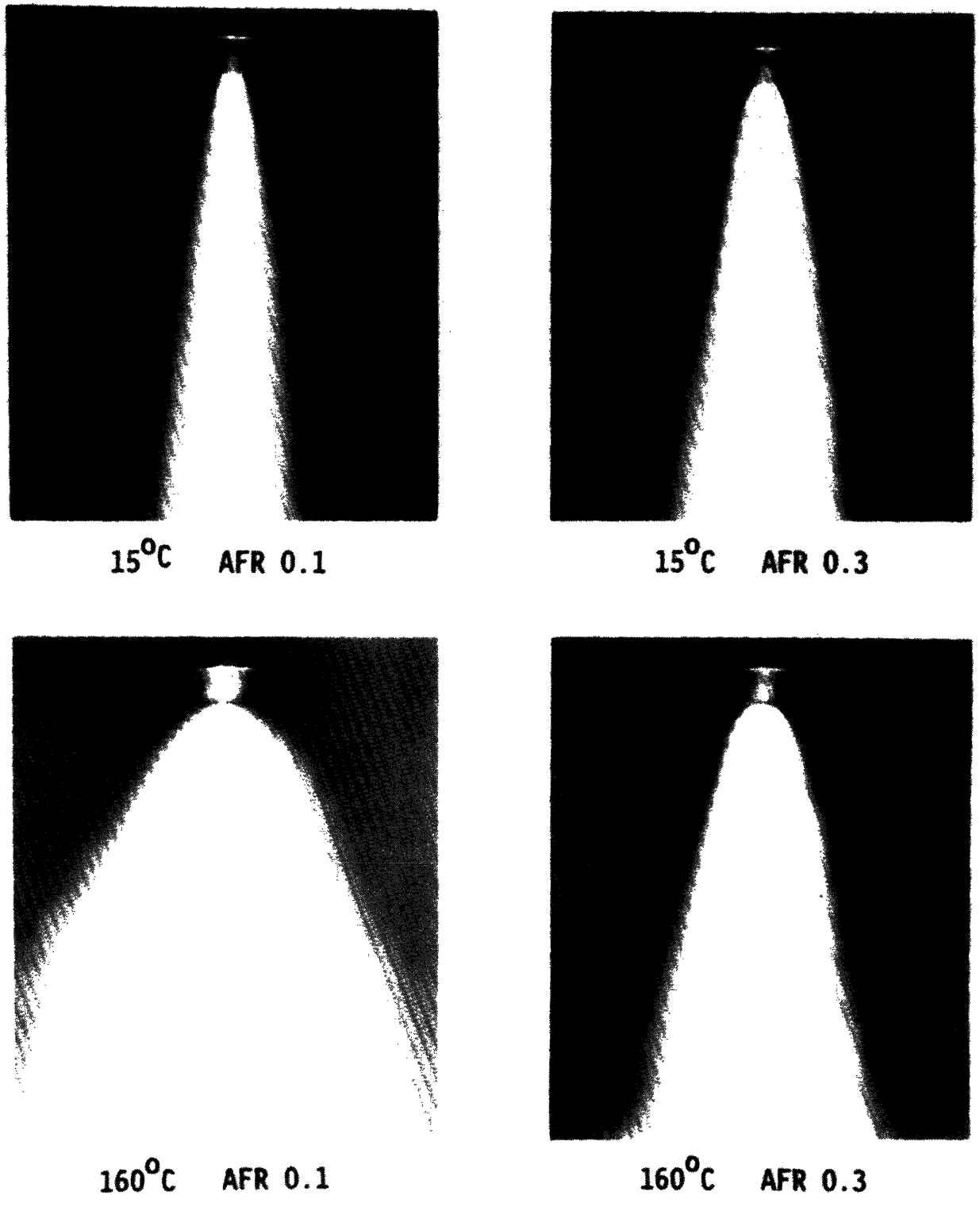

Figure 5-4. Photographs of Water Sprays Taken at AFRs of 0.1 and 0.3 and at Water Temperatures of 15°C and 150°C, Water Flow Rate: 1.4 kg/min

Table 1. Specifications of CWFs used*

	CWF-A	CWF-B
Solids loading (%) (as received)	67.35	61.3
pH	8.28	7.98
MMD (μm)	7.937	9.58
% < 200 Mesh	99.67	98.6
% < 325 Mesh	97.76	96.4
Viscosity at 3000 sec^{-1}	263 cp	508 cp
at 5000 sec^{-1}	315 cp	610 cp

*Data provided by the CWF manufacturer (the OXCE Co.)

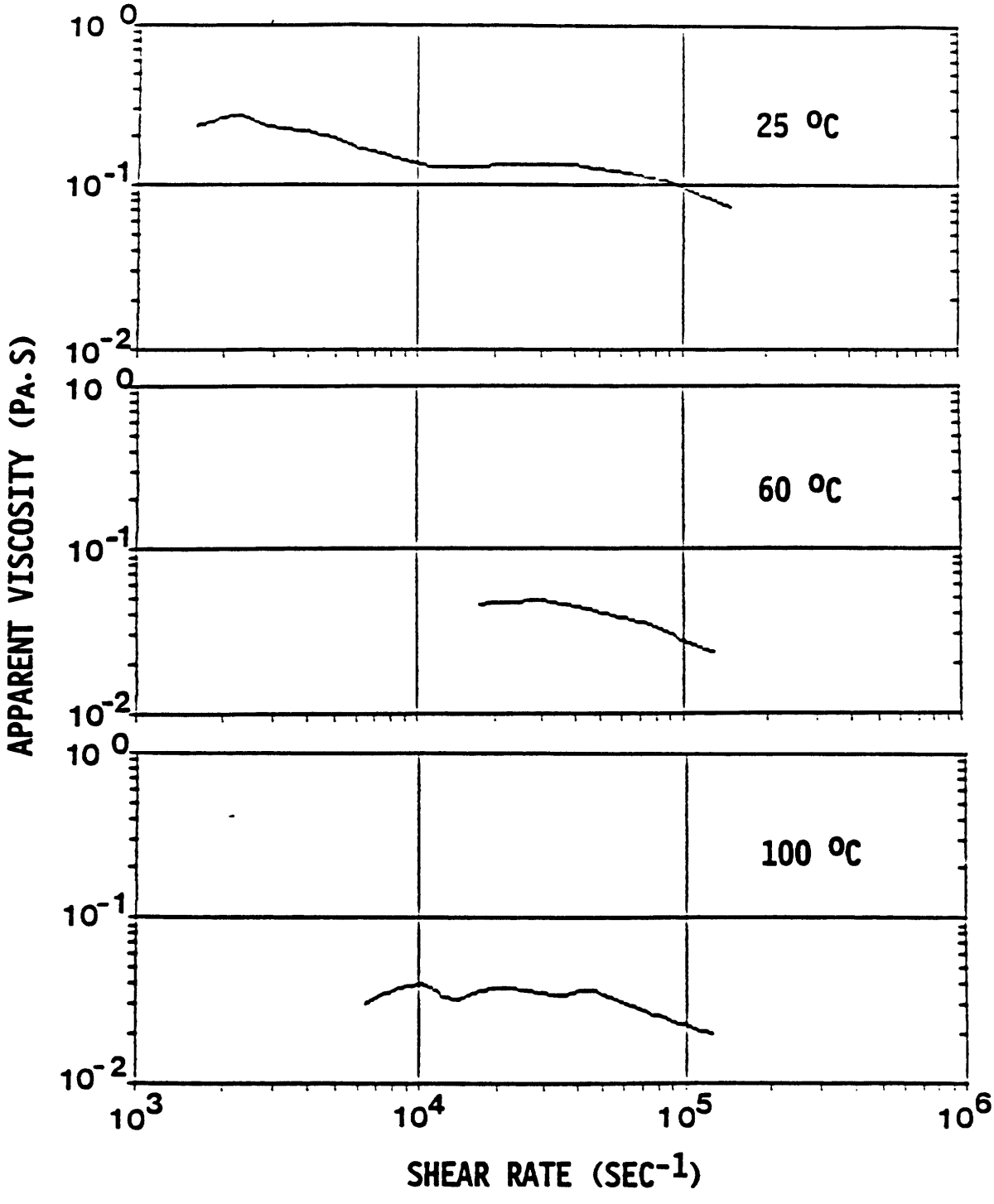

Figure 5-5. CWF-A (64/36) Viscosity at Various Shear Rates and Three Fuel Temperatures

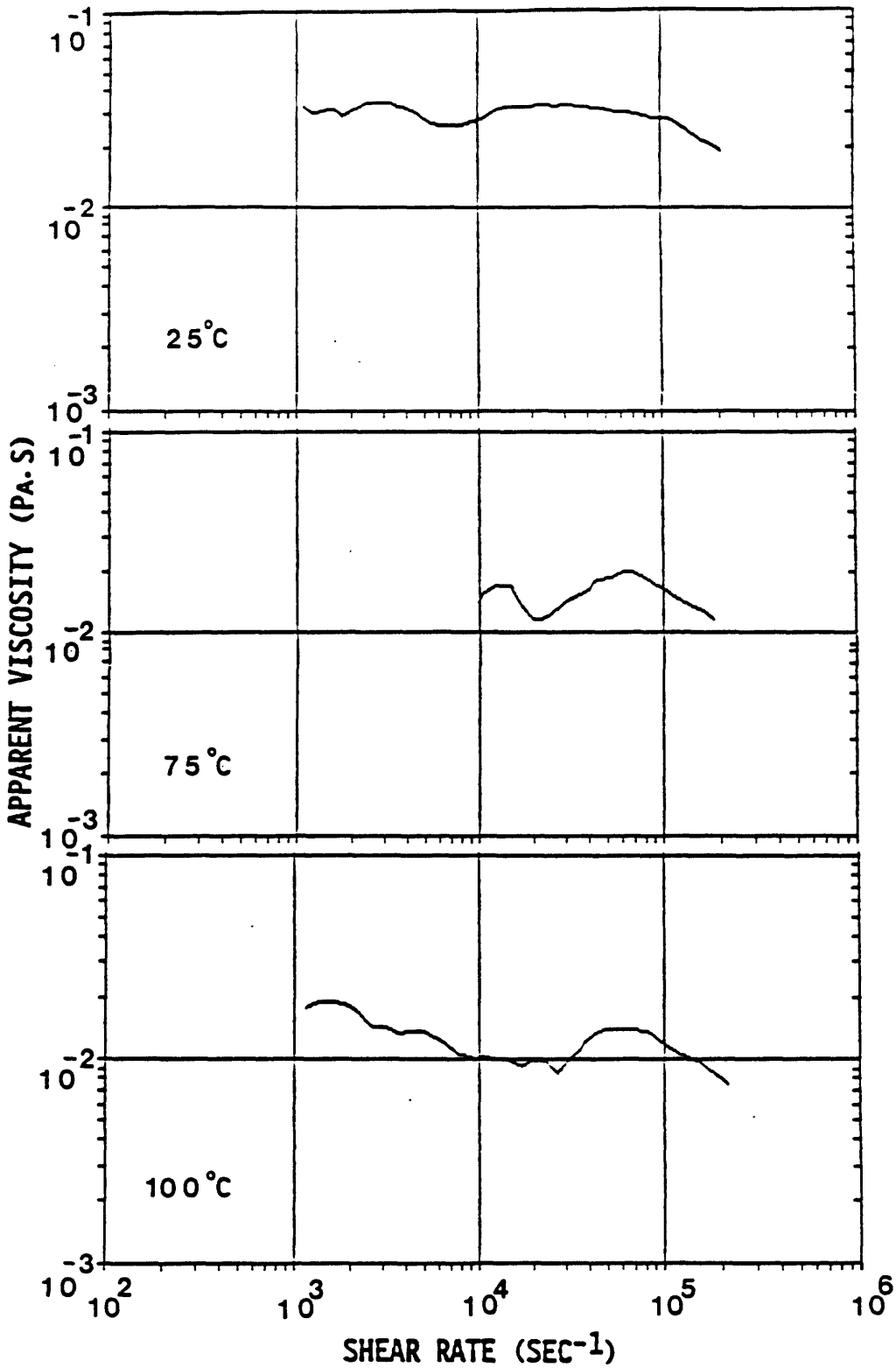

Figure 5-6. CWF-B (50/50) Viscosity at Various Shear Rates and Three Fuel Temperatures

measurements, CWFs were heated using the steam-jacketed CWF fuel line in the spray test rig and were fed directly to the capillary tube of the viscometer. It was found that the high shear viscosity of the CWF decreased substantially with temperature. Slight heating of the CWF from 25°C to 60° or 75°C resulted in large reductions of CWF viscosity at shear rates of 10^4 to 10^5 sec^{-1}. Further heating of the CWFs to 100°C showed continued but lesser reduction of high shear viscosity.

5.2.2 Droplet Size Measurement

5.2.2.1 Thermal Atomization

CWF sprays were tested at atmospheric pressure with the three fuel treatments proposed. The OR-KVB and GE nozzles were used.

Average droplet sizes (mass median diameters) of CWF sprays were measured at various temperatures using the laser diffraction size analyzer. Experimental results of MMDs obtained with the OR-KVB atomizer are shown in Figure 5-7. Droplet sizes of water sprays obtained previously (Figure 5-1) are also included for comparison. MMDs are seen to decrease with increasing CWF temperature. The progressive reduction of average droplet size, observed as the CWF is heated to a temperature of 100°C, should be due to the reduction of CWF viscosity in this temperature range, as in the experiments with the capillary tube viscometer. The large reduction in CWF viscosity of CWF-B from 25°C to 75°C should be responsible for the relatively sharp reduction of the average droplet size from 55 μm to 45 μm in this temperature range. However, as observed also with the water spray, the reduction of droplet size observed when heating the CWF beyond 100°C is considered to be due to disruptive atomization with partial contribution from reduced viscosity.

When the initial droplet size is larger, as obtained at the smaller air/fuel ratios of AFR = 0.08 to 0.09, greater reductions of MMD are achieved with flash-atomization beyond 100°C. This is probably due to the lower surface tension acting on the larger droplets in the spray which makes them a more receptive target for disruptive secondary atomization.

Results of drop size reduction by thermal atomization using the OR-KVB and GE atomizers are plotted in Figure 5-8. The trends of the data are similar to those obtained with water sprays (Figure 5-1) with the droplet sizes decreasing monotonically with increasing CWF temperature. However, there is more scatter in the data in Figure 5-8, especially in the temperature range above 100°C. Radial droplet size distributions of CWF sprays obtained with the OR-KVB and GE nozzles are shown in Figure 5-9. The overwhelming effect of the atomizing air-to-fuel ratio upon MMD of the spray is illustrated in Figures 5-8 and 5-9 by comparing the performance of the OR-KVB and GE atomizers.

5.2.2.2 CO_2 Absorption

Similar to the results of the water spray studies, CO_2 absorption in CWF yielded no observable reduction of the CWF spray MMD. Data obtained with the two nozzles are shown in Figure 5-3. As the CO_2 concentration in the CWF was increased, limits were reached beyond which low-frequency

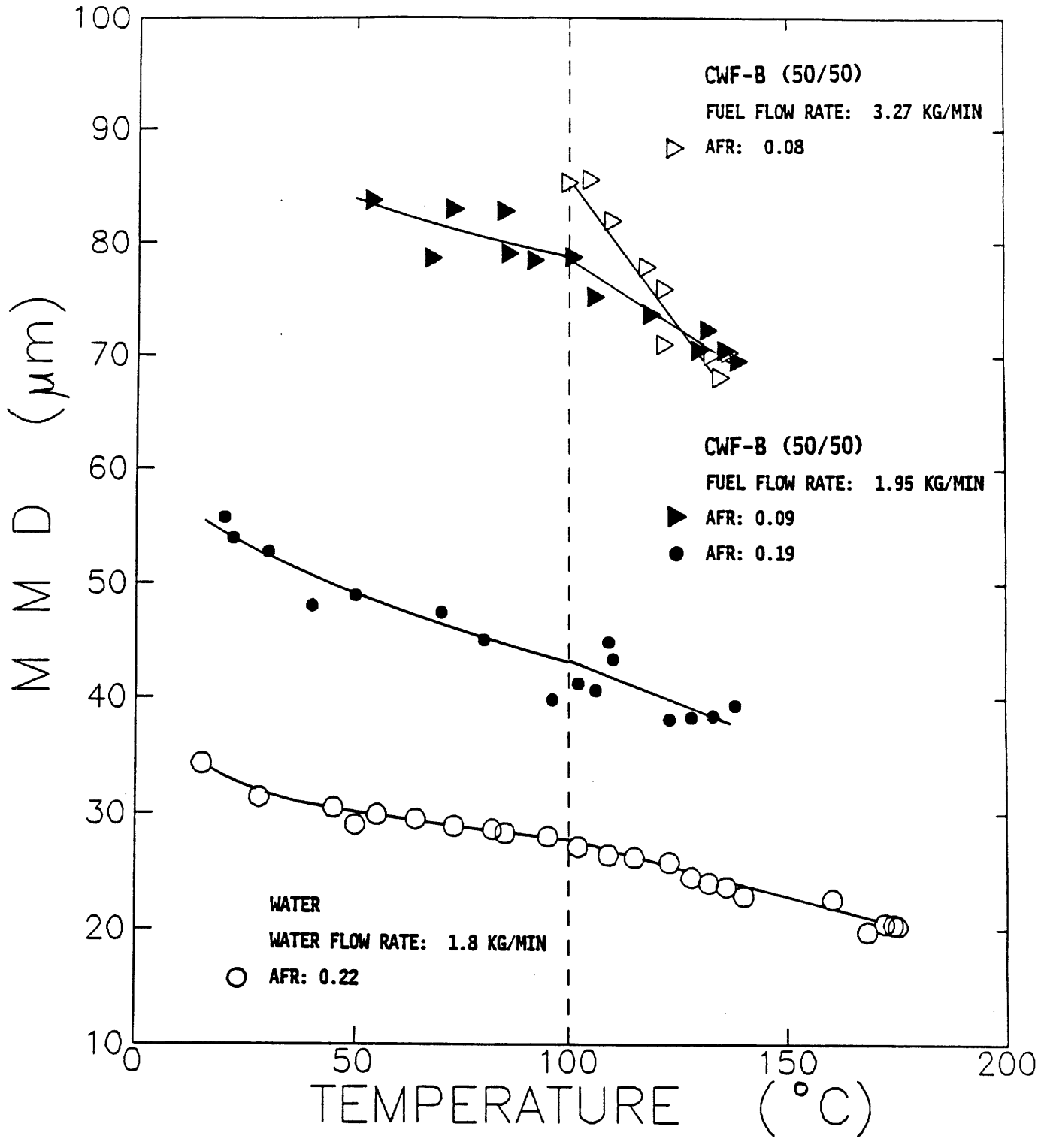

Figure 5-7. Effect of Liquid Temperature on Mass Median Diameter of Water and CWF Sprays at Atmospheric Pressure (OR-KVB Nozzle)

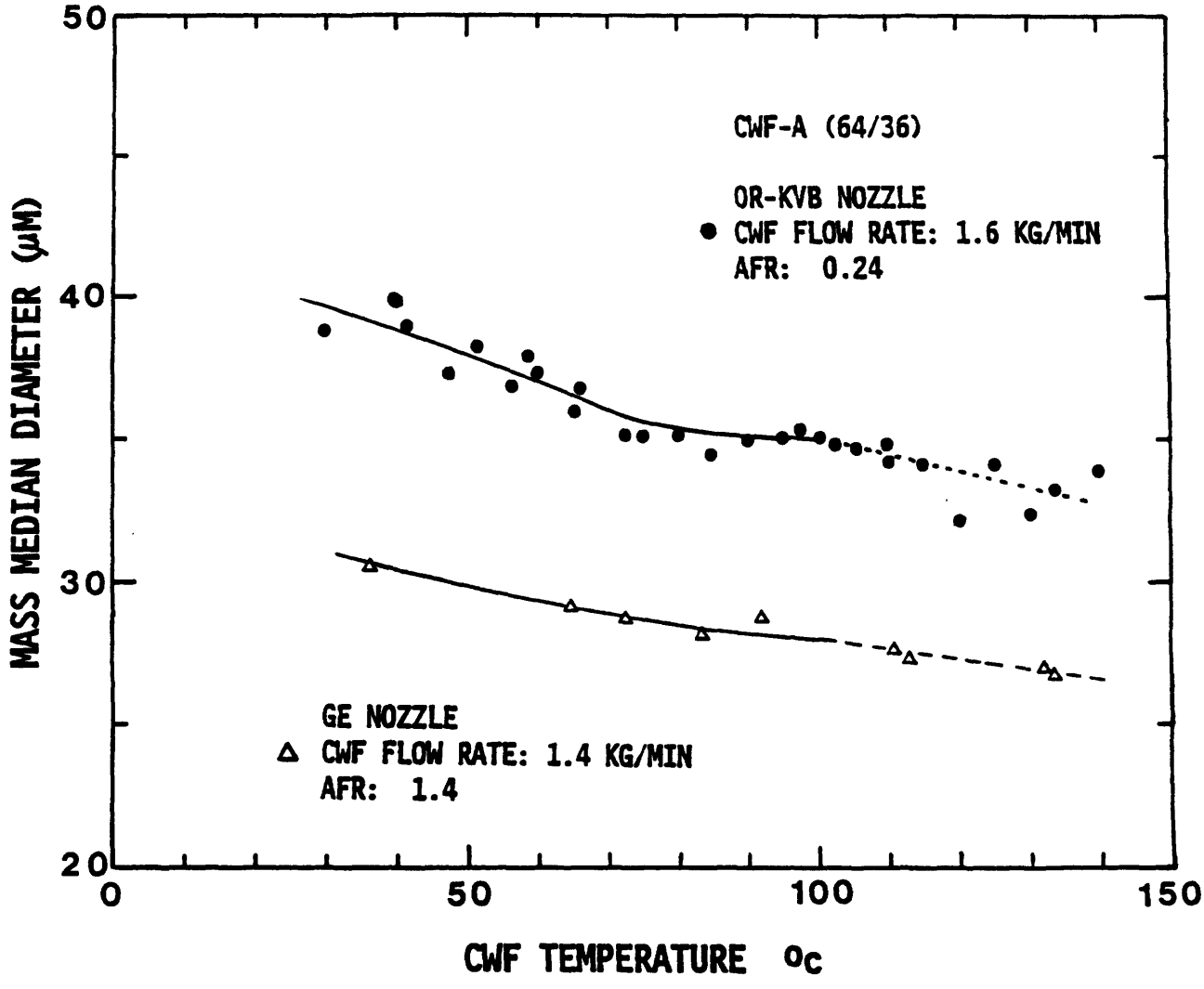

Figure 5-8. Effect of Fuel Temperature on Mass Median Diameter of CWF Sprays produced by OR-KVB and GE Nozzles

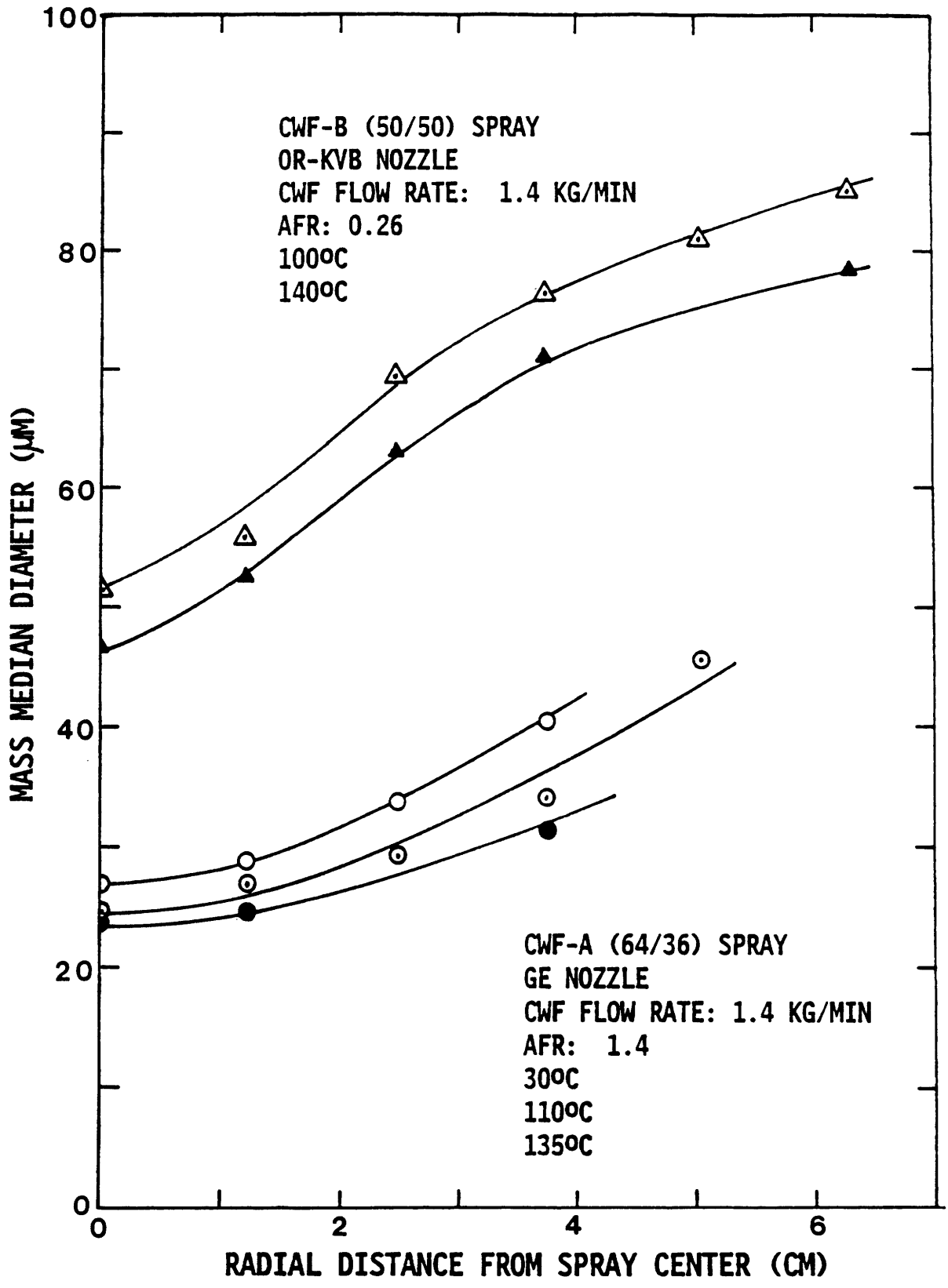

Figure 5-9. Radial Distributions of Mass Median Diameter of CWF Sprays produced by OR-KVB and GE Nozzles at Atmospheric Pressure

fluctuations of the spray were observed, as was the case with the water spray tests. The limiting CO_2/water mass concentration ratio was 1.4% for the OR-KVB nozzle (line pressure of 150 psig); the corresponding limiting ratio for the GE nozzle was 0.8% (line pressure of 25 psig).

5.2.3 Photographic Study of Spray Angle and Shape

Figure 5-10 shows four photographs of water and CWF sprays taken at the atomizing AFR of 0.1 and temperatures of 100°C and 150°C. The spray angle change for the sprays of CWF with solids loading of 50% was found to be smaller than that for water spray. This smaller angle change of CWF spray is attributable to the lesser amount of water in CWF (50%) and the higher linear momentum of the solids-laden spray.

5.3 MODELS OF CWF FLASH-ATOMIZATION

If a pressurized liquid is heated to a value approaching its saturation temperatures and is then discharged for atomization into an environment at a lower pressure through a nozzle, the liquid flash-vaporizes as its pressure is rapidly reduced. During flash-vaporization, nucleation and subsequent bubble growth take place within atomized droplets, ligaments or the liquid jet. These actions of internal bubble generation cause additional breakups of droplets and ligaments, and lead to the formation of new liquid surfaces in the spray produced by primary atomization. Such disruption is called flash-atomization or secondary atomization.

5.3.1 Nucleation and Bubble Growth

Bubble generation has two separate processes: 1) the formation of bubbles (nucleation), and 2) the subsequent growth. Three types of idealized media for nucleation have been considered (19):

(1) Pure liquid; no suspended foreign matter

(2) Liquid with suspended submicroscopic, nonwettable material that contains permanent gas pockets from which bubble nuclei emerge on volume heating

(3) Surface with cavities containing gas and/or vapor.

However, it has been shown that the nucleation usually occurs at solid surfaces (20).

CWF consists of micronized coal particles, water, and a small fraction of chemical additive. During flash-atomization of CWF, bubbles form and grow in the interstitial water of CWF. The possible nucleation sites include: macropores and micropores of coal particles (heterogeneous nucleation), micropores of suspended submicroscopic coal particles in the interstitial water (heterogeneous nucleation), and interstitial water itself (homogeneous nucleation). However, heterogeneous nucleation is much more likely to occur compared to homogeneous nucleation (20). Therefore, vapor bubble formation (nucleation) during CWF flash-atomization will mainly take place in the pores of the coal particles, including those of suspended submicroscopic coal particles.

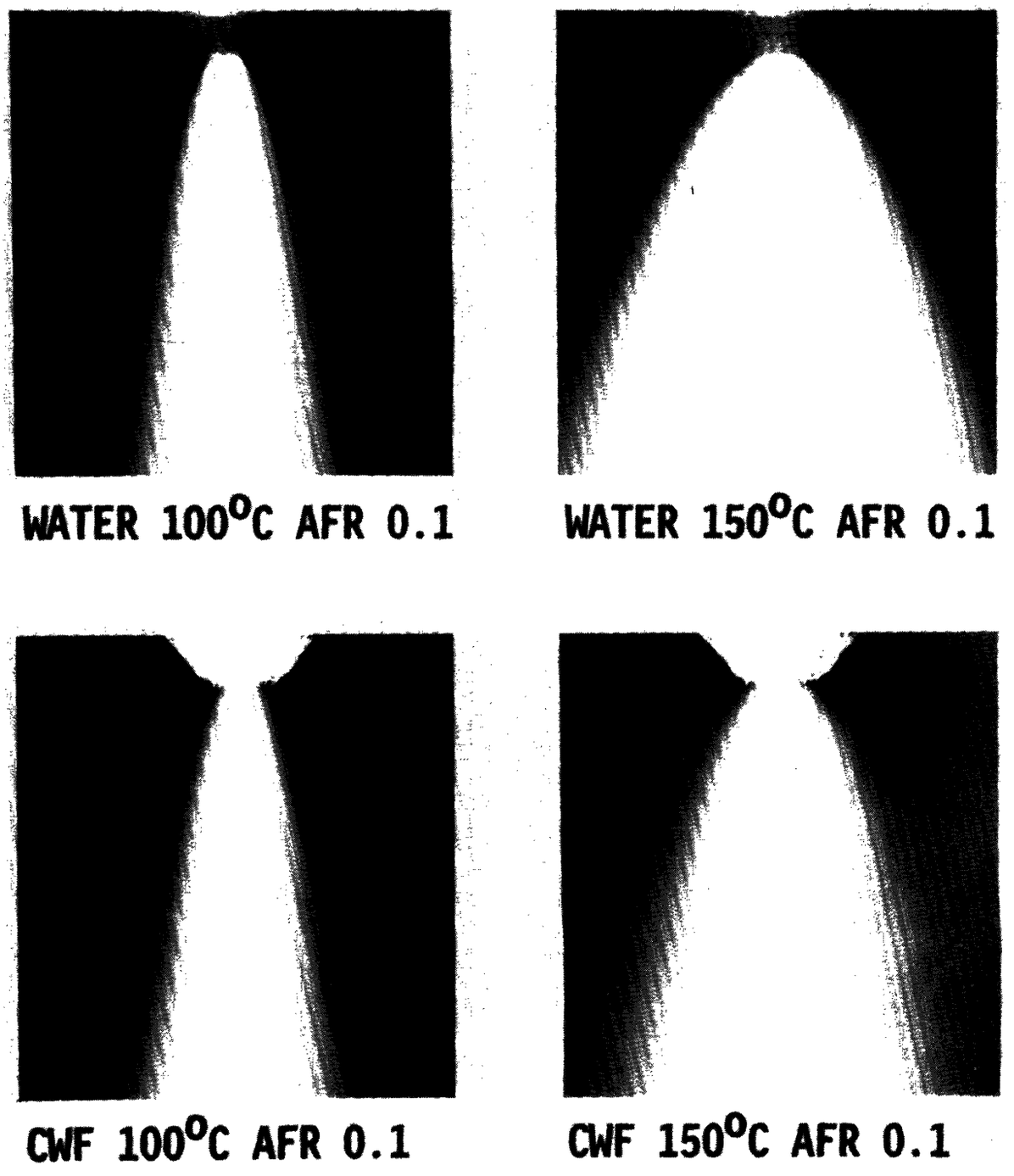

Figure 5-10. Photographs of Water and CWF Sprays taken at Liquid Temperatures of 100°C and 150°C, Water or CWF-B (50/50) Flow Rate: 1.4 kg/min

When the heated CWF undergoes a sudden pressure drop, an air pocket in an active nucleation pore grows by evaporation at the liquid/vapor interface. Figure 5-11 shows the sequential process of bubble growth within the atomized CWF droplet, ligament, or liquid jet of the heated CWF. The entrapped air pocket in the active nucleation pore grows from the bottom of the pore to the top of the pore, and forms a hemispherical bubble at the mouth of the pore (Figure 5-11a). The vapor bubbles grow (Figure 5-11b), until bubble growth is restricted through mutual interference (Figure 5-11c). As the growing bubbles touch each other, they will start to burst and coalesce into big vapor bubbles (Figure 5-11d). The coalescent bubbles separate and disperse the coal particles (Figure 5-11e). The water isolated by the coalescence of vapor bubbles will instantaneously form a spherical water droplet due to the surface tension of the water and will be suspended in the vapor region. The water remaining on the surface of the coal particle will instantly spread on the coal surface due to wetting behavior between the water and the coal surface, and will uniformly surround the coal particle.

However, it should be noted that even before the bubbles within a CWF droplet or CWF liquid jet reach the growth stage of Figure 5-11c, the CWF liquid could be much more easily shattered by the high-speed motion of the atomizing air than would be the case in a CWF liquid without growing bubbles.

5.3.2 Bubble Growth Dynamics

Bubble growth dynamics play an important role during flash-vaporization. This section uses the models of bubble nucleation at a nucleation pore and of bubble growth limited by heat diffusion to explain bubble growth behavior during the flash-atomization of CWF.

The model of vapor bubble growth to a critical size from a pore at a solid surface was formulated by Thirunavukkarasu (21). His model describes the bubble growth in the early stages prior to the bubble reaching the critical size (i.e., a hemispherical shape of the vapor/liquid interface at the pore mouth--see Figure 5-12d) in a liquid which becomes superheated due to a sudden pressure drop.

Figure 5-12a shows the initial stage of an entrapped vapor and/or air pocket in the active nucleation pore. Figures 5-12b and 5-12c show the vapor growing up to the top of the nucleation pore. The time Δt_1, taken to reach the top of the nucleation pore (Figure 5-12c) from the bottom of the pore (Figure 5-12a), is derived from the energy equation in the liquid for a plane interface, and expressed as follows (21):

$$\Delta t_1 = \left[\frac{\pi \rho_v^2 h_{fg}^2}{4 \rho_\ell^2 c_\ell^2 \alpha_\ell}\right] \left(\frac{\ell}{\Delta T}\right)^2 \qquad (17)$$

where ℓ = depth of cylindrical nucleation pore
ΔT = superheat of liquid
ρ_v = density of vapor
ρ_ℓ = density of liquid

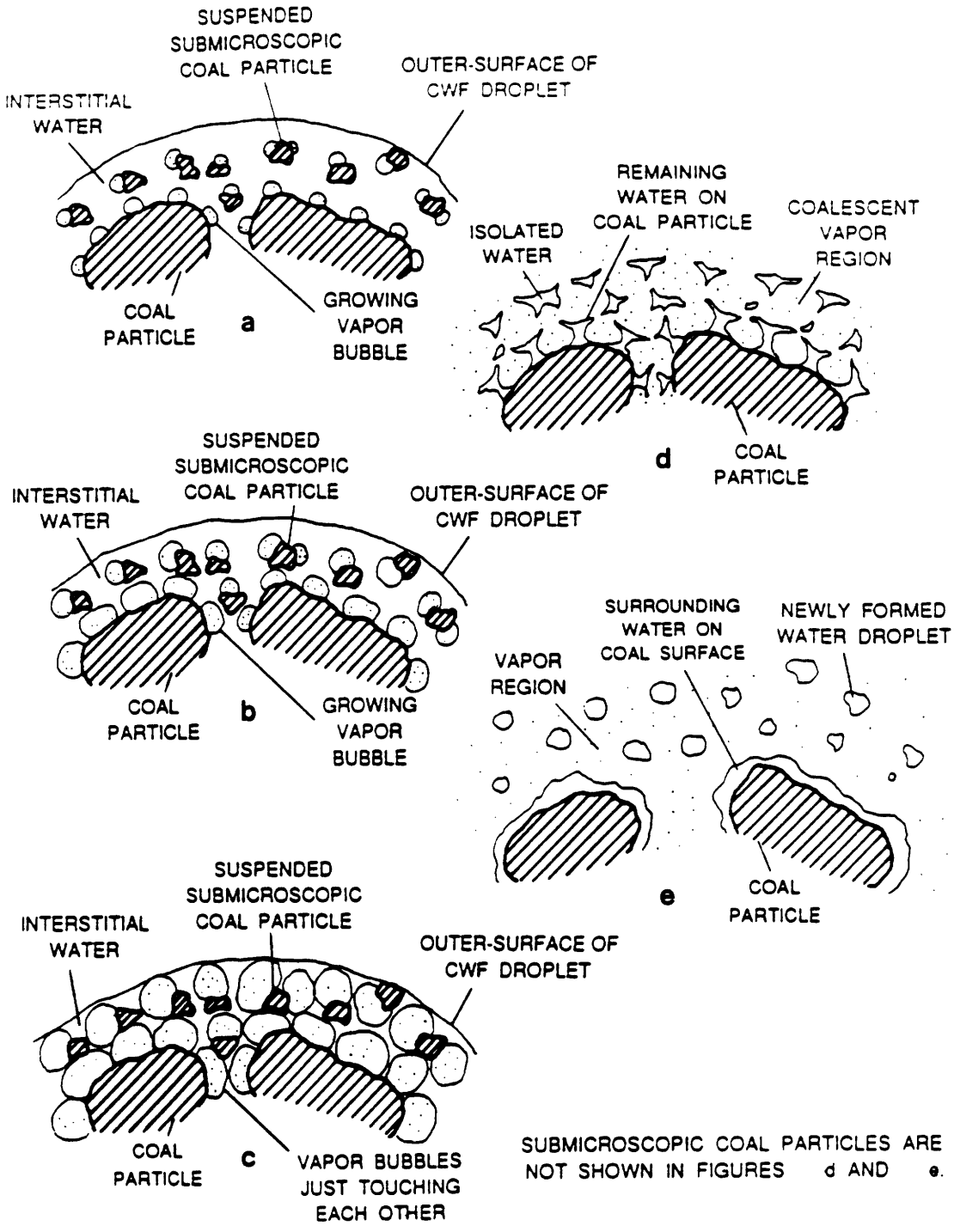

Figure 5-11. Sequential Process of Flash-Atomization on CWF Droplet Surface

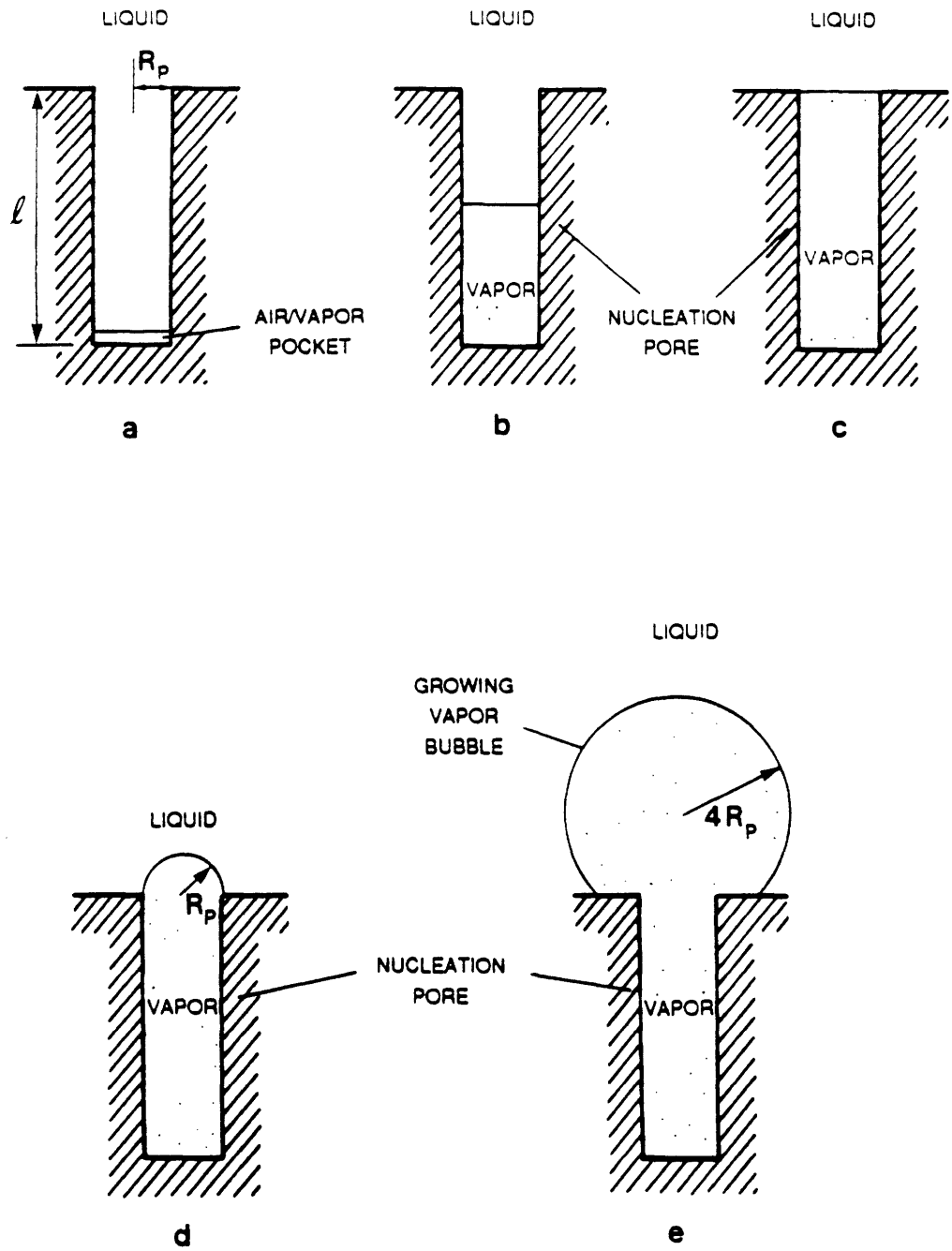

Figure 5-12. Sequential Process of Vapor Bubble Growth at Nucleation Pore of Coal Particle

c_ℓ = specific heat of liquid
α_ℓ = thermal diffusivity of liquid
h_{fg} = latent heat of evaporation

As the vapor reaches the top of the nucleation pore (Figure 5-12c), it grows and forms a hemispherical bubble (radius of R_p) at the nucleation pore (Figure 5-12d). The bubble growth rate between the stages of Figures 5-12c and 5-12d is obtained from the energy equations in the liquid and vapor regions, and expressed as

$$\frac{dR}{dt} = \frac{-2\pi R_p^2 k_\ell \rho_\ell c_\ell}{3XY} (\Delta T)^2 \tag{18}$$

where $\frac{dR}{dt}$ = bubble growth rate
R = radius of bubble
R_p = radius of nucleation pore mouth
X, Y = functions of bubble radius R and vapor temperature
k_ℓ = thermal conductivity of liquid
ΔT = superheat of liquid

The negative sign of Eq. (18) takes account of the radius reduction from R_∞ ($= \infty$) to R_p. Hence, the time Δt_2, required to reach the hemispherical stage (Figure 5-12d) from the bubble radius of R_∞ (Figure 5-12c), is given by

$$\Delta t_2 = \int_{R_\infty}^{R_p} \frac{-3XY}{2\pi R_p^2 k_\ell \rho_\ell c_\ell (\Delta T)^2} dR \tag{19}$$

Thirunavakkarasu found that beyond the hemispherical stage the bubble growth rate remains the same as given by Eq. (19), until the bubble radius reaches about four times the pore radius, that is, $R = 4\ Rp$ (Figure 5-12e). Beyond this the bubble growth rate is limited by thermal conduction. Zwick and Plesset (22), Plesset and Zwick (23,24), Forster and Zuber (25), and others (26,27) studied the asymptotic bubble growth that is limited by conduction. Their results, applicable to the isobaric bubble growth, show that the bubble growth rate is proportional to superheat, and inversely proportional to the square root of bubble growth time, as follows:

$$\frac{dR}{dt} = \left[\frac{12}{\pi}\right]^{1/2} \frac{\rho_\ell c_\ell \alpha_\ell^{1/2} \Delta T}{2 \rho_v h_{fg} t^{1/2}} \tag{20}$$

Hence, the asymptotic bubble growth time Δt_3, taken to reach a final bubble radius of R_2 from an initial bubble radius of R_1, is given by

$$\Delta t_3 = \frac{\pi \rho_v^2 h_{fg}^2}{12 \rho_\ell^2 c_\ell^2 \alpha_\ell (\Delta T)^2} (R_2 - R_1)^2 \tag{21}$$

Therefore, the total time Δt_{tot} required to reach the final bubble radius of R^* from the entrapped air and/or vapor pocket at the bottom of the pore can be obtained as

$$\Delta t_{tot} = \Delta t_1 + \Delta t_2 + \Delta t_3$$

$$= \left[\frac{\pi \rho_v^2 h_{fg}^2}{4 \rho_\ell c_\ell^2 \alpha_\ell^2}\right] \left(\frac{\ell}{\Delta T}\right)^2 + \int_{\infty}^{R_p} \frac{-3 XY}{2\pi R_p^2 k_\ell \rho_\ell c_\ell (\Delta T)^2} dR$$

$$+ \int_{R_p}^{4R_p} \frac{+3 XY}{2\pi R_p^2 k_\ell \rho_\ell c_\ell (\Delta T)^2} dR$$

$$+ \left[\frac{\pi \rho_v^2 h_{fg}^2}{12 \rho_\ell^2 c_\ell^2 \alpha_\ell (\Delta T)^2}\right] (R^* - 4R_p)^2 \qquad (22)$$

Here, in addition to Eq. (19), Δt_2 is modified to include the bubble growth time from Rp to $4R_p$. Δt_3 is obtained by substituting $4R_p$ and R^* the initial and final bubble radii, in Eq. (21).

The total bubble growth time Δt_{tot} is inversely proportional to the square of superheat ΔT. Hence it is concluded that as the superheat ΔT increases and/or the final bubble radius R^* decreases, the total bubble growth time Δt_{tot} decreases. Also, the total bubble growth time Δt_{tot} is dependent upon the dimensions of the nucleation pore (R_p and ℓ) and the properties of the liquid and vapor.

5.3.3 Effect of Superheat on CWF Flash-Atomization

Coal particles within a CWF droplet have a large number of micropores and macropores. These pores are assumed to have the size distribution shown in Figure 5-13, which illustrates the number of pores of a particular size range versus the diameter of pore.

In accordance with Staniszewski's (28) observation, as the superheat ΔT is increased, the number of activated nucleation pores increases and more pores become activated at pore diameters spread on either side of the critical pore diameter D_{crit} (Figure 5-13). On the other hand, as the number of activated nucleation pores increases (i.e., density of nucleation sites increases), the average distance between each activated nucleation pore, and hence the average diameter of touching bubbles, decreases. Therefore, at a higher superheat, the total bubble growth time to form touching bubbles is reduced due to the smaller average bubble diameter and also because bubble growth time is inversely proportional to the square of superheat.

Figure 5-14 compares two cases of bubble growth at two different levels of superheat. The time corresponding to each event illustrated in Figure 5-14a (small superheat) is much longer than that in Figure 5-14b (large superheat). Therefore, when the superheat of the CWF is smaller, probability of secondary breakup by flash-vaporization would be reduced due to the longer bubble growth time. Figure 5-14 shows that at a higher

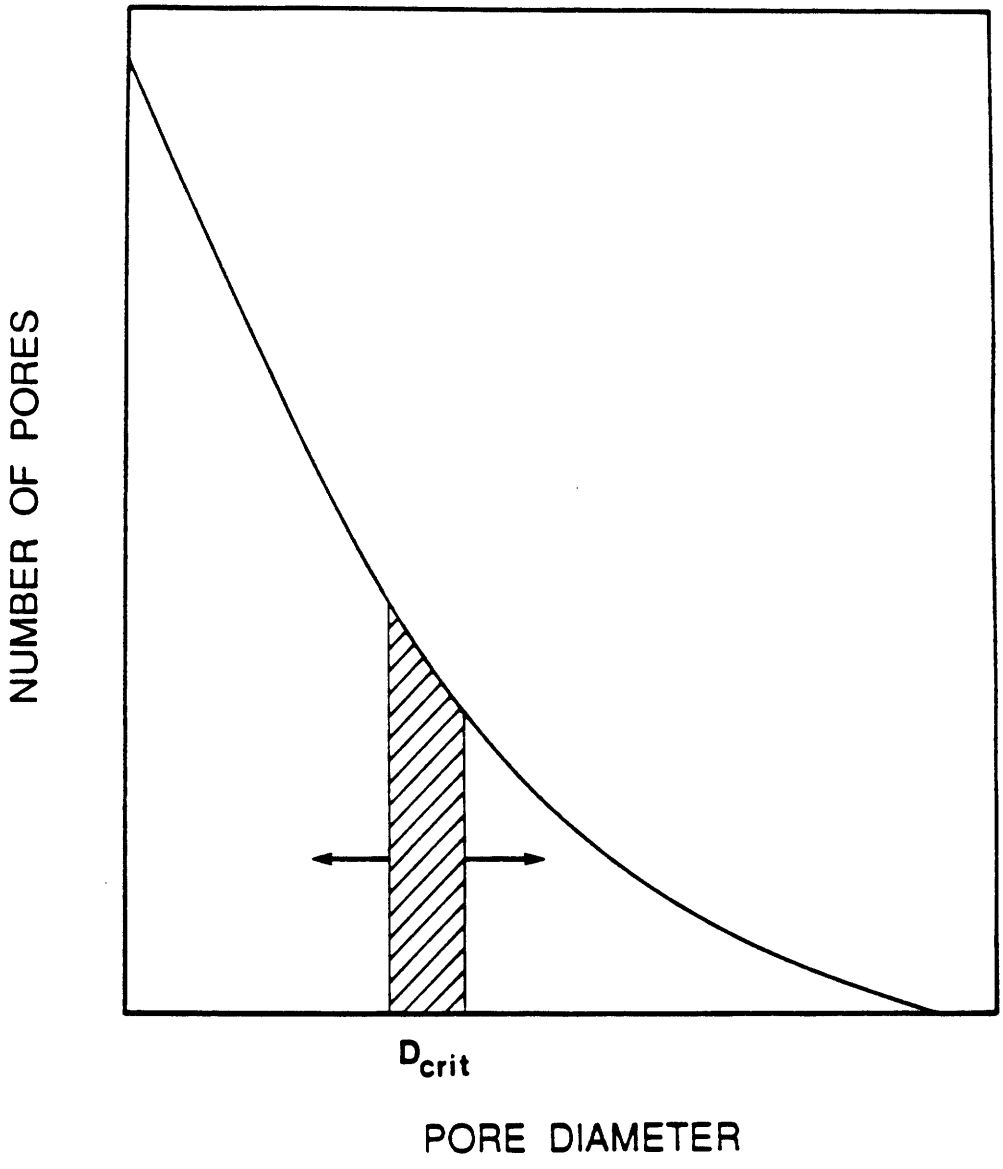

Figure 5-13. Pore Size Distribution of Coal Particle

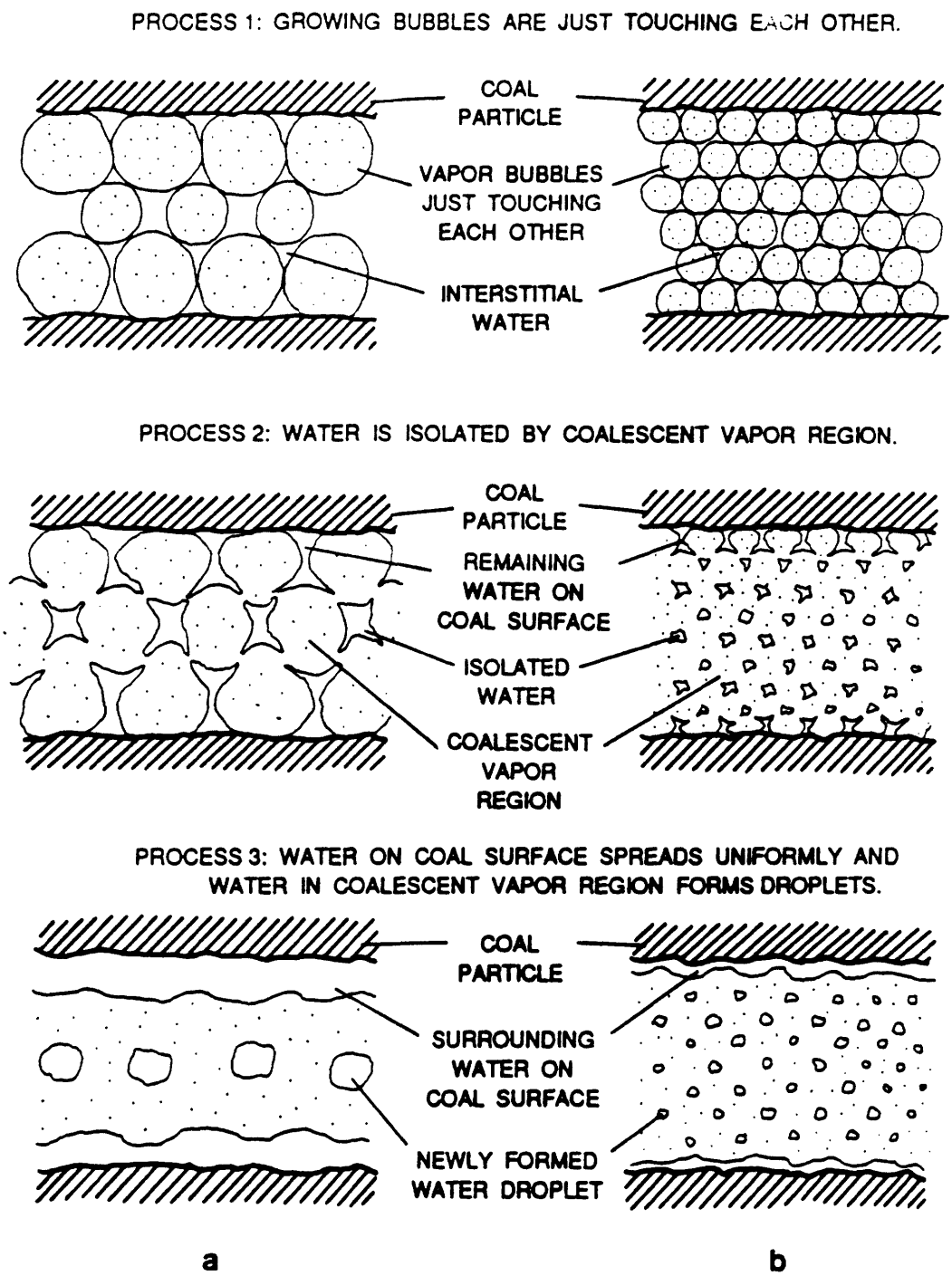

Figure 5-14. Comparison of Amount of Remaining Water on Coal Particle Surface with Different Superheat ΔT
(a) Small Superheat ΔT, (b) Large Superheat ΔT

superheat, as the average diameter of touching bubbles decreases, both the amount of the remaining water on the coal surface and the size of the interstitial water droplets (situated between the vapor bubbles) decreases with the concurrent increase in the number of these droplets.

As newly formed water droplets and CWF droplets are scattered, some fraction of them may collide and coalesce (Figure 5-15). The extent of adhesion during droplet collision depends on their relative motion and the thickness of the water film in the CWF droplets. As shown in Figure 5-16, the adhesive force between two CWF droplets is determined by the surface tension of water (γ) multiplied by the circumference (ℓ) at the neck region. The circumference of the neck region is proportional to the amount of the surrounding film water. If the amount of surrounding water is very small, colliding CWF droplets may fall apart easily due to the weak surface tension force. However, if the amount of surrounding water is large enough, it is very much likely that the CWF droplets will adhere and coalesce.

Using an ultrafine-grind CWF over a regular or fine-grind CWF has several advantages with respect to improving secondary atomization. The ultrafine CWF has a higher water mass fraction, say 50%, than coal-water fuels intended for boiler use (30%). Figure A-1 illustrates the effect of water fraction (γ) on volume change and mass fraction of steam induced by flash-vaporization at atmospheric pressure. It can be seen from Figure A-1 that the increase of water mass fraction from 30% to 50% corresponds to more than 50% increase of flash-vaporization strength (i.e., volume change and steam mass fraction). Therefore, the higher water fraction should produce more steam through flash-atomization. For the CO_2 absorption technique this higher fraction of water can absorb more CO_2 gas and thereby generate stronger CO_2 bubbling effects.

6. PRIMARY ATOMIZATION AT ELEVATED PRESSURE

It is known that spray quality (droplet size and spray shape) changes with chamber pressure (16,29,30). For example, with an increase in the combustor chamber pressure, the atomization air velocity at the nozzle exit will decrease if the atomization air mass flow rate remains constant. Therefore, resulting droplet size will increase. For the application of coal-water fuel to gas turbines, effects of chamber pressure on atomization quality (droplet size distribution and spray shape) were examined.

6.1 EXPERIMENTAL APPARATUS

The high-pressure spray test rig (Section 3.2) was used for experiments at elevated pressure. Droplet sizes of CWF sprays were measured at various chamber pressures and AFRs using the laser diffraction droplet size analyzer (Section 3.3), which was installed perpendicular to the spray (Figure 3-2). The twin-fluid OR-KVB atomizer (Section 3.6) was used for this study. The CWF flow rate remained constant and the AFR was varied. The atomizing air flow rate, in turn, determined the atomizing air velocity at the nozzle exit for a given chamber pressure; it was calculated as the atomizing air flow rate divided by the nozzle exit area (diameter: 2.79 mm) and the chamber air density.

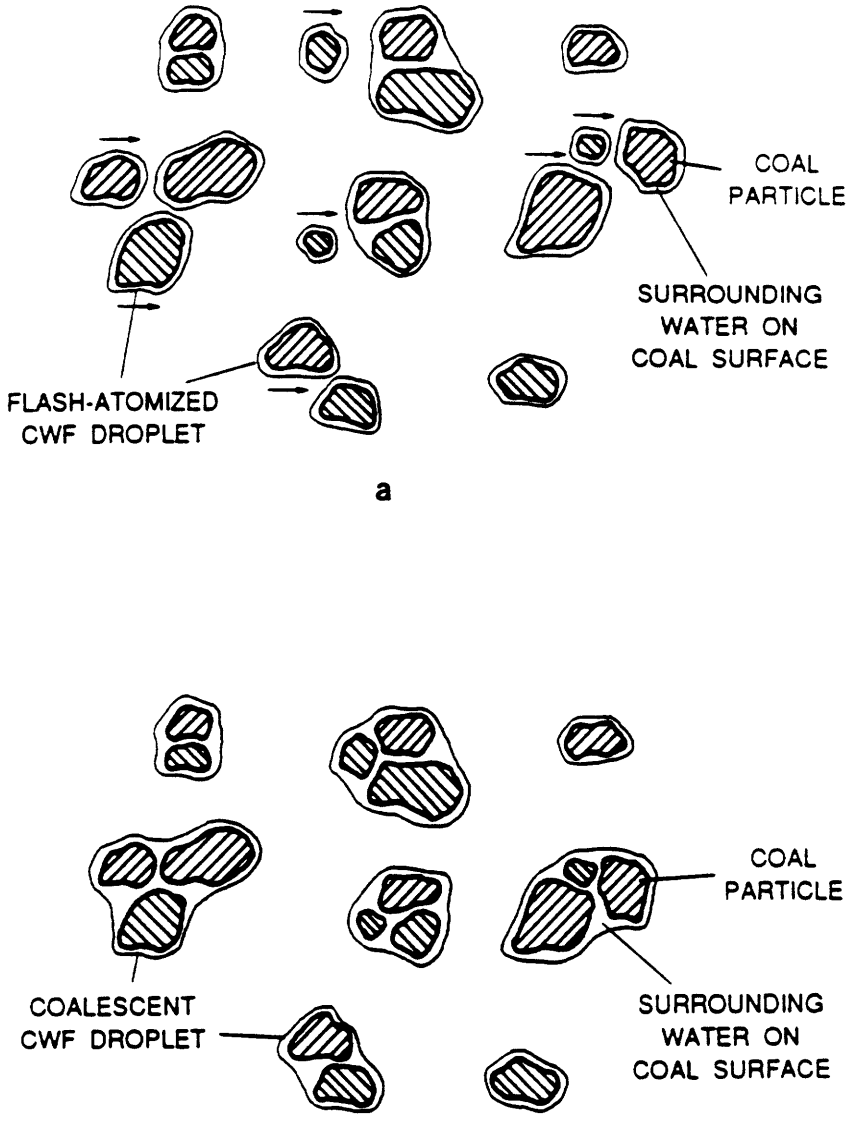

Figure 5-15. Adhesion Process of Flash-Atomized CWF Droplets
(a) Before Collision, (b) After Collision

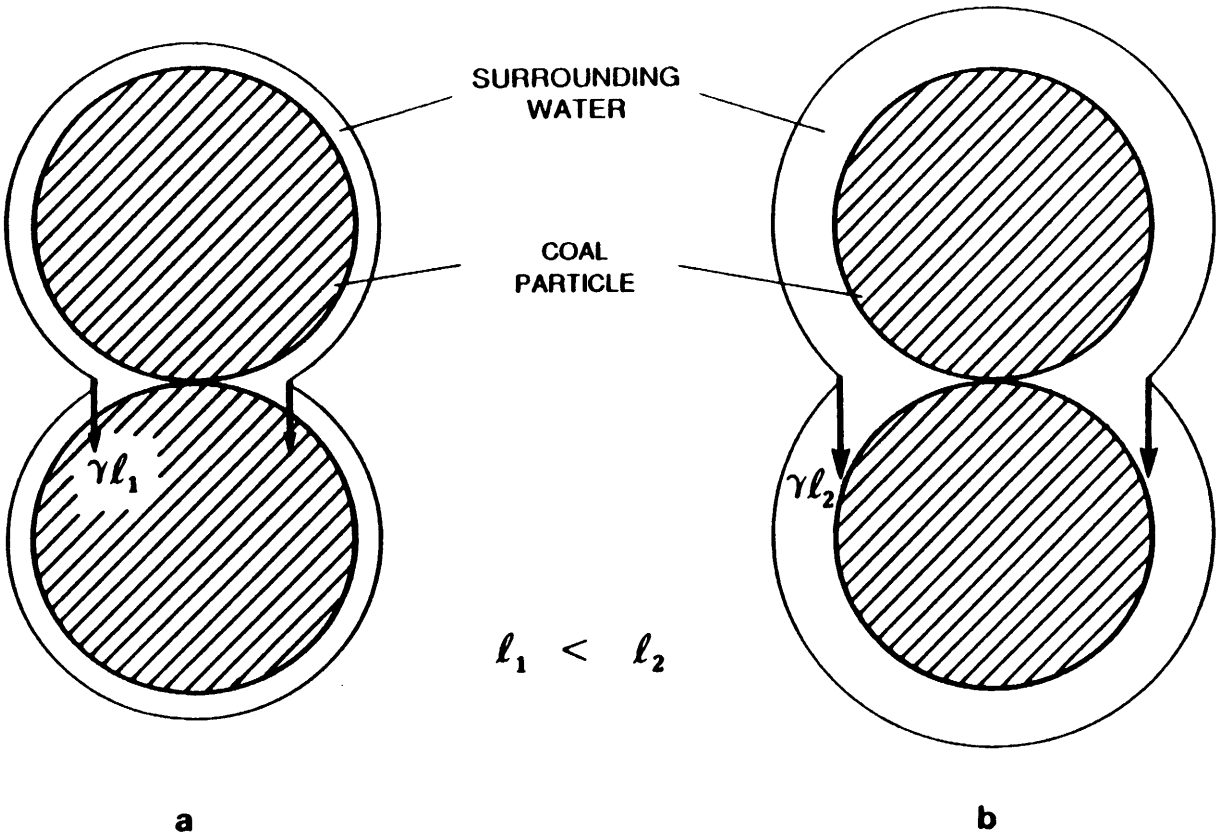

Figure 5-16. Comparison of Surface Tension Force with Different Amount of Surrounding Water in Coalescent CWF Droplets (a) Thin Water Layer, (b) Thick Water Layer

6.2 DROPLET SIZE MEASUREMENT IN WATER AND CWF SPRAYS

Measured average droplet sizes at various chamber pressures are plotted as a function of AFRs for water sprays in Figures 6-1 and 6-2, and for CWF sprays in Figures 6-3 and 6-4. At a given chamber pressure the MMDs of water sprays and CWF sprays decrease with increasing AFR (see Figures 6-1 and 6-3) because the atomizing air velocity at the nozzle exit is increasing with the AFR. But at a fixed AFR, the MMD increases with the chamber pressure. This is because the chamber air density increases with increasing chamber pressure and, thus, at a fixed AFR, the atomizing air velocity at the nozzle exit decreases. Although the atomization quality is expected to improve with increasing ambient air density, these results show that the effect of increasing air density is more than compensated for by the effect of the reduced atomizing air velocity, leading to coarser atomization.

However when the experimental data of Figures 6-1 and 6-3 are replotted as a function of atomizing air velocity at the nozzle exit (see Figures 6-2 and 6-4), the results indicate that spray droplet sizes are decreasing with increasing chamber pressure at a given atomizing air velocity. Atomization quality improves under the higher ambient air density as long as the atomizing air velocity at the nozzle exit remains constant (see Figure 6-5).

6.3 PHOTOGRAPHIC STUDY OF SPRAY ANGLE AND SHAPE

Photographs of sprays were taken through the windows installed on the high pressure spray rig to characterize changes of spray shape and angle as a function of chamber pressure and AFR. Photographs of water sprays and CWF sprays at four chamber pressures and two AFRs are shown in Figures 6-6 and 6-7, respectively. Half angles of the sprays were measured from the photographs at two spray axial locations. One location was the exit of the nozzle (axial location: 0 cm) and the other was 4 cm from the nozzle exit. The measured half angles of the water and CWF sprays are plotted in Figures 6-8 and 6-9, respectively. For water, the spray angle was significantly reduced when chamber pressure increased for given atomization conditions (AFR, fuel flow rate, nozzle); for the CWF the reduction was rather moderate.

For given atomization conditions (AFR, fuel flow rate, nozzle geometry), the entrainment mass flow rate per unit length of spray remains constant with increasing chamber pressure. It follows that the volume flow rate of air entrainment decreases with increasing chamber pressure. This decreasing entrainment of the volume flow rate of air per unit length of the sprays is mainly responsible for the reduction of the spray angle with increasing chamber pressure. When comparing water and CWF sprays, it should be noted that the density of the CWF spray droplets is higher than that of the water droplets. Therefore, water sprays, compared to CWF sprays, are more sensitive to the change in chamber pressure; the angles of water sprays are narrower than those of CWF sprays at the same chamber pressure and corresponding atomizing conditions. As mentioned, the liquid mass flow rates for both the water and CWF sprays were kept constant at 1.4 kg/min; therefore, the liquid volume flow rates of the CWF spray were actually less than those of the water spray. This difference is thought to be responsible for the wider angle of the CWF sprays than those of the water sprays.

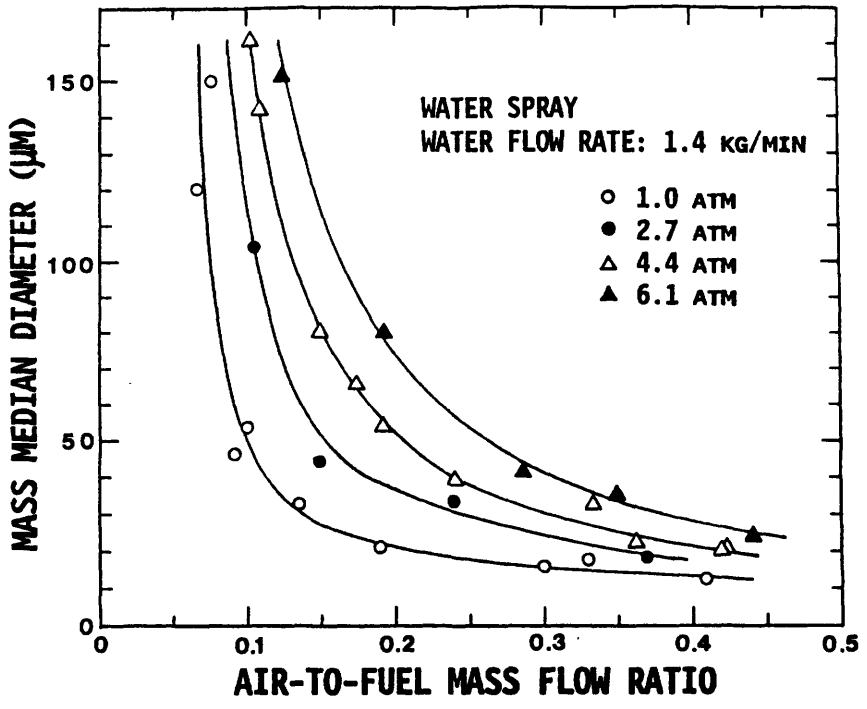

Figure 6-1. Effects of AFR and Chamber Pressure on Mass Median Diameter of Water Sprays

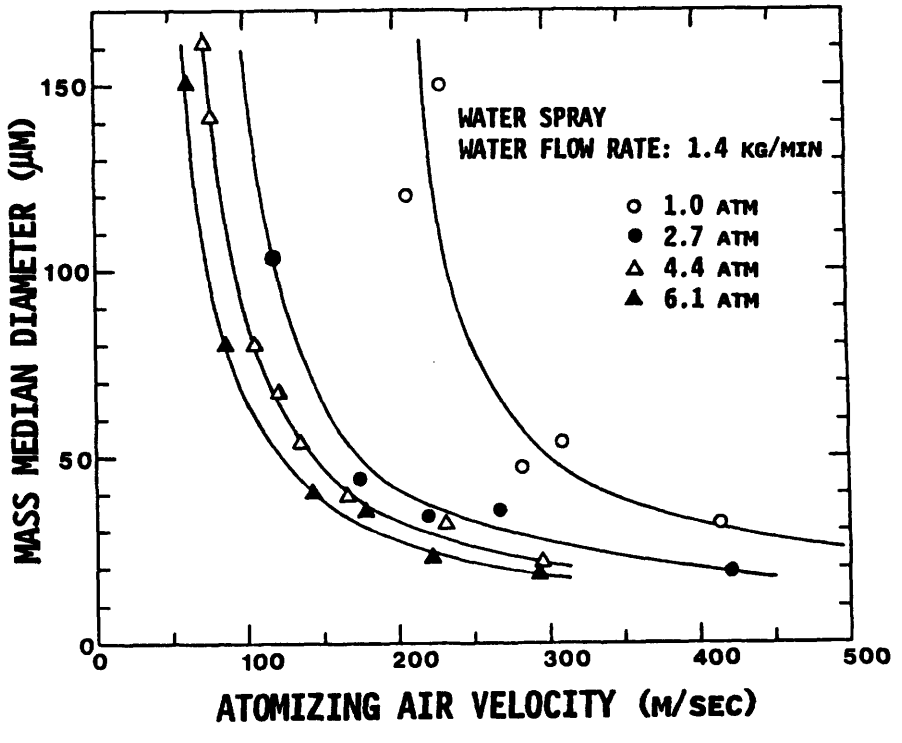

Figure 6-2. Effects of Atomizing Air Velocity and Chamber Pressure on Mass Median Diameter of Water Sprays

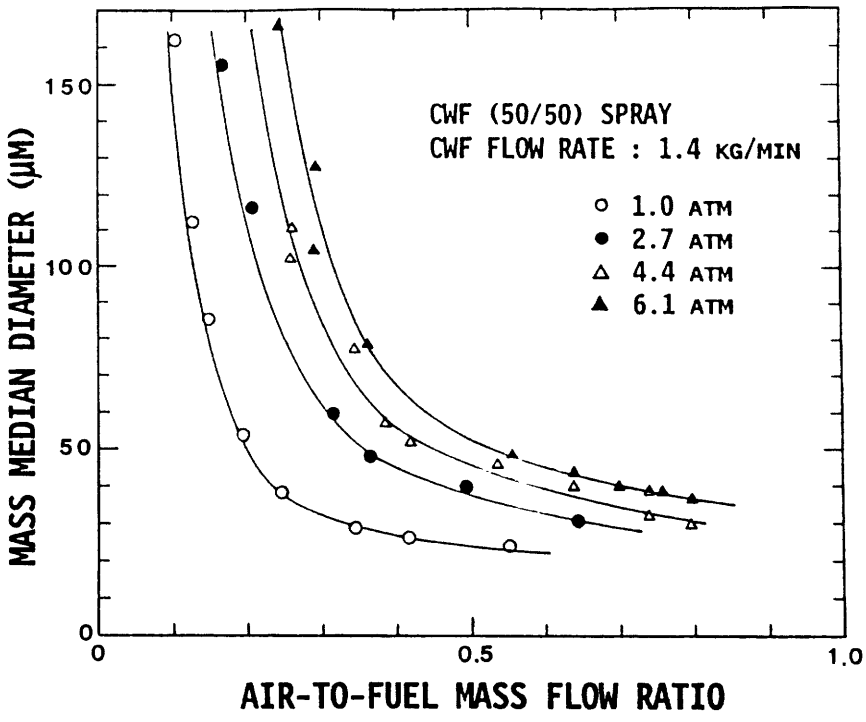

Figure 6-3. Effects of AFR and Chamber Pressure on Mass Median Diameter of CWF Sprays

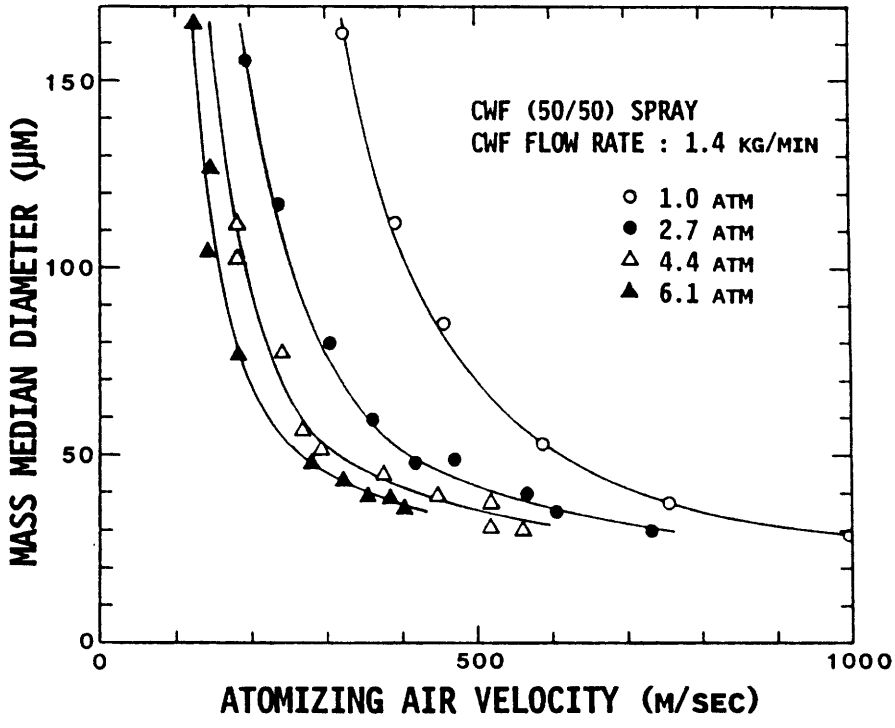

Figure 6-4. Effects of Atomizing Air Velocity and Chamber Pressure on Mass Median Diameter of CWF Sprays

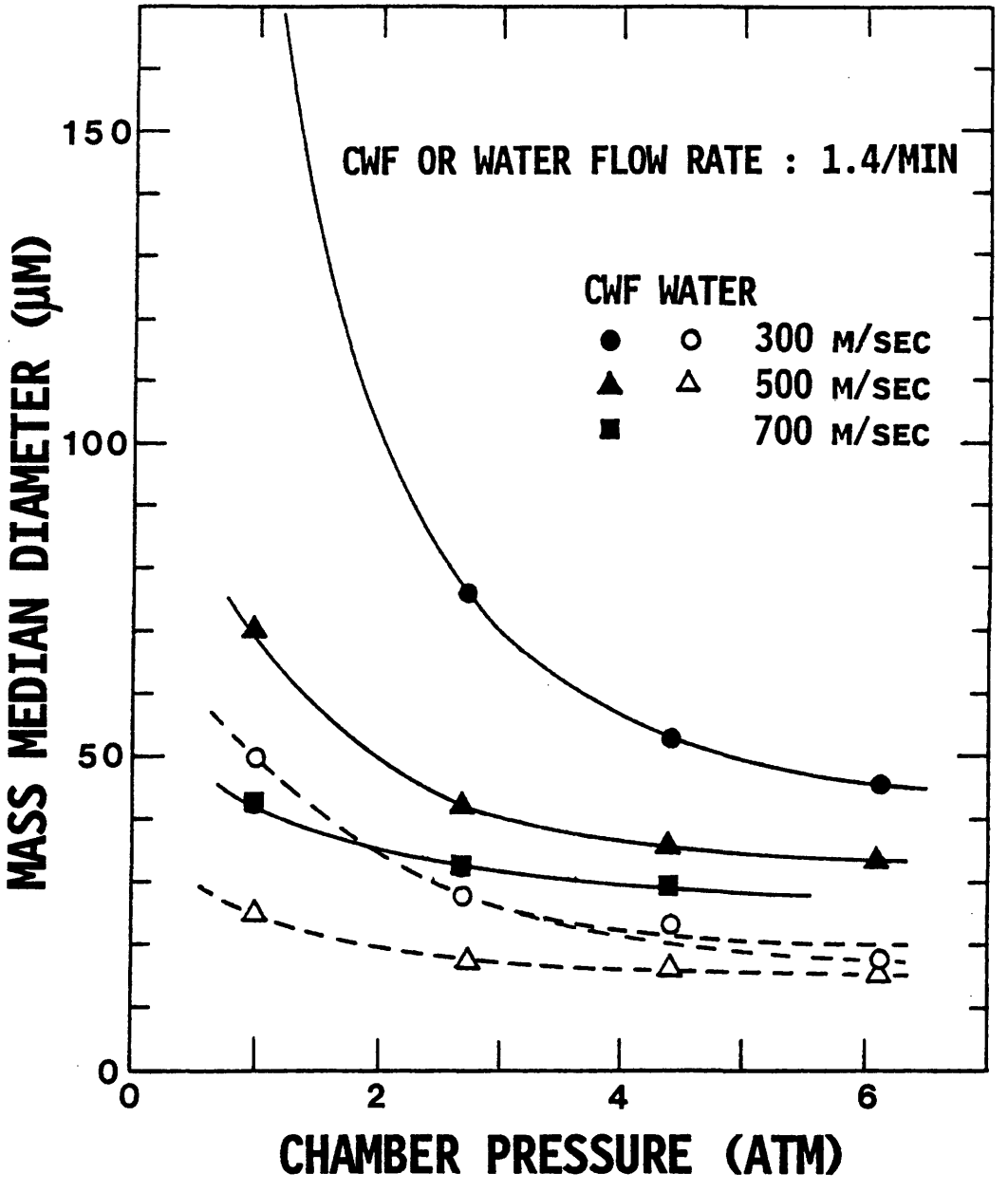

Figure 6-5. Effect of Chamber Pressure on Mass Median Diameter of Sprays at Different Atomizing Air Velocities

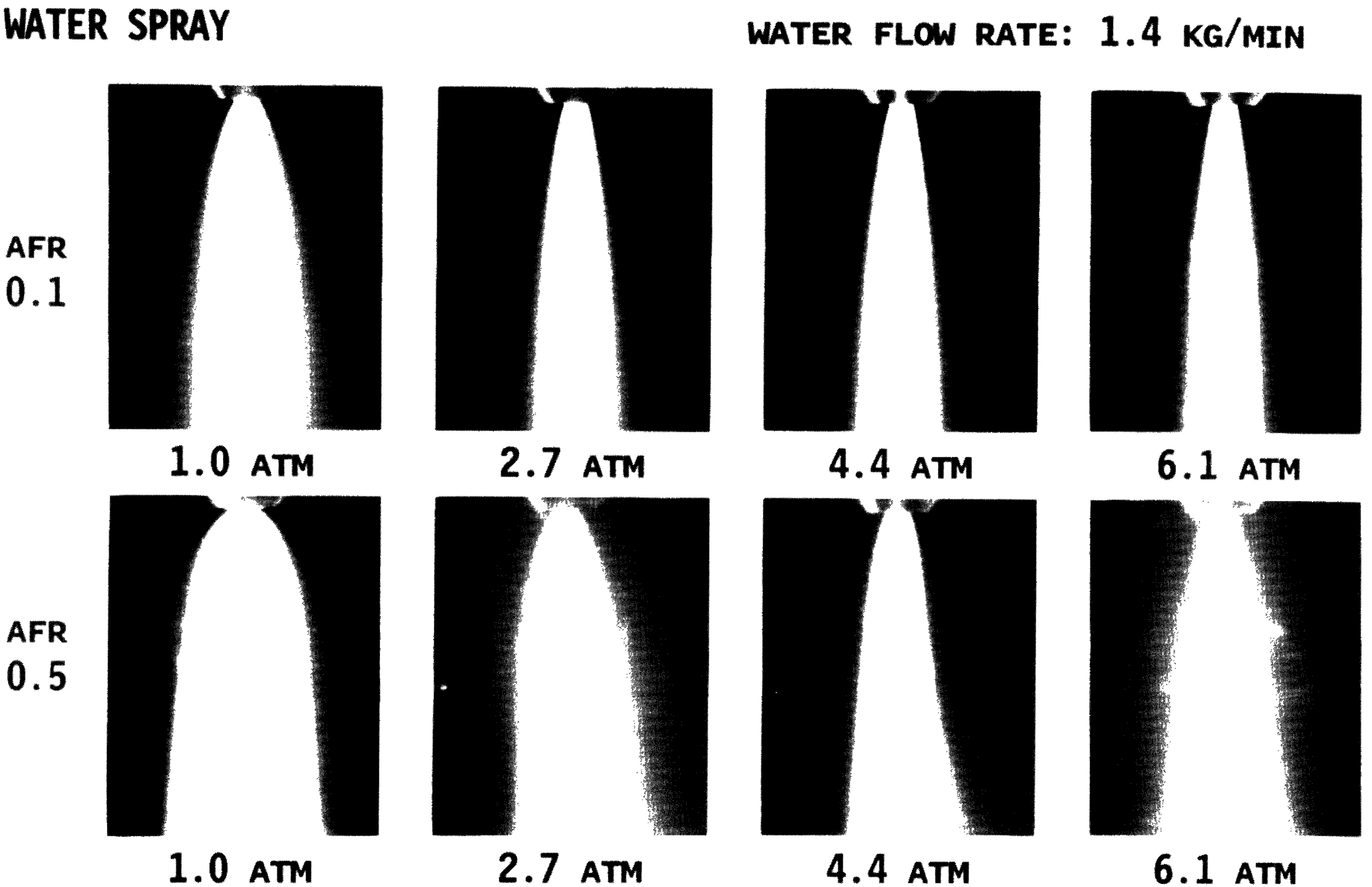

Figure 6-6. Photographs of Water Sprays taken at Four Different Chamber Pressures and Two AFRs, Water Flow Rate: 1.4 kg/min, 25°C

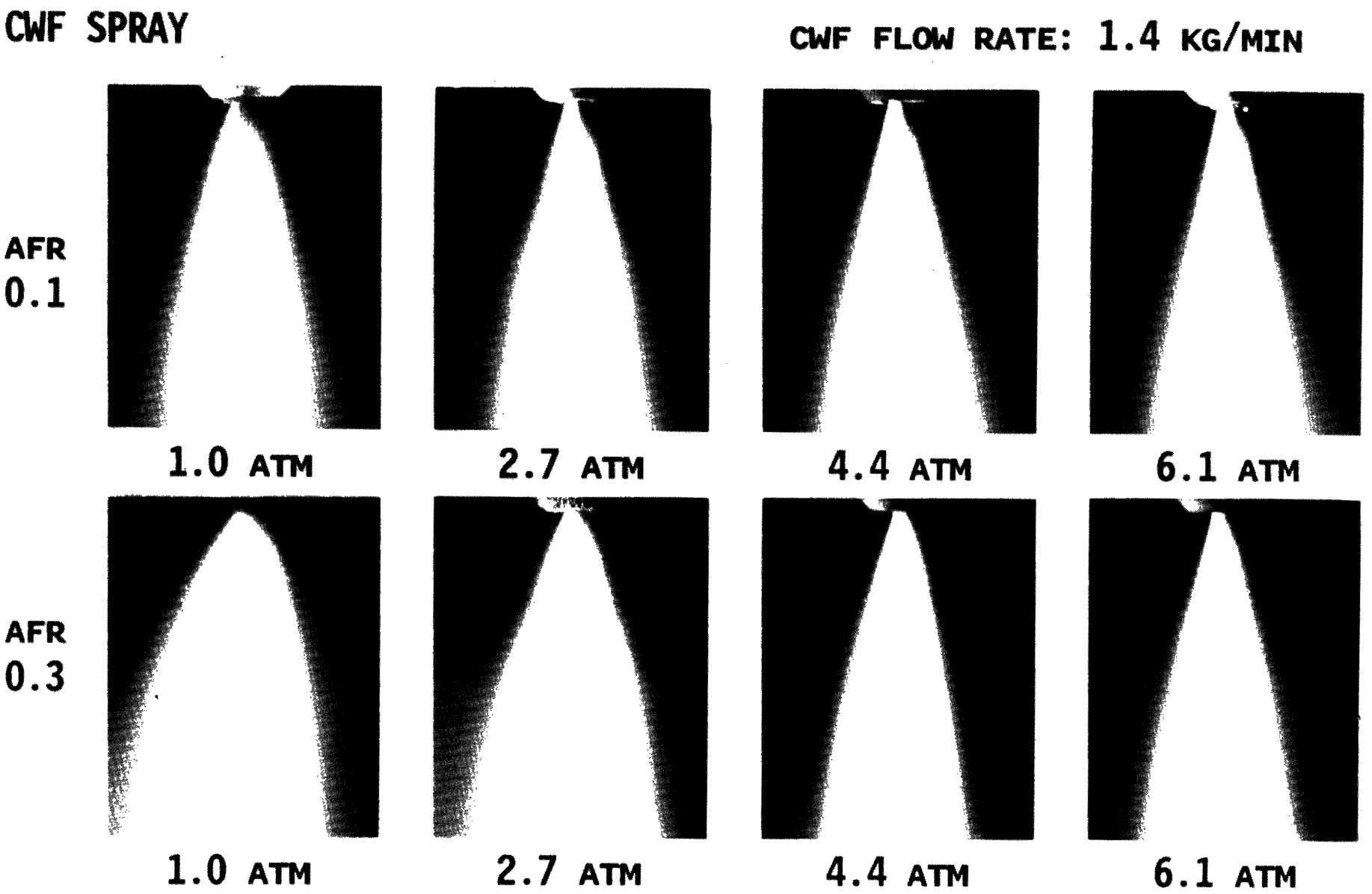

Figure 6-7. Photographs of CWF Sprays taken at Four Different Chamber Pressures and Two AFRs, CWF-B (50/50) Flow Rate: 1.4 kg/min, 25°C

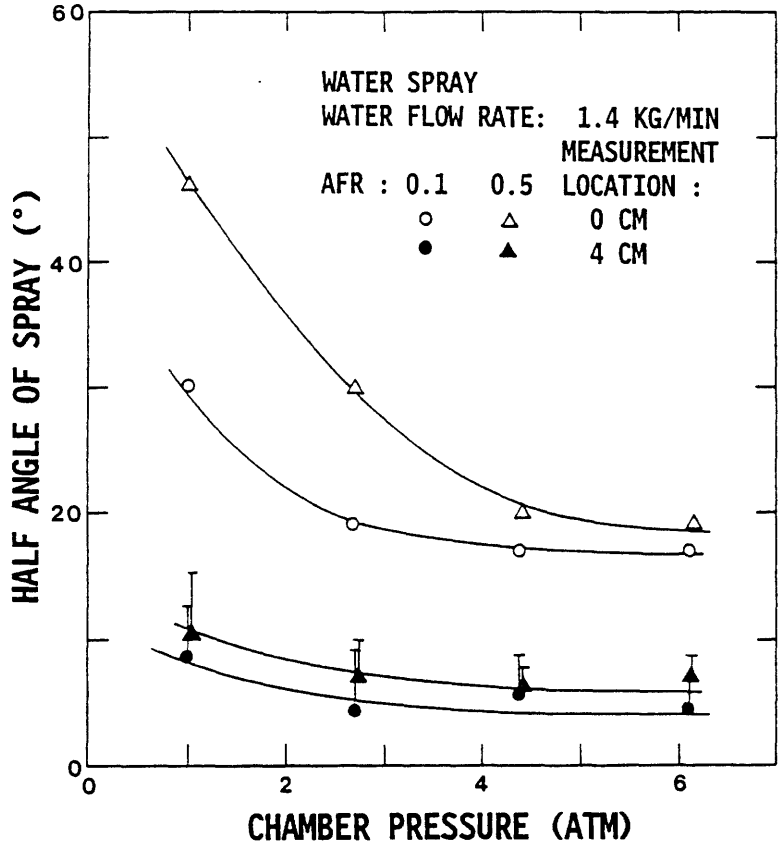

Figure 6-8. Effects of Chamber Pressure on Half Angle of Water Sprays.

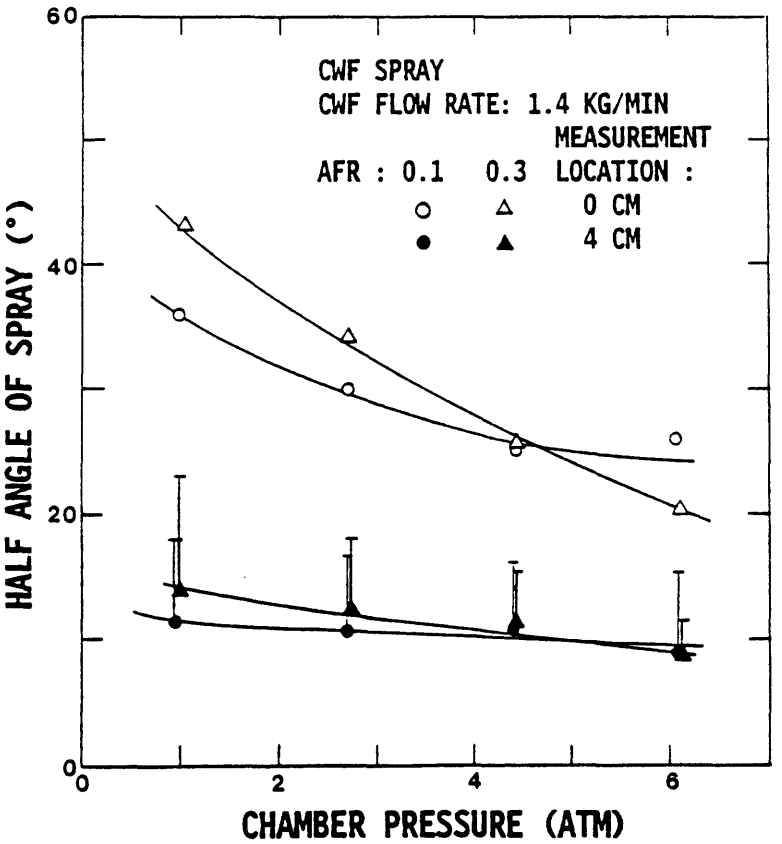

Figure 6-9. Effects of Chamber Pressure on Half Angle of CWF Sprays.

7. SECONDARY ATOMIZATION AT ELEVATED PRESSURE

In order to determine whether the three fuel treatment techniques can be applied to CWF-burning gas turbines, they were tested at gas turbine operating conditions (i.e., atomization was at elevated pressure). It was considered that if certain conditions were maintained constant with increasing ambient pressure, secondary atomization techniques could be applied to high ambient pressure conditions without any loss of secondary atomization effects. For the case of CWF heating, the steam mass fraction produced by flash-vaporization would remain approximately constant with increasing combustor pressure if the difference between the fuel temperature and the water saturation temperature at the combustor chamber pressure were maintained constant. However, volume change produced by the vaporized steam would decrease due to increased steam density at ambient pressure. Also, at increasing chamber pressures it may be difficult to maintain the temperature difference constant between that of the CWF in the atomizing gun and that of the saturated steam at the chamber pressure, because the saturation pressure required in the fuel line increases as a steep power function of the saturation temperature (in Kelvin). If a practical limit of nozzle fuel line pressure is taken to be 500 psia, at which the saturation temperature becomes 240°C, and the fuel is injected into a combustor pressurized at 100 psia, 0.085 lb of steam per pound of 50/50 CWF will be vaporized, resulting in about a 25-fold volume increase. It is expected that this would be enough to produce strong shattering effects on the CWF spray.

7.1 EXPERIMENTAL APPARATUS

The high-pressure spray test rig (Section 3.2) was used for experiments at elevated pressure. As in the corresponding primary atomization studies (Section 6), droplet sizes of CWF sprays were measured at various chamber pressures and AFRs using the laser diffraction droplet size analyzer (Section 3.3) which was installed perpendicular to the spray (Figure 3-2). The OR-KVB atomizer (Section 3.6) (air-assisted) was also used for this study. The CWF flow rate was maintained constant, and thus the AFR was controlled by the variation of the atomizing air flow rates which, in turn, determined the atomizing air velocity at the nozzle exit for a given chamber pressure.

7.2 DROPLET SIZE MEASUREMENT

Effects of fuel heating (secondary atomization) on atomization quality were studied for applications at elevated pressure. Droplet sizes of CWF sprays measured as a function of fuel temperature at several different chamber pressures are plotted in Figure 7-1. Saturation temperatures corresponding to each chamber pressure are marked in the figure by arrows. MMDs were observed to decrease steadily with increasing temperature, but for each chamber pressure the rate of reduction of MMD sharply increases as temperature approaches the corresponding saturation temperature.

As discussed in Section 5, the reduction of the average droplet size observed near the saturation temperature of the liquid is due to the decrease of the CWF viscosity with heating. The reduction of MMD observed for temperatures beyond the saturation temperature is probably due to the combination of disruptive thermal atomization and further reduction of the

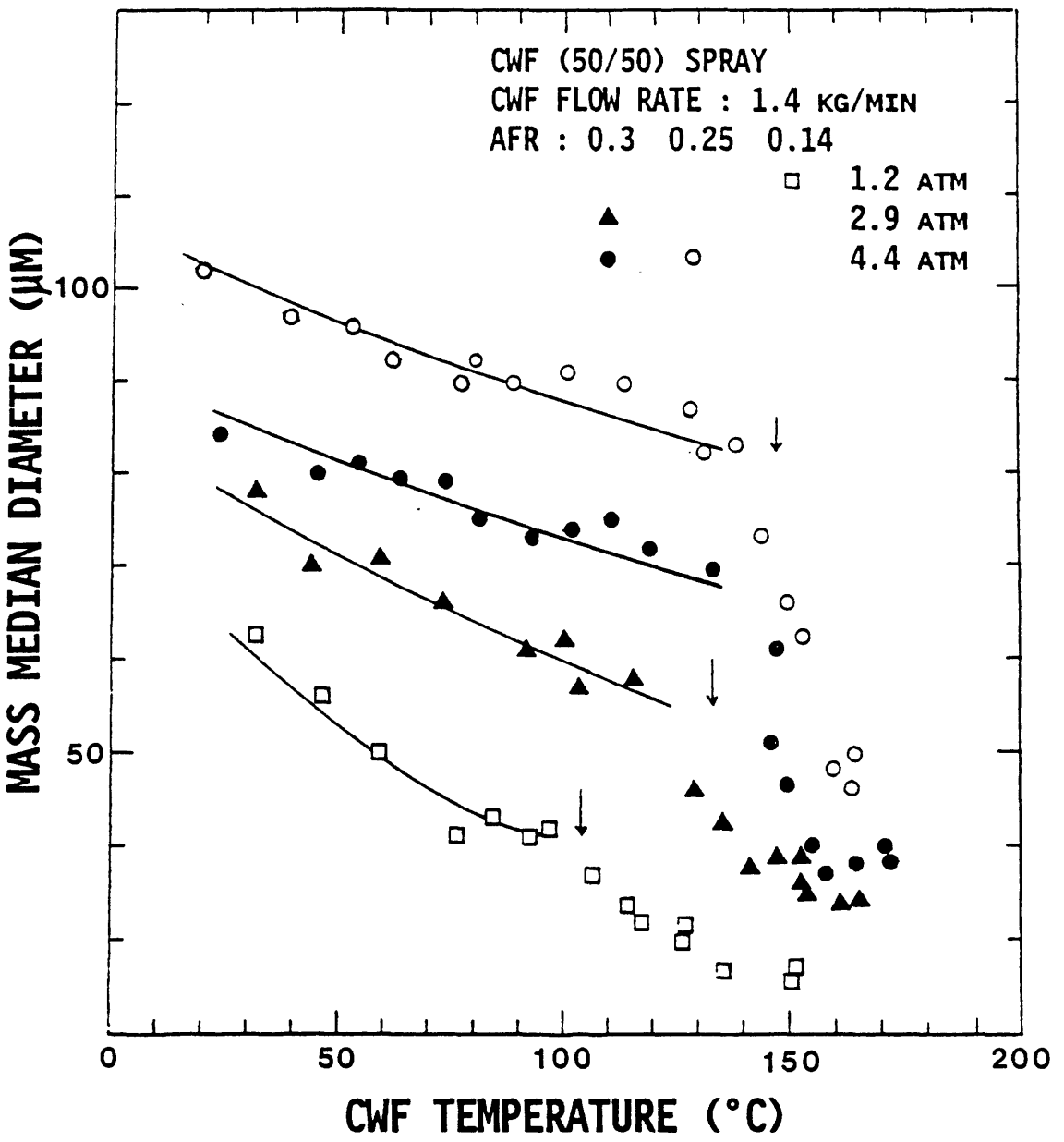

Figure 7-1. Effect of Fuel Temperature on Mass Median Diameter of CWF Sprays at Elevated Pressure

effective viscosity. However, the experimental results of Figure 7-1 show that at elevated pressures the sharp reduction of MMD starts to appear before the saturation temperature is reached, and the rate of MMD reduction is higher than for atmospheric pressure conditions. Further investigations are required to clarify these unexpected favorable results.

The authors consider that the fine mist generated upon the condensation of the steam might have an effect on the laser diffraction measurement. This effect, however, is not considered to be sufficiently strong to explain the significant reduction in the MMD under conditions of secondary atomization at elevated pressures.

7.3 PHOTOGRAPHIC STUDY OF SPRAY ANGLE AND SHAPE

Photographic studies were also made to characterize changes of spray shape and angle when flash-atomization was used at elevated pressure. Figures 7-2 and 7-3 show pictures of water sprays with heating taken at three chamber pressures, and two values of AFR. Figure 7-4 shows pictures of CWF sprays with heating at two elevated pressures. In all these cases one effect of heating is seen to be an increase in spray angle, as was observed in the corresponding experiments at atmospheric pressure (see Figures 5-4 and 5-10). The change in the spray angle was reduced, however, with increasing chamber pressure. The CWF sprays expand much less than the water sprays, primarily because of the smaller water fraction of the CWF (~50%).

8. A MODEL OF SPRAY ANGLE CHANGE DURING FLASH-ATOMIZATION

8.1 INTRODUCTION

When water or coal-water fuel is heated near its saturation temperature at high fuel line pressure and discharged to the environment at a lower pressure through an atomizer, the water flash-vaporizes. This action of volumetric increase causes the spray angle to increase as seen in Figures 5-4 and 5-10 at atmospheric pressure, and Figures 7-2, 7-3 and 7-4 at elevated pressure. The increase of the spray angle during flash-atomization is accompanied by the reductions of not only droplet size but also droplet axial velocities. Therefore, during combustion of CWF sprays these reductions result in improved flame stability and carbon conversion efficiency.

Section 8.2 describes a theoretical model of the angle change of water and CWF sprays due to flash-atomization. Section 8.3 presents a correlation of water and CWF spray angles with superheat of water and mass flow rates of both water or CWF and atomizing air.

8.2 THE THEORETICAL MODEL

If a pressurized liquid is heated to a temperature approaching its saturation temperature, the liquid flash-vaporizes as its pressure is suddenly reduced in the atomizing nozzle.

The available energy of a superheated liquid ($\Delta\psi$) in the isobaric process can be obtained as

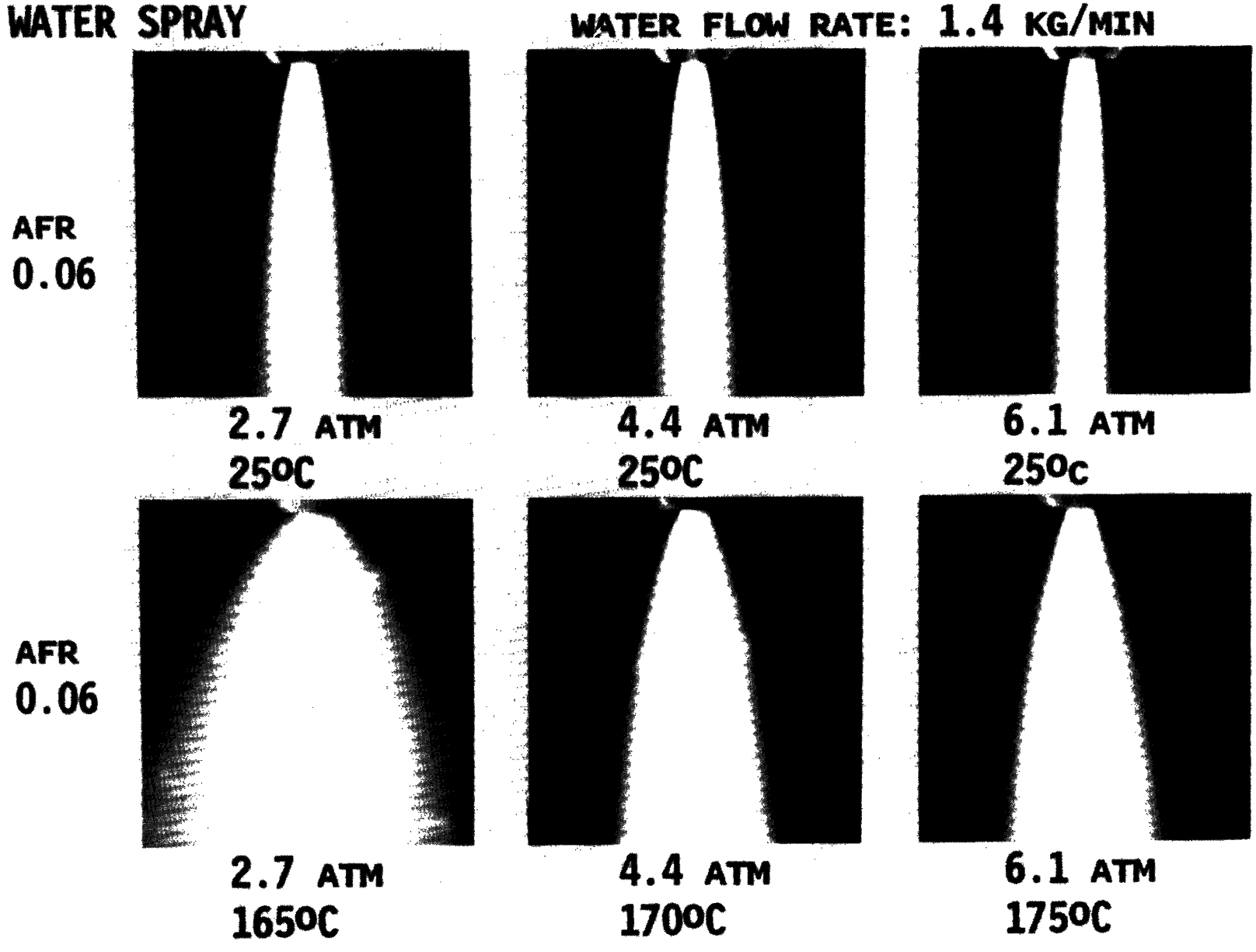

Figure 7-2. Photographs of Water Sprays taken with and without Heating at Three Elevated Chamber Pressures. Water Flow Rate: 1.4 kg/min, AFR: 0.06

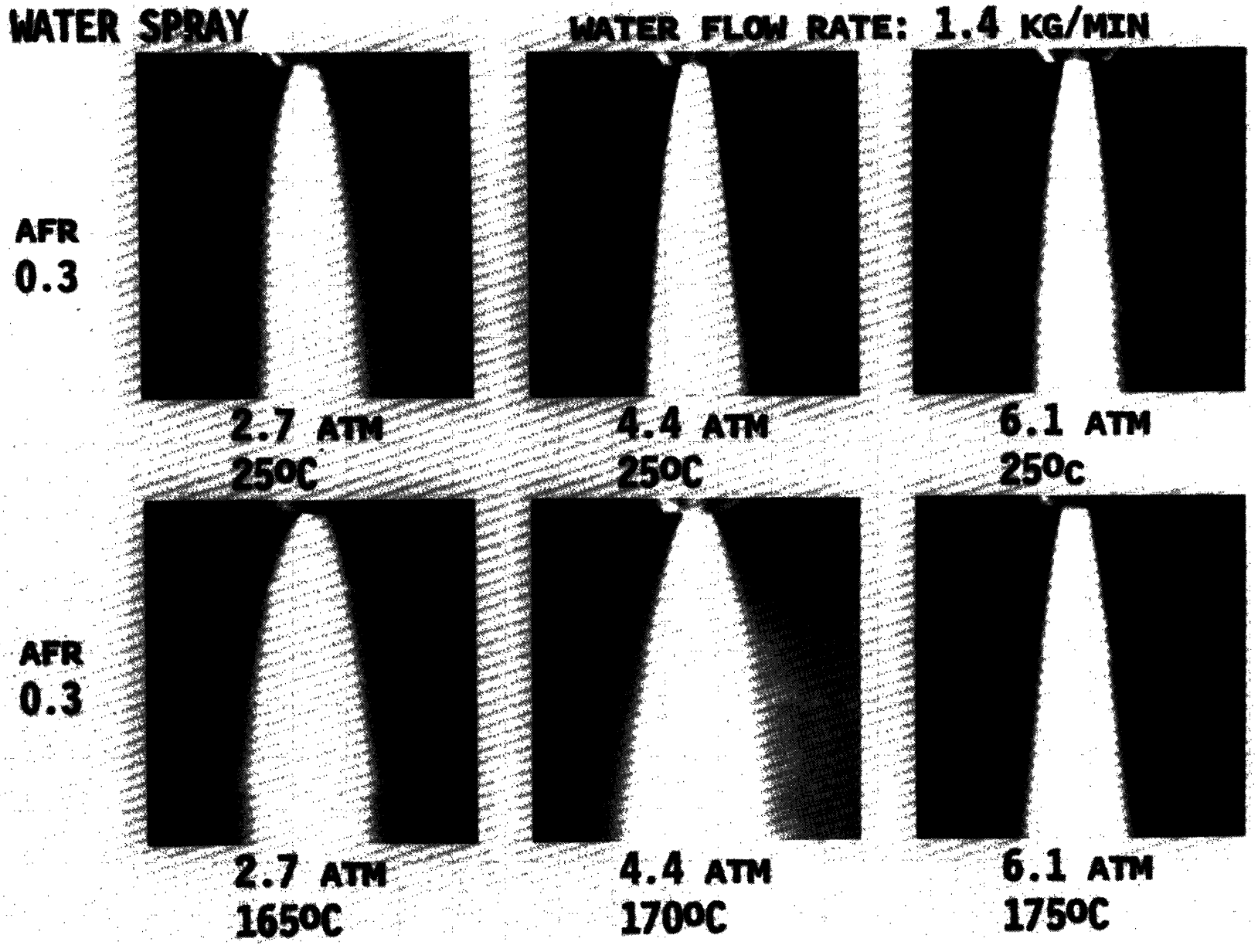

Figure 7-3. Photographs of Water Sprays taken with and without Heating at three Elevated Chamber Pressures.
Water Flow Rate: 1.4 kg/min, AFR: 0.3

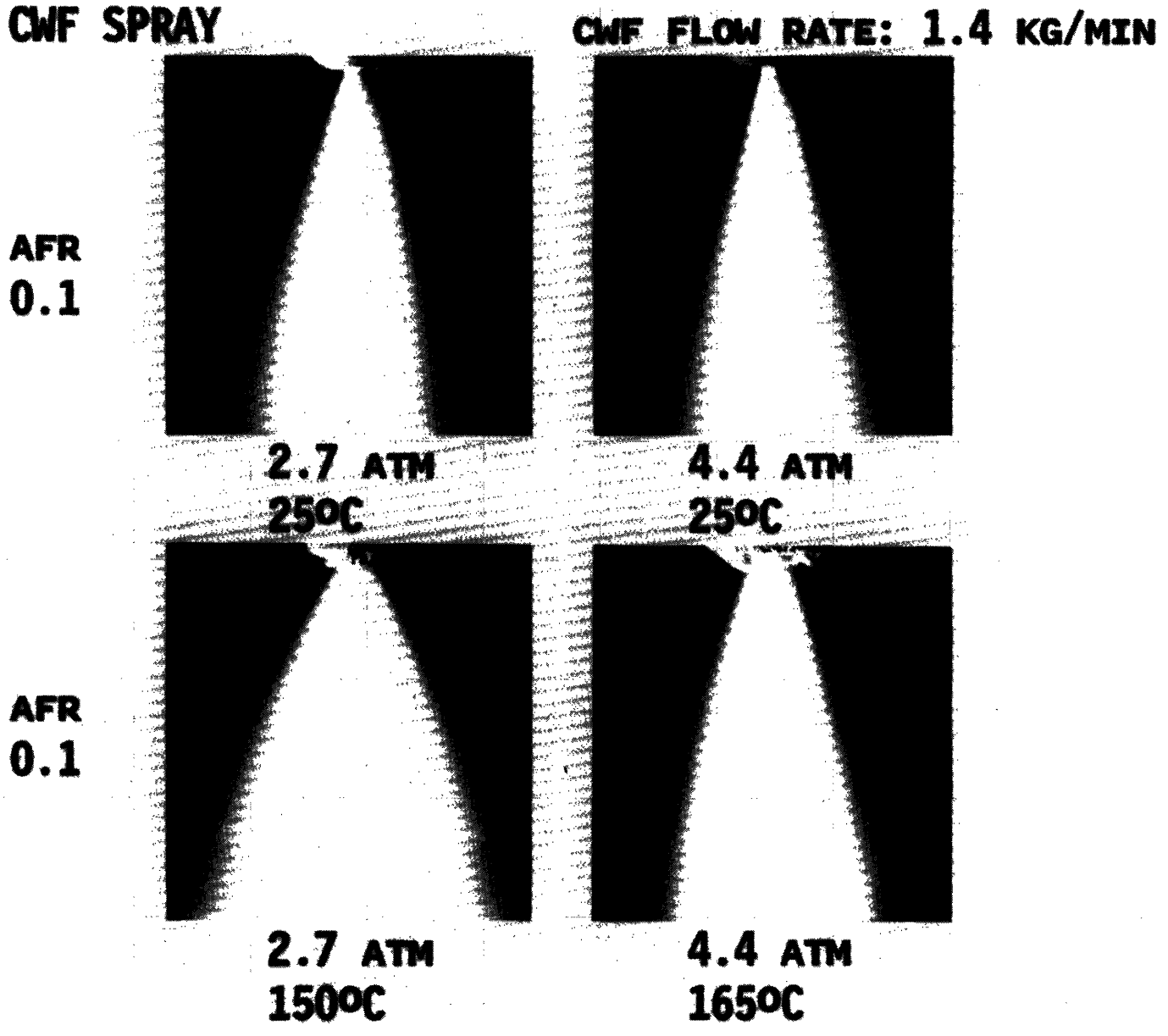

Figure 7-4. Photographs of CWF Sprays taken with and without Heating at two elevated Chamber Pressures, CWF-B (50/50) Flow Rate: 1.41 kg/min, AFR: 0.1

$$\Delta\psi = \Delta h - T_{sat}\Delta s \tag{23}$$

where Δh = difference in enthalpies between the superheated and saturated liquids
T_{sat} = saturation temperature of the liquid at ambient pressure
Δs = difference in entropies between the superheated and saturated liquids

Specific heat, c_p, is nearly constant in the temperature range of interest, and so Eq. (23) can be expressed as

$$\Delta\psi = c_p \left[\Delta T - T_{sat} \ln \left(\frac{T}{T_{sat}} \right) \right] \tag{24}$$

where c_p = specific heat of liquid at constant pressure
ΔT = superheat of liquid
T = temperature of superheated liquid, given by
$T = \Delta T + T_{sat}$

Therefore, the available energy of a superheated liquid ($\Delta\psi$) in the isobaric process can be rewritten as

$$\Delta\psi = c_p \left[\Delta T - T_{sat} \ln \left(\frac{\Delta T + T_{sat}}{T_{sat}} \right) \right] \tag{25}$$

The available energy of a superheated liquid can be manifested through an increase in the kinetic energy of the spray or as new surface energy during atomization. Lienhard (31) showed that the magnitude of the new surface energy is not of primary importance compared to that of the kinetic energy.

During atomization, two components of spray velocity can be defined: one is the axial velocity of spray V_a, and the other is the radially propagating velocity of spray V_r (Figure 8-1a). In the case of atomization with flash-vaporization an additional velocity of V_f, generated due to the additional kinetic energy of the superheated liquid, should be considered (Figure 8-1b).

As shown in Figure 8-1a, the half angle α_o of the spray without flash-atomization is expressed as

$$\sin \alpha_o = \frac{V_r}{V_a} \tag{26}$$

In Figure 8-1b the half angle α of the spray with flash-atomization is expressed as

$$\sin \alpha = \frac{V_r + V_f}{V_a} \tag{27}$$

If all of the available energy were to go into radial translational kinetic

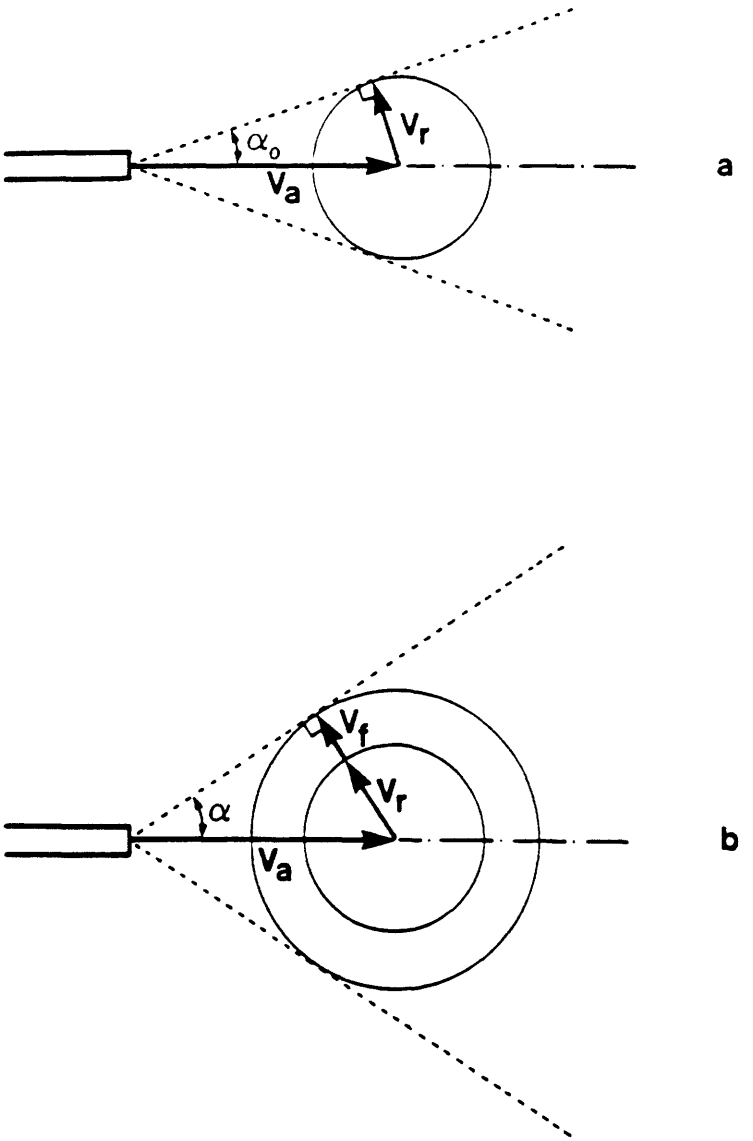

Figure 8-1. Schematic Diagram of Twin-Fluid Atomization
a) Without Flash-Atomization
b) With Flash-Atomization

energy, the maximum velocity $V_{f_{max}}$, generated by flash-vaporization, would be

$$V_{f_{max}} = (2\ c_p)^{1/2} \left[\Delta T - T_{sat} \ln \left(\frac{\Delta T + T_{sat}}{T_{sat}} \right) \right]^{1/2} \tag{28}$$

In reality, however, only a fraction of the superheated liquid will fully return to a saturated condition and contribute to the process of spray angle change during flash-atomization. Therefore, the actual velocity (V_f) achievable from flash-atomization can be related to the maximum radial velocity generated with flash-atomization ($V_{f_{max}}$) multiplied by the efficiency factor ξ, which is

$$V_f = \xi\ V_{f_{max}} \tag{29}$$

Here, the efficiency factor ξ will be some constant much less than unity, and can be obtained experimentally.

From Eqs. (26) through (29), actual velocity V_f generated by flash-atomization is correlated as

$$\begin{aligned} V_f &= V_a\ (\sin \alpha - \sin \alpha_o) \\ &= \xi\ V_{f_{max}} \\ &= \xi\ (2\ c_p)^{1/2} \left[\Delta T - T_{sat} \ln \left(\frac{\Delta T + T_{sat}}{T_{sat}} \right) \right]^{1/2} \end{aligned} \tag{30}$$

Hence, the half angle α of the spray with flash-atomization is correlated with superheat of liquid ΔT, efficiency factor ξ, and axial velocity of spray V_a, as follows:

$$\alpha = \sin^{-1} \left[\frac{\xi}{V_a} (2c_p)^{1/2} \left[\Delta T - T_{sat} \ln \left(\frac{\Delta T + T_{sat}}{T_{sat}} \right) \right]^{1/2} + \sin \alpha_o \right] \tag{31}$$

where α = half angle of spray with flash-atomization
α_o = half angle of spray without flash-atomization
T_{sat} = saturation temperature of liquid at ambient pressure
ΔT = superheat of liquid
ξ = efficiency factor
V_a = axial velocity of spray
c_p = specific heat at constant pressure P_{amb}

In a twin-fluid atomized spray, the axial velocity of spray V_a varies with the mass flow rate of atomizing air $\dot{m}_a$ and that of fuel $\dot{m}_f$. The term ξ/V_a will be correlated with $\dot{m}_a$ and $\dot{m}_f$ in Section 8.3.

8.3 CORRELATION WITH EXPERIMENTAL DATA

Calculation of the spray angle by means of Eq. (31) requires knowledge of the value of ξ/V_a. The value of ξ/V_a could be determined experimentally by measuring spray angles as a function of the superheat of liquid. Still photos taken during the studies described in Sections 5.1.2 and 5.2.3 were used to measure spray angles. The spray angles were measured at the position of 4.0 cm downstream from the atomizer tip, as shown in Figure 8-2. The spray half angles at the temperature of 100°C (α_o) and those obtained at a higher temperature (α) were plotted in Figure 8-3 as functions of water temperature (T) but at fixed mass flow rates of both atomizing air ($\dot{m}_a$) and water ($\dot{m}_f$). Figure 8-3 shows that ($\sin\alpha - \sin\alpha_o$) varies linearly with

$$(2c_p)^{\frac{1}{2}} \left[\Delta T - T_{sat} \ln \frac{\Delta T + T_{sat}}{T_{sat}} \right]^{\frac{1}{2}}$$

for fixed $\dot{m}_f$ and $\dot{m}_a$. The slope of the data line in this figure represents the value of ξ/V_a for the corresponding $\dot{m}_a$ and $\dot{m}_f$. Values of ξ/V_a obtained as functions of $\dot{m}_a$ and $\dot{m}_f$ are plotted in Figure 8-4. Based upon the data in Figure 8-4, the term of ξ/V_a is correlated with $\dot{m}_f$ and $\dot{m}_a$ as follows:

$$\frac{\xi}{V_a} = \frac{0.0068}{\dot{m}_f} - \left(2.2 \times 10^{-10} \dot{m}_a \right)^{0.0293 \dot{m}_f + 0.190} \tag{32}$$

where the units of physical variables are as follows:

ξ/V_a : sec/m
$\dot{m}_a$: kg/min
$\dot{m}_f$: kg/min

Finally, the half angle α of the water spray during flash-atomization is correlated with water temperature, mass flow rates of both water and atomizing air, and the half angle α_o of the water spray at the water temperature of 100°C, by substituting ξ/V_a from Eq. (32) into Eq. (31), which becomes

$$\alpha = \sin^{-1} \left[(2c_p)^{\frac{1}{2}} \left(\frac{0.0068}{\dot{m}_f} - \left(2.2 \times 10^{-10} \dot{m}_a \right)^{0.0293 \dot{m}_f + 0.190} \right) \times \left(\Delta T - T_{sat} \ln \left(\frac{\Delta T + T_{sat}}{T_{sat}} \right) \right)^{\frac{1}{2}} + \sin\alpha_o \right]$$

Values of ξ/V_a for CWF sprays with solids loading of 50% were also obtained and are shown in Figure 8-4. When the data of ξ/V_a determined for CWF sprays are compared with those of water sprays at the corresponding water flow rates, ξ/V_a values of CWF sprays are seen to be approximately half of those of water sprays (which is proportional to the water fraction of the CWF). This is because of the lesser amount of water in the CWF spray, which leads to reduced efficiency of expansion upon heating.

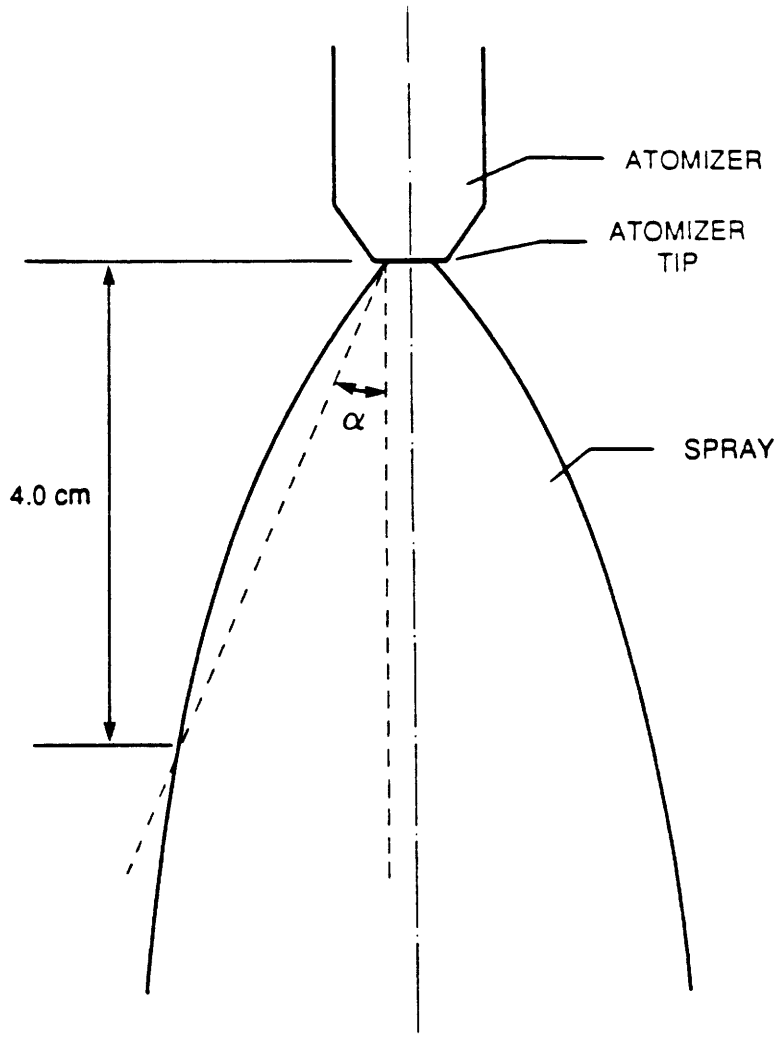

Figure 8-2. Measurement of Spray Angle α.

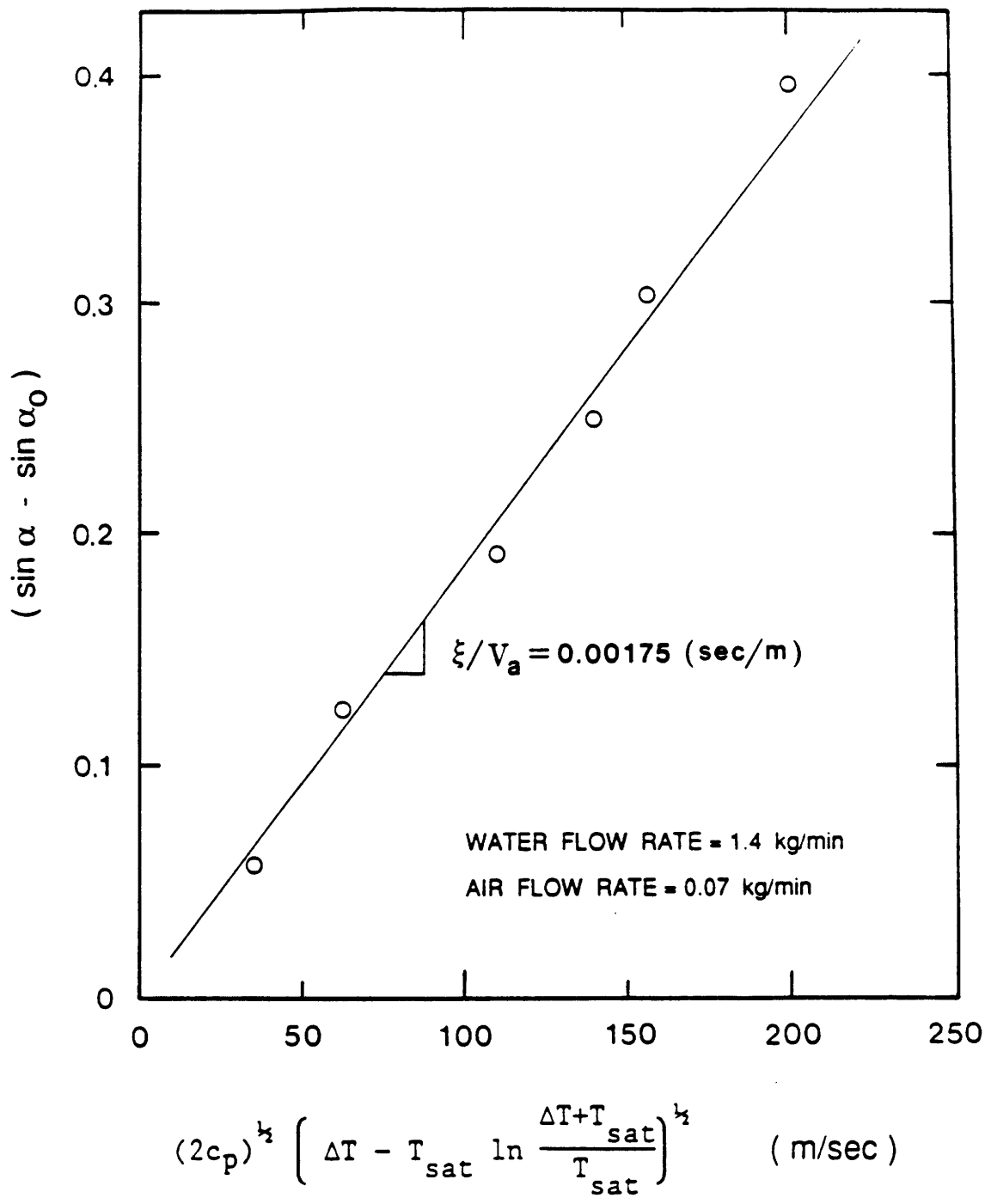

Figure 8-3. Variation of (Sin α-Sin α_o) with $(2\ c_p)^{1/2}\left[\Delta T - T_{sat} \ln \frac{\Delta T + T_{sat}}{T_{sat}}\right]^{1/2}$

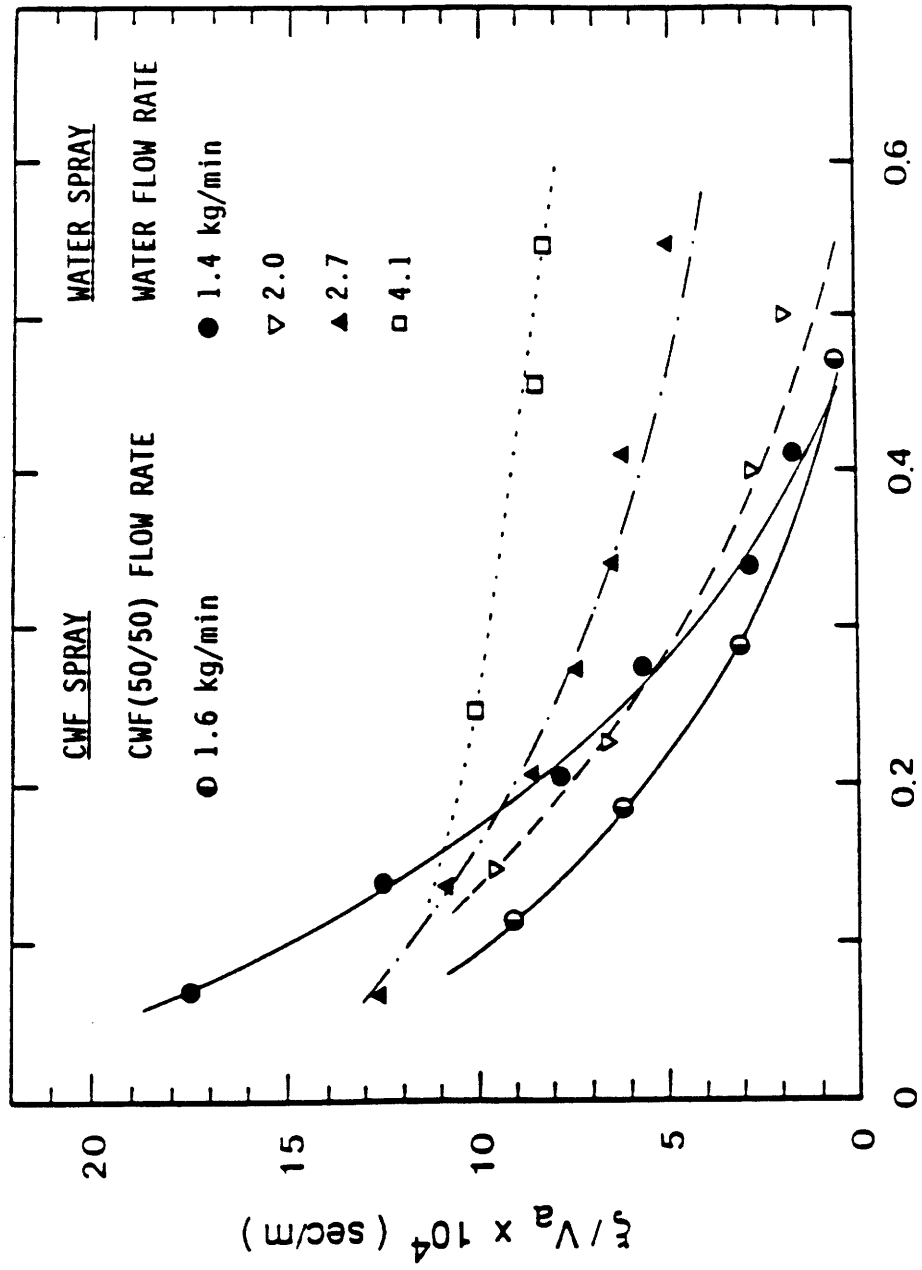

Figure 8-4. Variation of ξ/V_a with Atomizing Air Flow Rates

9. CONCLUSIONS AND RECOMMENDATIONS

9.1 CONCLUSIONS

The main conclusions of the experimental and theoretical (modeling) studies are as follows:

(1) A correlation, shown below, has been developed giving the CWF spray droplet size as a function of the characteristic dimensions of the twin-fluid atomizer, the air-to-fuel mass ratio (AFR) and the effective viscosity of the CWF at high shear rate representative of the shear rate within a twin fluid atomizer.

$$\frac{MMD}{D_o} = 0.0263 \left[\frac{\sigma_L}{\rho_A U_R^2 D_o}\right]^{0.25} \left[1 + \frac{1}{AFR}\right]^{0.5}$$

$$+ 0.0050 \left[\frac{(K\dot{\gamma}^{n-1})^2}{\rho_L \sigma_L D_o}\right]^{0.5} \left[1 + \frac{1}{AFR}\right]^{0.75}$$

The correlation was tested experimentally and good agreement was found between calculated and measured drop sizes when high shear rate viscosity data were used.

2) A model has been developed to predict spray angle change for the effects of flash (secondary) atomization. A relationship is given between the change in the spray angle on the one hand, and the superheat of the water in the CWF and the mass flow rates of the CWF and the atomizing air, on the other. The half angle of the flash-atomized spray, α, is given as

$$\alpha = \sin^{-1}\left[(2c_p)^{1/2}\left[\frac{0.0068}{\dot{m}_f} - \left[2.2 \times 10^{-10}\ \dot{m}_a\right]^{0.0293\ \dot{m}_f + 0.190}\right]\right.$$

$$\left. \times \left[\Delta T - T_{sat} \ln\left(\frac{\Delta T + T_{sat}}{T_{sat}}\right)\right]^{1/2} + \sin\alpha_o\right]$$

(3) The mass median droplet size in twin-fluid atomized sprays was found to increase with chamber pressure if both the atomizing air and the fuel mass flow rates were kept constant, but the droplet size decreased for the case when the atomizing air velocity was kept constant during an increase in chamber pressure (with concomitant increase of the atomizing air flow rate).

(4) Droplet size measurements of heated CWF sprays showed that thermal atomization effectively reduces the spray droplet size, not only at atmospheric but also at elevated pressures. Reduction in droplet

size for the effect of CWF temperature up to levels of the saturation temperature of the CWF is explained by the corresponding reduction in the CWF effective viscosity; above this temperature the superheated liquid flash vaporizes upon its passage through the atomizer with the result of droplet disintegration and hence finer atomization. As flash-atomization works on the water fraction of the CWF, its effect is proportional to the water content of the fuel. The effect of secondary (flash) atomization upon the spray size distribution depends also on the original (primary) atomized droplet sizes: large droplets are more likely to be disrupted because of their smaller surface tension. This is an especially favorable feature of secondary atomization because large droplets are likely to cause difficulties with burnout and impingement on structural parts of the combustor or gas turbine.

(5) Photographic studies of the spray angle revealed that the angle decreases with increasing chamber pressure, but the spray angle will increase even at elevated pressure as a result of heating of the CWF to produce flash-atomization. The effect of flash atomization on the spray angle change is important because a wider angle makes for improved flame stability and promotes carbon burnout efficiency.

(6) Secondary atomization by CO_2 absorption which in a previous study produced favorable results on CWF combustion, did not seem to have an observable effect on the droplet size distribution of the CWF spray at room temperature. It is considered that the improvements found in flame stability and carbon burnout in sprays with CO_2 absorption in the CWF were due to the rapid bubble formation in the atomized droplets upon their injection into the flame, an effect that does not occur at room temperature.

9.2 Recommendations

(1) The correlations for droplet size and spray angle should be tested for a wide range of atomizer types, fuel types, and chamber pressures, to broaden the areas in which they are applicable.

(2) The effect of the high-temperature combustion environment on the droplet size and shape of flash-atomized CWF sprays would need to be determined as a function of the ambient pressure.

(3) Existing atomizers should be characterized for their amenability to operation under conditions of flash-atomization. The relationship between spray angle, linear momentum of the spray, and droplet size on the one hand and flame stability, carbon burnout, and fly ash formation on the other should be studied with the objective of establishing a better mechanistic understanding of the effect of atomization quality upon gas turbine combustion characteristics.

REFERENCES

1. Merten, M., and Homer, M., Section in Final Report on Combustion of Coal Water Suspension Power Plant, Lignite Mining Association, Essen, Germany, January, 1979.

2. Daley, R.D., Farthing, G.A., and Vecci, S.J., "Coal-Water Slurry Evaluation Volume 2: Laboratory and Combustion Test Results," Electric Power Research Institute, CS-3413, 1984.

3. Reid, R.C., Sarofim, A.F., and Beér, J.M., MIT, Cambridge, MA, private communication (1983).

4. Yu, T.U., Kang, S.W., Toqan, M.A., Walsh, P.M., Beér, J.M., and Sarofim, A.F., "Secondary Atomization of Coal-Water Slurry Fuels," Seventh International Symposium on Coal Slurry Combustion and Technology, New Orleans, Louisiana, May 22-24, 1985.

5. Yu, T.U., Kang, S.W. Toqan, M.A., Walsh, P.M., Teare, J.D., Beér, J.M. and Sarofim, A.F., "Effects of Fuel Treatment on Coal-Water Fuel Combustion," 21st Symposium (Int.) on Combustion, Combustion Institute, 1986.

6. Farmayan, W.F., Walsh, P.M., Teare, J.D., and Beér, J.M., "Coal-Water Slurry Ignition and Flame Stability: Mechanisms and Effects of Major Input Variables," ASME Winter Annual Meeting, New Orleans, December 9-14, 1984.

7. Swithenbank, J., Beér, J.M., Taylor, J.M.D.S., Abbot, D., and McCreath, G.C., "A Laser Diagnostic Technique for Measurement of Droplet and Particle Size Distribution", AIAA 14th Aerospace Sciences Meeting, Washington, D.C., AIAA Paper No. 76-69, pp. 1-9, January 1976.

8. Dodge, L.G., "Change of Calibration of Diffraction Based Particle Sizers in Dense Sprays," Optical Engineering, Vol. 23, No. 6, 1984.

9. Yu, T.U., Rah, S.C., Kang, S.W., and Beér, J.M., "Measurement of Viscosity of Coal-Water Fuels at High Shear Rate," 8th International Symposium on Coal Slurry Preparation and Utilization, Florida, May 1986.

10. Tsai, S.C. and Knell, E.W., "Rheology and Its Effects on Atomization of Coal Water Slurry," 1st Pittsburgh Coal Conference, Pittsburgh, PA, September 1984.

11. Probstein, R.F., Private Communication, MIT, Cambridge, MA, 1987.

12. Yu, T.U., Kang, S.W., and Beér, J.M., "Fuel Type Effects on Coal-Water Slurry Atomization", AIAA-86-0298, AIAA 24th Aerospace Sciences Meeting, Reno, Nevada, January 6-9, 1986.

13. Yu, T.U., Kang, S.W., Beér, J.M., Sarofim, A.F. and Teare, J.D., "Atomization Quality and High Shear Rate Viscosity of Coal-Water Fuels," 12th International Conference on Slurry Technology, March 1987.

14. Kang, S.W., "Combustion and Atomization Studies of Coal-Water Fuel in a Laminar Flow Reactor and in a Pilot-Scale Furnace," Ph.D. Thesis, Department of Mechanical Engineering, MIT, Cambridge, MA, February, 1988.

15. Miesse, C.C., "Recent Advances in Spray Technology," Appl. Mech. Reviews, Vol. 9, No. 8, pp 321-323, 1956.

16. Lefebvre, A.H., "Gas Turbine Combustion," McGraw-Hill Book Company, 1983.

17. Mellor, R., Chigier, N.A. and Beér, J.M., "Hollow Cone Liquid Spray in Uniform Air Stream," Combustion and Heat Transfer in Gas Turbine Systems, Cranfield Symposium, No. 11, Pergamon Press, London, 1971.

18. Yu, T.U., "Mathematical Modeling of Atomization of Liquids, A Review on Fluid Mechanics," unpublished work, 1985.

19. Rohsenow, W.M., "Nucleation with Boiling Heat Transfer," ASME 70-HT-18, pp. 2-11, 1970.

20. Rohsenow, W.M., Developments in Heat Transfer, MIT Press, 1964.

21. Thirunavukkarasu, K., "Bubble Growth from a Cavity at a Solid Surface," ASME 70-HT-13, pp. 1-9, 1970.

22. Zwick, S.A. and Plesset, M.S., "On the Dynamics of Small Vapor Bubbles in Liquids," J. Math. Phys., Vol. 33, pp. 308-330, 1955.

23. Plesset, M.S., and Zwick, S.A., "A Nonsteady Heat Diffusion Problem with Spherical Symmetry," J. Appl. Phys., Vol. 23, p. 95, 1952.

24. Plesset, M.S., and Zwick, S.A., "The Growth of Vapor Bubbles in Superheated Liquids," J. Appl. Phys., Vol. 25, pp. 393-400, 1954.

25. Forster, H.K. and Zuber, N., "Growth of a Vapor Bubble in a Superheated Liquid," J. Appl. Phys., Vol. 25, pp. 474-478, 1954.

26. Scriven, L.E., "On the Dynamics of Phase Growth," Chem. Eng. Sci., Vol. 10, p. 1, 1959.

27. Birkhoff, G., Margulies, R.S. and Horning, W.A., "Spherical Bubble Growth," Phys. of Fluids, Vol. 1, p. 201, 1958.

28. Staniszewski, B.E., "Nucleate Boiling Bubble Growth and Departure," Tech. Report. 16, DSR 7673, Office of Naval Research Contract NONR-1841 (39), MIT Heat Transfer Lab, August 1959.

29. Parsons, J.A., and Jasuja, A.K., "Effect of Air Pressure Upon Spray Angle/Width Characteristics of Simplex Pressure Swirl Atomizers," ASME Paper No. 86-GT-176, Int. Gas Turbine Conf. and Exhibit, West Germany, June 8-12, 1986.

30. Ingebo, R.D., "Atomization of Liquid Sheets in High Pressure Airflow," ASME Paper No. 84-Wa/Ht-27, 1984.

31. Lienhard, J.H., "An Influence of Superheat Upon the Spray Configuration of Superheated Liquid Jets," Journal of Basic Engineering, Transactions of the ASME, pp. 685-687, September 1966.

APPENDIX A

CHARACTERISTICS OF FUEL TREATMENT TECHNIQUES

A.1 THERMAL ATOMIZATION

If water is heated to 200°C (saturated vapor pressure then being 225 psia, or 1550 kPa), its enthalpy in the liquid state is 366.5 BTU/lb. On sudden expansion to atmospheric pressure the water temperature must decrease to ~ 100°C, which represents a drop in enthalpy of ~ 186 BTU per lb of H_2O. This is sufficient to vaporize ~ 0.2 lb/lb H_2O, since the heat of vaporization of water at 100°C is ~ 970 BTU/lb. Thus the net result of a sudden expansion of water at 200°C is the conversion of ~ 20% of the water into steam, with a 300-fold increase in specific volume.

If the water forms part of a 70/30 coal/water fuel, the instantaneous flash-vaporization produces ~ 0.06 lb of steam per pound of CWF, representing a net specific volume change of the mixture of ~ 100-fold increase. Transfer of the heat stored in the coal particles (initially at ~ 200°C) to the remaining water would add to the extent of flash-vaporization and enhance the specific volume increase. The effect of water fraction of CWF on volume change and mass fraction of steam is shown in Figure A-1.

When the water or CWF is expanded through an atomizing nozzle, it has been demonstrated that the overall effect of the flash-vaporization is to shatter the droplets initially formed by the nozzle, thereby yielding a substantial decrease in p.s.d.

In principle the CWF could be heated to its saturated vapor temperature at the line pressure. The major operational problem arises from clogging due to deposition of the coal particles on the heated metal surfaces, so that provision must be made for rapid dismantling and cleaning of the line.

When a 50/50 CWF heated to 220°C (which has a saturation pressure of 335 psia) is sprayed into a pressurized environment at ~ 100 psia (representative of gas turbine applications), approximately 0.06 lb/lb CWF could be vaporized by flash vaporization; however, the volume change could be as small as ~ 18-fold increase due to the high-pressure environment. In order to have greater volume change it is necessary to increase the CWF temperature, but the temperature range achievable is limited by the fact that the saturation pressure increases as the 10^{th} power of the saturation temperature in Kelvins. If a practical limit of nozzle pressure is taken to be 500 psia, at which the saturation temperature becomes 240°C, then the flash-vaporization of a 50/50 CWF at 100 psia will generate ~ 0.085 lb steam/lb CWF and a ~ 25-fold volume increase.

A2. CARBON DIOXIDE INJECTION

At 31°C the solubility of CO_2 in water is ~ 0.65 P cc(NTP) per gram of H_2O, with P in atmospheres. Thus at a nozzle pressure of 100 psi the saturation level would be ~ 4 cc/g H_2O, or 0.008 g/g H_2O, corresponding to ~ 0.0024 g/g CWF (for a 70/30 slurry), or ~ 0.0040 g/g CWF (for a 50/50

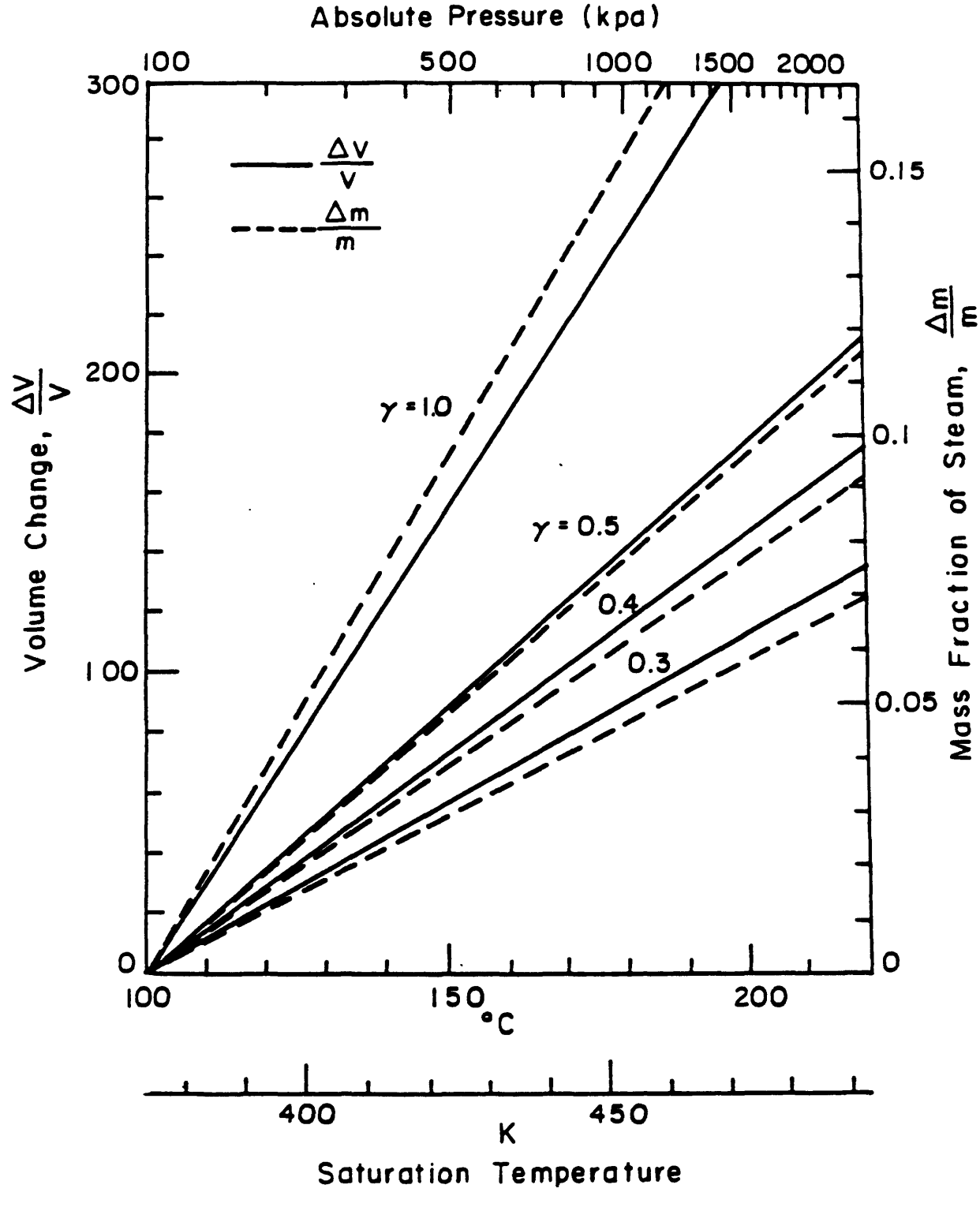

Figure A-1. Volume and Mass Fraction of Steam Generated from CWF as a Function of Saturation Temperature at Atmospheric Pressure, γ: Water Mass Fraction in CWF

slurry). It was originally expected that pronounced secondary atomization effects might be observed with lesser amounts of dissolved CO_2, below the saturation level for the fuel line pressure.

When CO_2 is dissolved in a heated CWF for the combination technique of heating and CO_2 dissolution, the solubility of CO_2 decreases: at 100° to 120°C it is expected to be about 1×10^{-3} P cc/g H_2O (with P in kPa). However, the dissolved CO_2 at reduced solubility should still provide additional secondary atomization effects.

APPENDIX B

SUMMARY OF PREVIOUS WORK ON COAL-WATER FUEL COMBUSTION WITH FUEL TREATMENTS

Three methods have been studied for using secondary atomization to produce a better quality of spray droplet size distribution and, hence, finer fly ash particle size distribution. The studies were made in the MIT Combustion Research Facility (CRF), and they include (1) thermally assisted, (2) CO_2-assisted, and (3) chemically assisted atomization.

In-flame measurements made during the CRF combustion experiments served to determine the effects of the three methods of secondary atomization on flame stability and carbon burnout, with particular emphasis on identifying the effectiveness of each method in reducing the fly ash p.s.d. From a close observation of the still photos it was evident that different treatments could bring improvements in flame stability and fuel-air mixing. Especially when CWF was heated, better burnout of CWF flames was noted, which could be explained by increased flame length. Particle size distributions of residual char and fly ash at the end of the flames for different secondary atomization techniques are shown in Figure B-1. Thermally-assisted atomization was the most effective method, judged by the reduction of solids concentrations and size distributions determined along the length of the flames. While not as effective as thermal atomization, CO_2 and picric acid additions to the slurry have also yielded beneficial results. The improvements in atomization quality due to CO_2 absorption were greater in the flame than in sprays introduced into a cold environment. The chemically assisted atomization gave a noticeable but only slight improvement over the base case (no secondary atomization); it was in the third place in ranking behind thermal and CO_2-assisted atomization.

In-flame measurements made on the best case, the secondary atomization with CWF heating, provided detailed information for comparison with the base case. The CWF heating improved flame stabilization and the combustion of solid particles, and reduced the resultant fly ash p.s.d.

Experimental results indicate that the secondary atomization technique may be used as an effective means of improving the quality of CWF atomization and hence carbon conversion efficiency. It seems that secondary atomization may lead also to finer fly ash p.s.d., which, in turn, would reduce the need for derating of performance on retrofitting oil-designed boilers for CWF combustion.

The work summarized above has been reported in References 4, 5, and 14, and in a DOE Final Report, Number DOE/PC 70268-F2, entitled "Fundamental Aspects of Coal-Water Fuel Droplet Combustion and Secondary Atomization of Coal-Water Mixtures", Volume II, November, 1986.

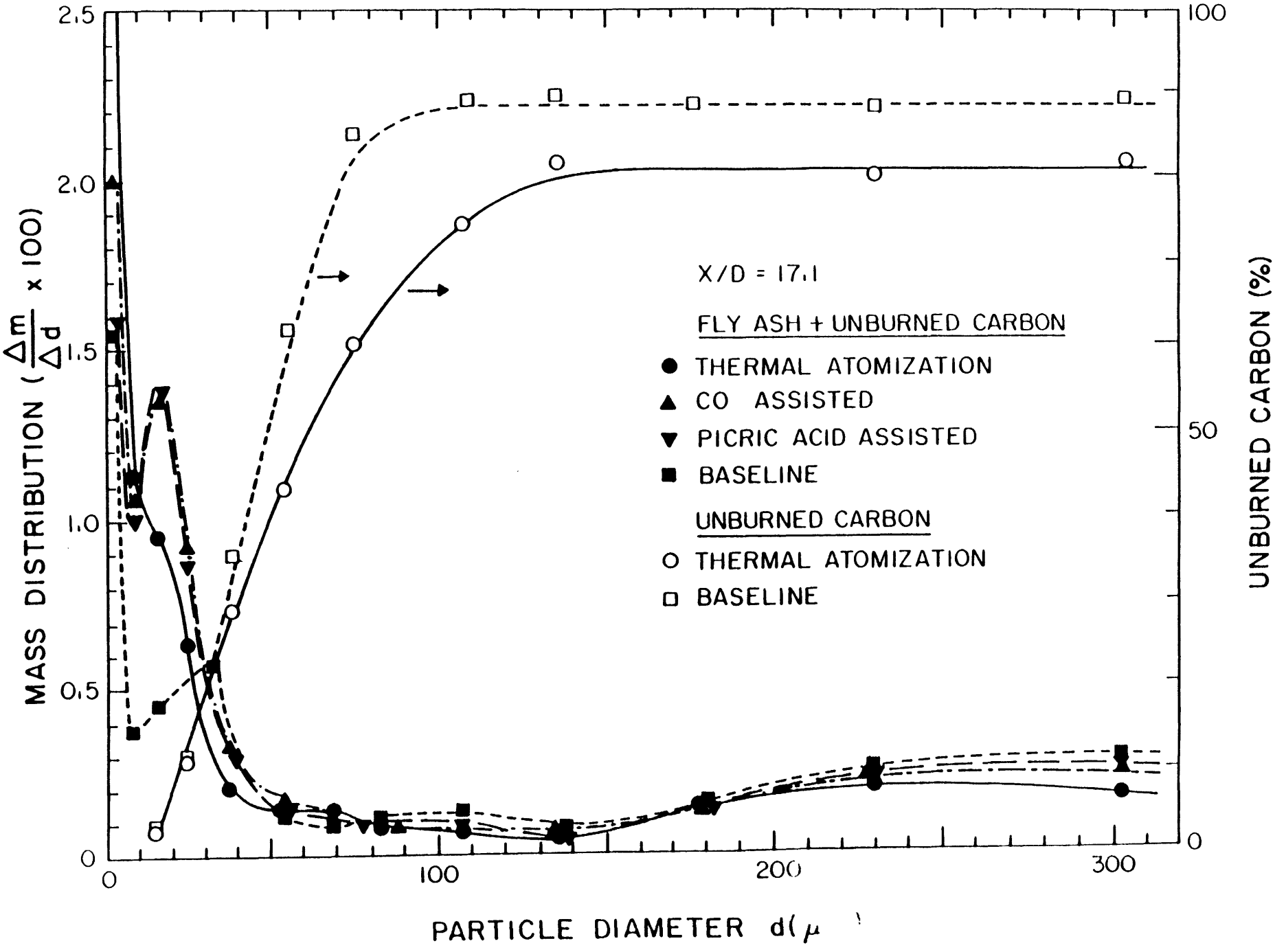

Figure B-1. Particle Size Distribution of Fly Ash and Residual Char at the End of Flame for Different Fuel Treatments

APPENDIX C
DETAIL DRAWINGS OF PRESSURE VESSELS

Figure C-1. High-Pressure Spray Test Rig - Vertical Vessel

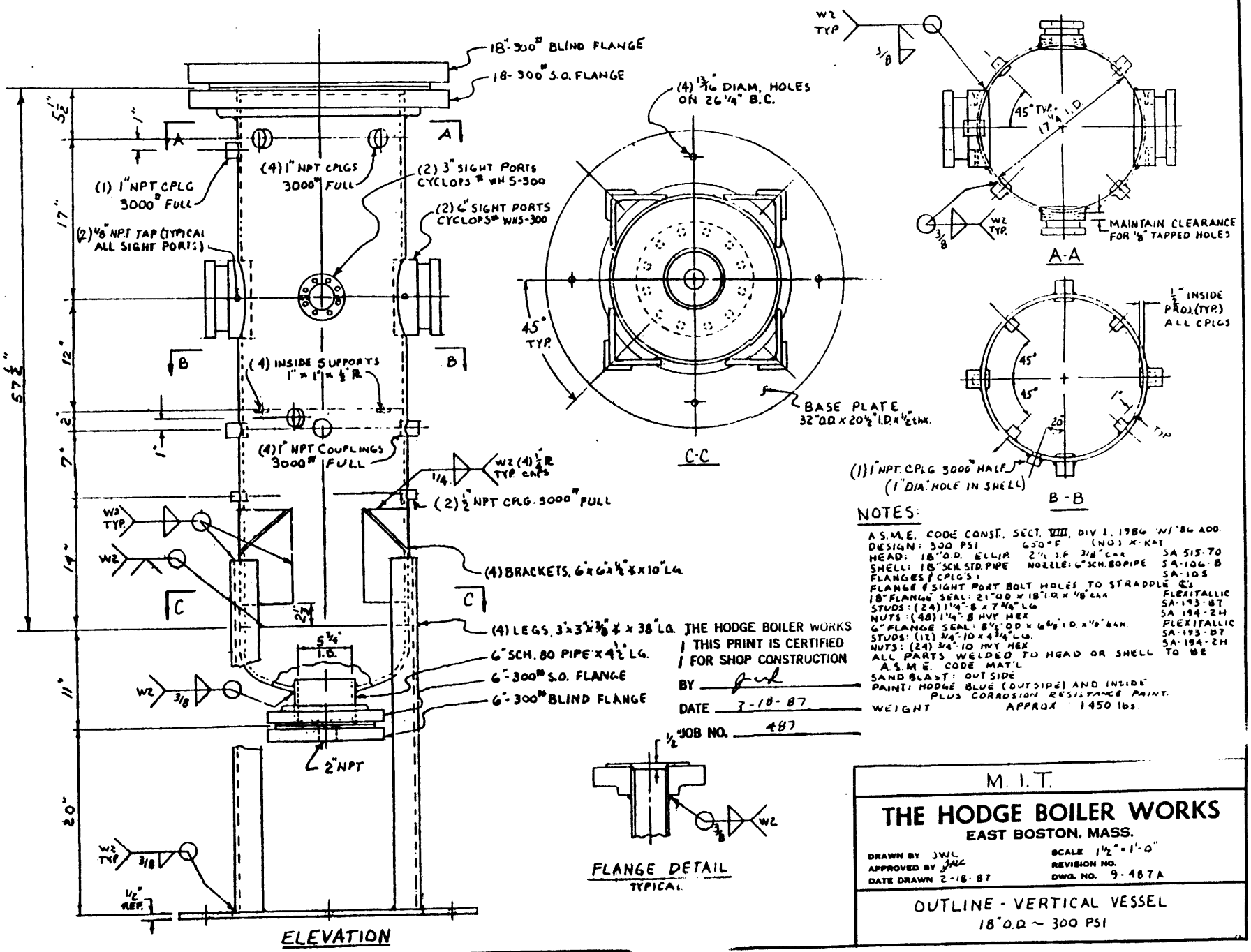

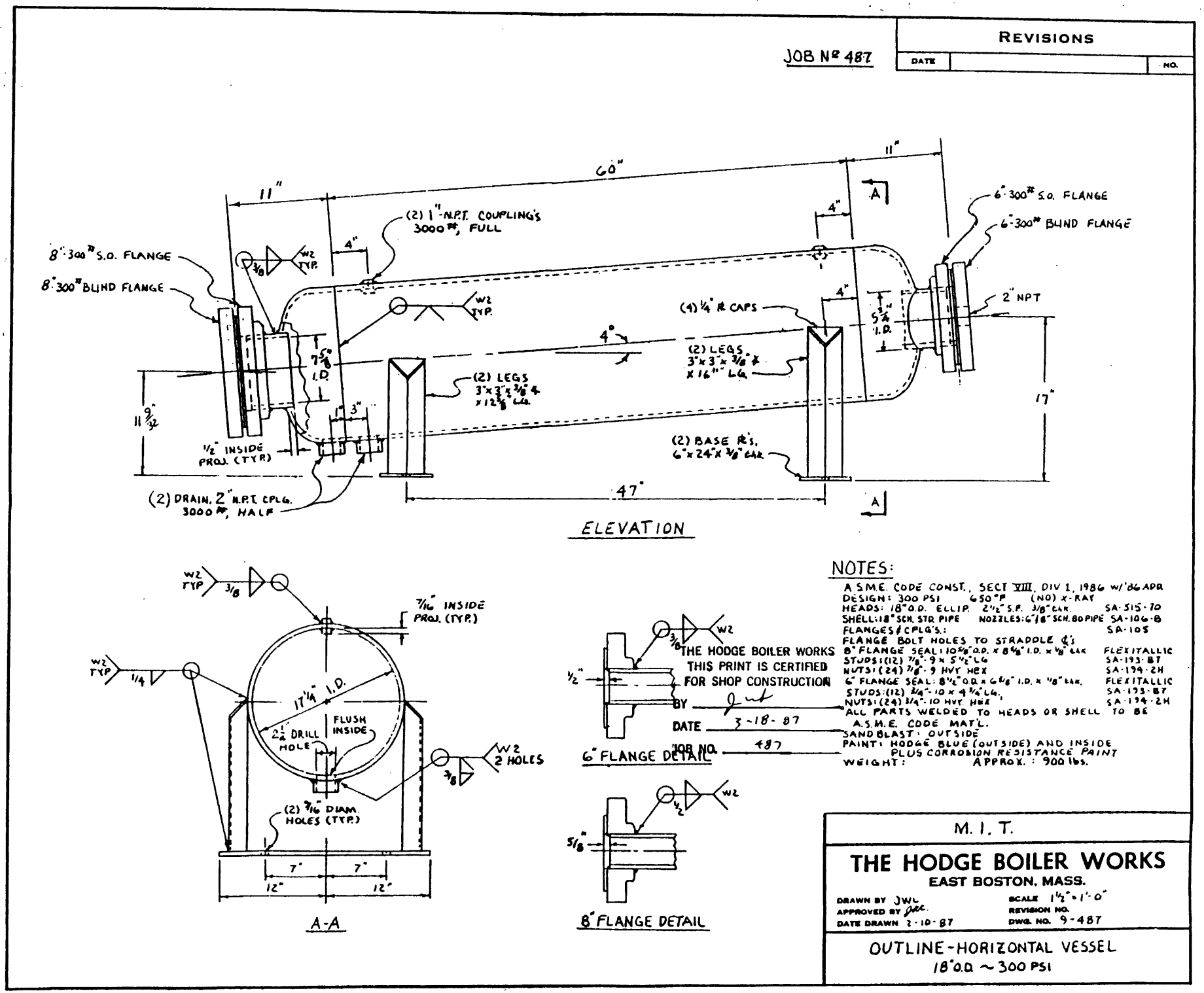

Figure C-2. High-Pressure Spray Test Rig - Horizontal Vessel